Techniques for Enhancing the PLD Growth of Superconducting YBCO Thin Films

Graham Lyall Hardie

Thesis presented in partial fulfilment of the requirements for the degree of Master of Engineering (Research) in theFaculty of Engineering at Stellenbosch University

Department of Electrical and Electronic Engineering
University of Stellenbosch
Private Bag X1, 7602 Matieland, South Africa

Supervisor:

Prof. W.J. Perold

December 2014

Declaration

By submitting this thesis electronically, I declare that the entirety of the work contained therein is my own, original work, that I am the sole author thereof (save to the extent explicitly otherwise stated), that reproduction and publication thereof by Stellenbosch University will not infringe any third party rights and that I have not previously in its entirety or in part submitted it for obtaining any qualification.

Date: December 2014

Abstract

Techniques for Enhancing the PLD Growth of Superconducting YBCO Thin Films

G.L. Hardie

Department of Electrical and Electronic Engineering
Stellenbosch University, South Africa

Thesis: MEng (Research), December 2014

High Temperature Superconductors (HTS) exhibit exceptional electrical properties that make them attractive candidates for numerous electronic devices and applications. However, constructing working devices can be challenging due to fabrication difficulties of these brittle ceramics. This thesis investigates new methods to make the fabrication of high quality $YBa_2Cu_3O_7$ (YBCO) thin films easier and compatible with more materials.

We present the development of a universal add-on method that can be used in situ to improve the quality of superconducting thin films deposited by Pulsed Laser deposition (PLD). We investigate the in situ application of electric fields and voltage biasing to improve the thin film growth. Considering various electrode configurations, we have developed a final electrode design that is stable and produces reproducible results. By introducing an insulated high voltage (HV) electrode into the chamber during deposition, the quality of the deposited thin films can be modulated depending on the polarity of the voltage applied. Applying a positive voltage improves the film quality obtained. Applying a negative voltage degrades the superconducting properties of the films.

A simple proof-of-concept HTS dual-mode microwave filter was designed, fabricated and tested. Only the filter produced using our novel PLD technique displayed the correct filtering action upon cooling to 77K. This is attributed to the thin films better superconducting properties due to our developed technique.

Opsomming

Tegnieke om die PLD groei van Supergeleidende YBCO dun films te verbeter

G.L. Hardie

Departement Elektriese en Elektroniese Ingenieurswese
Universiteit van Stellenbosch, Suid-Afrika

Tesis: MIng (Navorsing), Desember 2014

Hoë Temperatuur Supergeleiers (HTS) vertoon aantreklike elektriese eienskappe wat hulle goeie kandidate maak vir verskeie elektroniese toepassings. Om werkende toestelle te ontwikkel kan 'n uitdaging wees, as gevolg van die vervaardigings probleme wat bestaan vir hierdie bros keramiek materiaal. Hierdie tesis ondersoek nuwe metodes om die vervaardiging van 'n hoë gehalte $YBa_2Cu_3O_7$ (YBCO) dun films makliker en versoenbaar te maak met verskeie materiale.

Ons toon die ontwikkeling van 'n algemene metode wat maklik bygevoeg kan word om in situ die gehalte van supergeleidende dun films, wat deur gepulseerde laser deponering (PLD) gedeponeer is, te verbeter. Ons ondersoek die in situ toepassing van elektriese velde en spannings om die dun film groei te verbeter. Verder oorweeg ons verskeie elektrode konfigurasies en ontwikkel 'n finale elektrode ontwerp wat stabiel is en herhaalbare resultate produseer. Die kwaliteit van die gedeponeerde dun films kan gemoduleer word deur die byvoeging van 'n geïsoleerde hoogspannings (HV) elektrode tydens deponering, afhangende van die polariteit van die aangelegde spanning. 'n Positiewe spanning verhoog die film kwaliteit, terwyl 'n negatiewe spanning die supergeleidende eienskappe van die films verlaag.

'n Eenvoudige HTS dubbele-modus mikrogolffilter is ontwerp, vervaardig en getoets, om as toepassings voorbeeld te dien. Slegs die filter wat geproduseer was met behulp van ons nuwe PLD tegniek, vertoon die beste filter oordrag by 77K. Dit word toegeskryf aan die beter supergeleidende eienskappe van die dun film, as gevolg van die toepassing van ons ontwikkelde tegniek.

Acknowledgements

I would like to express my thanks and gratitude to the following people and organizations who have helped me during the course of this project and have contributed to making this work possible:

- My supervisor, Professor Willem Perold. Thank you for your constant enthusiasm and support during this project.
- Ulrich Butter for his friendship, amazing technical abilities and resourcefulness. Being able to make nearly anything I needed or could dream up. All the time, effort and enthusiasm you have invested in this project is much appreciated. Your countless ideas over many coffees and teas have been invaluable and much appreciated. Teaching me most of the techniques I have mastered during the course of this project.
- To Akram Elkaseh, my friend and fellow researcher, thanks for the help in running many of the susceptibility measurements.
- All my friends in Room E210, thanks for the magic and the good times.
- Uli Deutchslander and Johan Germishuisen help with the PLD system at physics whenever I had a problem or needed to borrow something.
- National Laser Centre (NLC) and Laser research institute (LRI) for the excimer laser for my PLD work.
- iThemba LABS for the shared use of the PLD system and the many borrowed parts.
- A huge thank you to my family who have been so supportive; a special thank you to my parents Caryle and Stewart Hardie for all the love and support over the many years of study!
- My beautiful wife Stephni for always being there for me, supporting me always and believing in me.
- The financial assistance of the National Research Foundation (NRF) towards this research is hereby acknowledged.

Finally, special thanks go to my lord and saviour Jesus Christ for giving me the grace to complete this project, to him goes all the glory and honour!

Contents

List of Figures

List of Tables

Nomenclature

CeO	Cerium Oxide
Δ	Energy Gap
ERSFQ/eSFQ	Energy-Efficient Single Flux Quantum
H_c	Critical Magnetic Field
HTS	High Temperature Superconductors
J_c	Critical Current Density
LN	Liquid Nitrogen
LTS	Low Temperature Superconductor
PLD	Pulsed Laser Deposition
SDR	Software Defined Radio
T_c	Transition Temperature
ξ	Coherence Length
YBCO	$YBa_2Cu_3O_{7-\delta}$
YBCO	Yittrium Barium Copper Oxide
YSZ	Yttria-Stabilized Zirconia

Chapter 1

Introduction

1.1 Introduction

High Temperature Superconductors (HTS) exhibit exceptional electrical properties that make them attractive candidates for numerous electronic devices and applications [1]. Their exceptionally low microwave losses make them ideal materials for microwave devices with much sharper frequency characteristics and less noise than conventional compact filters [2]. However, their exceptional performance must always be weighed against their manufacture difficulties, high cost and their extreme cryogenic cooling requirements [1]. These difficulties not only make the manufacturing process more challenging to construct working devices, they also limit the type of materials that can be used for device manufacture and the type of fabrication processes that can be used. This thesis is aimed at investigating new methods that make fabrication of YBCO thin films easier and compatible with more materials.

1.2 Motivation

HTS have attracted a lot of attention because of the reduced cost and complexity of running these systems at liquid nitrogen (LN) temperatures (77K). Cryocoolers have much higher cooling power here and larger superconducting devices can be cooled effectively. In some applications, HTS can also offer significant performance gains compared to their lower temperature counterparts. HTS offer increased power handling capabilities and higher switching speeds, and have found many applications as components and devices in radar, satellite communication, space, electronic warfare, medical diagnosis, electrical, and mechanical systems [1, 3]. However, HTS materials are complex multi-element oxides and pose many fabrication difficulties when trying to grow and fashion usable devices from them. HTS are hard and brittle Ceramics. They have to be grown as nearly perfect crystal thin films to exhibit superconducting behaviour and this requires extremely high

processing temperatures in high vacuum environments. These fabrication difficulties need to be overcome in order to engineer practical devices from them. The ability to produce practically useful and commercially exploitable devices is essential in driving the development and research of these materials [1].

Low Temperature Superconductors (LTS) are a much more established and mature technology than HTS and are important for extreme sensitivity and high efficiency applications [1]. However, LTS require much larger cryocoolers to reach the liquid helium temperatures (4.2K) where they operate. LTS dominate the area of digital superconducting electronics with a much simpler and better developed fabrication process [4]. These simple metal compounds are easily deposited and formed into the required circuits with acceptable parameter spreads for medium to large scale integrated circuit development. HTS processes have struggled to achieve acceptable process spreads [1, 5, 6]. However, simple devices have been demonstrated and HTS could therefore act as a vital link between the extreme cryogenic temperatures of LTS and the room temperature electronics used for testing and control.

Anders et al. [1] point out the important contributions that superconducting electronics and devices currently make to our society and their incredible potential for future applications. They highlight passive superconducting microwave filters, in the telecommunication and military market sectors, as one of the few commercial applications currently using superconductor technologies. Furthermore, with energy efficiency becoming of primary importance in the ICT industry and performance reaching the limits of Moore's law, faster and faster technologies are requiring immense investment costs [7]. Superconducting technology has the distinct advantage of high processing speed and intrinsically low power consumption [8]. More recently, superconductor digital technology has also moved towards higher energy efficiency designs [9]. Superconductors offer a possible solution to this bottleneck of performance with reduced power consumption. Additionally, the penalty of cooling is becoming lower compared to conventional semiconductors technologies which also require extensive cooling [9, 10]. This is particularly true in the application fields of supercomputers and data-centers. Nishijima et al. [7] refers to superconductivity as the *"ultimate energy-saving technology"*, and they provide a roadmap for how superconducting technologies could be used to address many of the major challenges (globally recognised by governments and the United Nations) confronting humanity. These challenges include: water purification, power distribution and storage, low-environmental impact transport, environmental sensing, earthquake and landmine detection, and energy efficient supercomputers. Furthermore, Anders et al. [1] consider the improvement of fabrication technologies a key aspect of being able to make superconductors a dominant technology in the market place, and that improved superconductors should be one of the main directions of these technological advances.

Digital superconductor technology and silicon semiconductor technology complement each other well. Superconductor technology is also dependent on semiconductor technology for its control and successful operation. Presently the complexity of silicon technology far exceeds that of su-

perconducting electronics. There is currently no solution for superconducting memory, an area where CMOS technology performs well [1]. However, the extreme speeds and low power dissipation offered by Energy-Efficient Single Flux Quantum (ERSFQ/eSFQ) logic and are unrivalled [7]. Harnessing the performance gains of LTS is challenging due to the large gap in operating temperature compared to room temperature electronics ($\sim$ 300K). Signal leads that carry information between the room temperature and superconductor electronics contaminate the low temperature electronics with heat and noise. This limits performance and can ultimately destroy superconductivity in the circuit. On the other hand, most standard semiconductor devices does not work well at the extreme cryogenic temperatures (lower than 30K) needed by LTS [11]. Interfacing between the two technologies therefore is critical. Here HTS can fill an important niche as mediators between ultra low temperatures of LTS and room temperature electronics. HTS wires and films have been highlighted as crucial interfacing components of next generation superconducting technologies [1, 8, 9]. HTS operate with larger signal levels and higher temperatures. HTS have also found extensive use as high quality compact microwave filters [12] and these could be used on-chip to remove excess noise. Particularly with the front-end receiver of software defined radios (SDR), where a on-chip HTS filter can be connected directly to the antenna to remove any unwanted noise signals [13].

To be able to integrate superconductor and semiconductor technology on the same chip is highly sought after [14]. As Anders et al. [1] state, "*Hybrid technologies, e.g., involving CMOS, should be chosen to take advantage of the strengths of superconducting logic, while sidestepping the weaknesses. Further work is needed on two-way hybrid interfaces with room temperature circuitry, and on integration with suitable 4 K cryocoolers.*" This integration would allow for the advantages of both technologies to be harnessed and to complement one another. In particular for digital electronics, the superconductors could be used for their brute force speed and semiconductors for their high storage capacity memory. Depositing HTS on silicon substrates would be advantageous, because both the semiconductor and LTS worlds make use of silicon substrates [15]. Sharing the same substrates makes cooling and signal routing between devices simpler and more reliable. Such a hybrid technology would also make it easier to interface superconducting cryogenic technologies to our non-optimal room-temperature world.

Silicon has long been the workhorse of the semiconductor industry, with highly advanced fabrication processes and specialized processing equipment exist for it as a substrate material. Silicon wafers have large scale demand and are much cheaper than many of the conventional substrates used for HTS. They are also readily available in a large variety of sizes. Single crystal Si (100) substrates have a good lattice match with YBCO (1.2% mismatch) and offer good mechanical support [11]. They have an excellent thermal conductivity (1000W/mK @ 77K) which is important as superconductivity is inherently a temperature dependent phenomenon.

YBCO is superconducting below 92K, allowing one to use liquid nitrogen to cool devices made from this material. Growing YBCO thin films on silicon substrates proves very challenging due

to the high processing temperatures (600-800°C) required to grow epitaxial thin films. These two materials chemically react at these high temperatures, resulting in thin films that are not superconducting [16]. The ambient oxygen atmosphere required during deposition complicates matters further by oxidizing the silicon substrate at the interface, producing amorphous silicon oxide. Silicon and YBCO also have a large mismatch in their thermal expansion coefficients. YBCO expands and contracts approximately four times more than silicon. The extreme thermal cycling that superconducting samples undergo inevitably leads to micro-cracking [17]. An intermediate buffer layer is required at the semiconductor/superconductor interface to better mate the two materials. Current solutions consist of buffer layers of yttria-stabilized zirconia (YSZ) and cerium oxide (CeO). Usually complex combinations of various buffer layers are required to obtain reasonable films.

Pulsed laser deposition (PLD) is a very versatile, convenient and conceptually simple technique that can be used for rapid prototyping of new materials and material combinations for thin films [18]. In 1987, it was first made famous for being able to grow $YBa_2Cu_3O_{7-\delta}$ (YBCO) superconducting thin films [19]. The stoichiometric transfer of target material to the substrate and growing film makes the preparation of complex multi-component materials, such as YBCO, possible. Not much target material is required and a wide variety of gasses can be introduced into the chamber to aid deposition. Additionally, the deposition inducing mechanism (the laser) can be completely removed from the deposition chamber and operated independently.

The flexibility of this method leads to different research groups producing many different deposition systems, each with there own unique optimal parameter set [20, 21]. The basic fundamentals remain the same: a laser, a target, a heated substrate, a vacuum chamber, and background gas. However, the specific details of the implementation vary considerably. It is therefore necessary to determine the PLD conditions specific to each system. Despite the conceptual simplicity in performing this deposition method and how easily it can be controlled and modified, the underlying physical processes and interactions between the various control parameters are highly complex. This makes optimisation time-consuming and therefore expensive.

It would be helpful if an additional non-essential parameter could be added and adjusted to compensate for essential deposition parameters that might be suboptimal, and thereby produce better films. Higher quality films could therefore be obtained for a much wider parameter range. This could help to make a deposition process more robust and less sensitive to parameter changes. A possible application would be where the researcher wants to adjust one of the deposition parameters to accommodate a certain substrate material into a deposition process. If this adjustment reduces the quality of the films produced, an additional parameter that can compensate for the sub-optimal parameter is required. A specific example of this to decrease the substrate temperature during YBCO thin film deposition, for material compatibility and the preservation of multilayer superconducting properties [22].

Being able to reduce the deposition temperatures of YBCO would make it compatible with a much

wider range of substrate and inter-layer materials. Silicon becomes a more viable substrate material at temperatures lower than 600°C and this would allow for better integration of HTS with semiconductor technology. Multilayer HTS technology would also benefit. The electrical characteristics of the superconducting layers are very sensitive processing temperatures. For multilayer fabrication, the health of the bottom layer electrode is highly dependent on the processing used to fabricate and pattern the subsequent upper layers [22]. High deposition temperatures can cause the lower superconducting layers to decompose, loose oxygen content and superconductivity [23]. Deposition conditions for upper superconducting layers should be kept as low as possible to try to preserve the superconducting characteristics of lower layers. Lower processing temperatures also help to minimize inter-facial diffusion between the substrate and the various inter-layer materials. However, YBCO has to be grown at temperatures in the range of 650-850°C in order to obtain films with good crystallinity and the right superconducting phase. Depositing thin films at lower temperatures is therefore a sub-optimal deposition process. We therefore require an additional parameter to compensate for the suboptimal process to be able to produce acceptable films.

Candidates for this non-essential parameter can be found from some novel solutions suggested in literature for improving PLD film quality [17, 24–26]. In situ application of electric fields, voltage biasing and plasmas into the deposition process, have been shown to improve the crystallinity of various PLD grown thin films. Particularly for the low temperature growth of YBCO thin films.

1.3 Project Objectives

This thesis is aimed at investigating new methods to make the fabrication of YBCO thin films by PLD easier and compatible with more materials. We seek a method that introduces an additional parameter, such as voltage bias, that can be controlled to compensate for sub-optimal deposition conditions, such as lower substrate temperatures or poorly optimised deposition parameter sets. The method should help to produce high-quality HTS thin-films suitable for manufacturing practical HTS devices.

The PLD system at Stellenbosch University has never been able to match the quality of the thin films produced using the inverted cylindrical magnetron (ICM) sputtering unit [27–29]. Therefore, we aim to improve the quality of the superconducting thin films produced using this local PLD equipment. However, the broader aim was to produce a universal method that can be used for any PLD system. As such, this method needs to be simple to implement as an *"add-on"* to any existing system. Therefore, we need a method that requires minimal modification of the deposition environment and one that works using existing deposition parameters. YBCO degrades rapidly with excessive handling and is sensitive to a variety of chemicals including water. Therefore, an in situ process is desired to avoid any additional processing steps. The in situ application of electric fields and voltage biasing is the starting point of our investigations, as it potentially satisfies many of the above mentioned considerations.

The secondary aim is to construct a proof-of-concept microwave filter device using the developed methods. Passive superconductive filters are relatively simple devices that have shown good commercial applications [1]. These filters can be constructed using a single superconducting layer and do not require any active devices. The quality of the superconducting layer directly affects the final device's performance. Therefore, this could serve as a practical application that provides a good indication of the value of the methods developed in this thesis.

1.4 Thesis Overview

This chapter gave a brief introduction and motivation for the research conducted in this thesis. We briefly covered the performance benefits that HTS hold and the fabrication difficulties they pose. The potential benefits of enhancing HTS YBCO fabrication processes to produce better films for more applications and to be compatible with more materials such as silicon was highlighted. The addition of electric fields in situ during PLD and their effect on film quality is mentioned and becomes the starting point of our research investigations. A HTS microwave filter is chosen as a suitable proof-of-concept device to demonstrate performance of the any techniques developed.

Chapter 2 introduces the fundamental properties of superconductors and provides background on microwave filter HTS devices and technologies, and some of the theory pertinent to their development.

Chapter 3 introduces the fundamental material properties of YBCO and the use of PLD to produce superconducting thin films. We also present a literature study of the use of electric fields, voltage biasing and plasmas to enhance the quality of PLD produced thin films. Previous research in this field and its pitfalls are highlighted. Although these techniques show great potential a research gap exists in the exact understanding of the processes involved. The lack of widespread adoption as a standard technique is also discussed.

In Chapter 4 we discuss the experimental methods used in this thesis, including thin film deposition, sample characterization, device patterning and device testing.

Chapter 5 details the initial experiments that were performed to recreate and test the results from literature. These were first performed to provide a basis for our research and provide a point of reference to work from and draw conclusions. We investigate the biasing of the target during PLD deposition and its effect on the resulting YBCO thin film quality. Problems with this technique are identified and addressed with a novel solution presented in the next chapter.

In Chapter 6 the experimental setup is considerably modified to produce a completely new deposition method. The new insulated electrode design employed allows for a much wider range of applied voltages and more stable control over deposition conditions. Various refinements in the electrode design are presented resulting in a final configuration that is stable and produces excellent results.

Chapter 7 summarizes the design, fabrication and testing of the superconducting band-pass filter. The fabrication of this device highlights the value of the preceding HV deposition technique that was developed. Only the devices fashioned from the films deposited using this method showed the desired response. The chapter shows some investigations on the practical challenges faced during device fabrication and offers possible solutions for future researchers.

Chapter 8 provides a conclusive summary of this research and the contributions made and highlights future work emanating from this research.

Chapter 2

Fundamental Superconducting Materials and Concepts

Superconductivity is a unique state of matter that exhibits two distinctive properties: perfect electrical conductivity (zero dc resistance) and perfect diamagnitism (the expulsion of all magnetic fields from its interior). These two characteristics are illustrated in Fig. 2.1. Superconductivity is intrinsically temperature dependent and only occurs below a certain critical transition temperature (T_c). These very low transition temperatures require cryogenic cooling and this makes superconductor's practical application challenging.

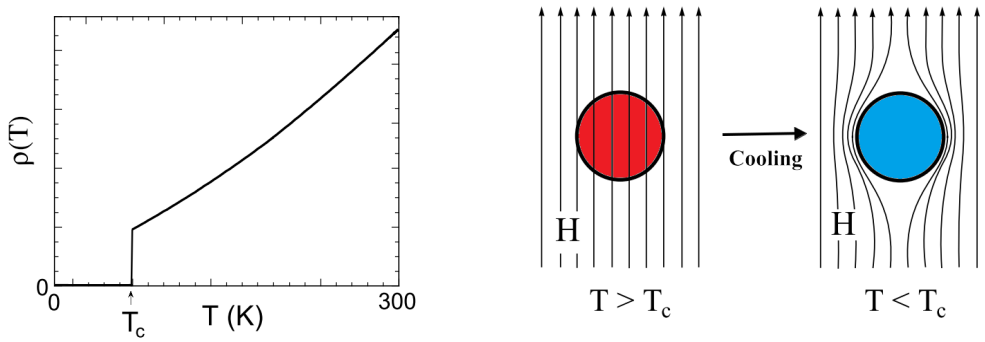

(a) (b)

Figure 2.1: The two characterising properties of the superconducting state. (a) Perfect electrical conductivity: electrical resistivity plotted against temperature showing a typical transition to the superconducting state (zero dc resistance) at T_c. (b) Perfect diamagnetism: the expulsion of all externally applied magnetic fields from the interior of a superconductor (The Meissner effect).

The dream of room temperature superconducting devices has always driven the search for higher temperature superconductors [30,31]. The discovery of superconductivity in $YBa_2Cu_3O_{7-\delta}$ (YBCO) [32] above the boiling point of liquid-nitrogen (77K) fuelled extensive research into the HTS cuprates. Since then many other HTS materials have been found that show superconductivity

at higher temperatures [33] (Fig. 2.2). However, YBCO still remains one of the most popular choices and its epitaxial growth and characterization has received more attention than any other HTS compound [34]. YBCO is the choice of superconducting material used in this thesis. Despite the successful development of numerous high-temperature superconducting materials, the physical mechanisms responsible for this type of superconductivity are still not completely understood [35]. They cannot be described by conventional low temperature BCS theory [36] and currently only speculations can be made as to the origin of their superconductivity.

This chapter aims to introduce the basic superconducting properties and theory. We will briefly present an electronic model for superconductivity and discuss the application of HTS for microwave filters. It would be impossible to give a complete review of the hundred plus years of intensive research into the rich topic of superconductors in the fields of physics, engineering and material science. There are a number of excellent books dedicated to these topics. Readers interested in a thorough coverage of the history, properties and theories of superconductors are referred to these textbooks [3, 30, 36].

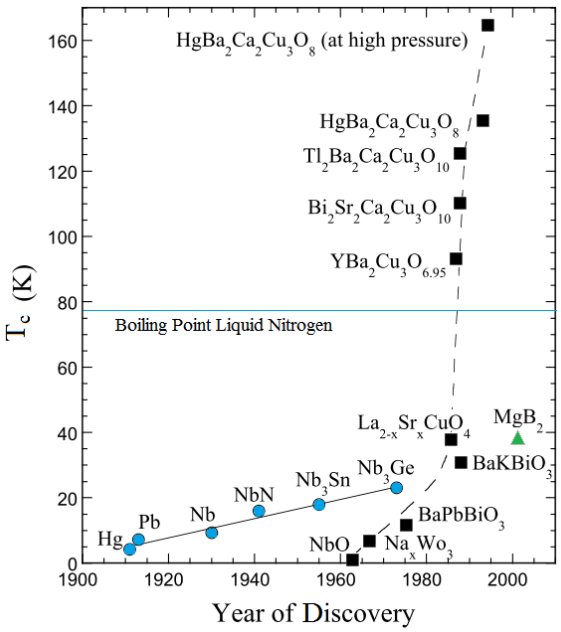

Figure 2.2: The evolution of the superconducting materials and their critical temperatures discovered over the years since 1911. Adapted from [30].

2.1 Transition to the Superconducting State

When a material becomes superconducting, it is not as instantaneous as a material's T_c might suggest. It is generally a gradual transition, fractions of a Kelvin to a few Kelvin wide, as shown in Fig. 2.3. The better crystalline quality, purity and uniformity of the thin film; the sharper and more

ideal this transition becomes. The transition width ($\triangle T_c$) provides an indication of the thin film uniformity and can be used together with the T_c to provide a measure of the crystalline quality of the film. High transition temperatures and small transition widths are therefore desirable and indicators of good film quality.

In this work, T_c refers to the temperature where the sample becomes completely superconducting ($T_c(0)$ shown in Fig. 2.3). There are two methods for measuring the transition temperature of a superconductor. Either the resistance of the sample or the magnetic susceptibility of the sample can be monitored while cooling the sample down past the transition temperature. As the resistance of the sample drops to zero the transition to the superconducting phase can be measured and visualised as is shown in Fig. 2.3. Alternatively, the magnetic susceptibility can be monitored [37].

Certain texts prefer to reference the onset temperature (where the sample starts entering the superconducting state $T_c(onset)$, as shown in Fig. 2.3) as T_c, because it is usually easier to define [38]. It is also higher and therefore more impressive. Others refer to T_c as the temperature half-way between $T_c(0)$ and $T_c(onset)$. However, only the final temperature where the sample is completely superconducting is of practical use. It indicates the absolute upper temperature limit where the device would stop working. Devices generally have to be operated well bellow this critical temperature. Anders et al. [1] suggest as a general guideline, that the maximum practical operating temperature of digital superconducting electronics is about 50% of T_c (eg. 40-50K for YBCO). Superconducting devices that are more passive (eg. filters) can be operated at about 80-90% of T_c (usually 77K for YBCO). Sensitive detectors need to be operated at as low a temperature as possible. The superconductor's properties become better the lower their operating temperature is. Operating a device too close to its transition temperature, one runs the risk that thermal fluctuations might drive the material into the normal state. $\triangle T_c$ is most commonly measured as the width of the transition between 90% and 10% of the measured value (resistivity or susceptibility) at $T_c(onset)$ [39]. We use this convention in this thesis.

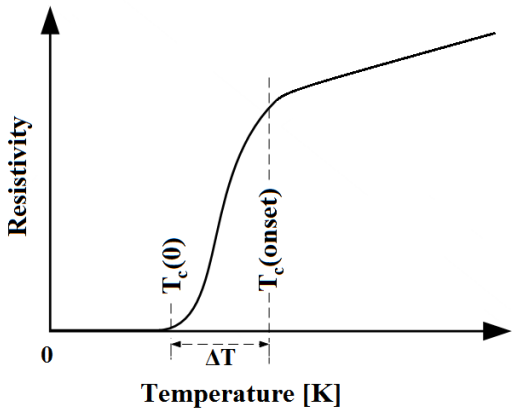

Figure 2.3: The non-ideal gradual transition to the superconducting state.

The cryogenic operating temperatures make achieving and maintaining superconductivity a challen-

ging task. Things are complicated further by two additional parameters which define the boundary between the superconducting and normal state: critical current density (J_c) and critical magnetic field (H_c) (Fig. 2.4).

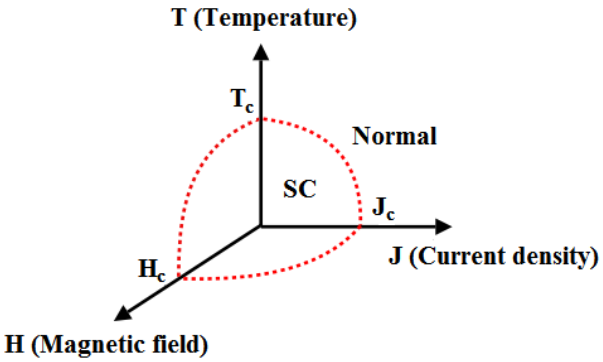

Figure 2.4: The physical parameter boundaries that exist between the superconducting (SC the region inside the dotted lines) and normal state (the outer region).

2.1.1 The Meissner effect

A superconductor is a perfect diamagnetic material maintaining zero magnetic flux at its interior. This is known as the Meissner effect. In contrast to a perfect conductor, a superconductor expels all flux regardless of its thermal and magnetic history (and the magnetic flux must be smaller than the critical magnetic flux H_c). Applying a magnetic field to a superconducting material before cooling it down past its critical temperature has the same net effect as applying the magnetic field after the material has become superconducting. The flux is expelled by induced surface currents flowing in such a way as to set up opposing fields which make the resultant field inside the superconductor zero. If we consider a similar case with a material that becomes only a perfect conductor, we find that the perfect conductor would merely maintain the magnetic field present inside the sample when the material becomes perfectly conducting (as prescribed by Lenz's law: $\frac{\partial \mathrm{B}}{\partial t} = 0$). Superconductivity is therefore more than just perfect conductivity and it is intrinsically a thermodynamic state. Strictly speaking, the flux does penetrate a small distance into the superconductor. The super-current flows in this thin layer and its thickness is defined as the London penetration depth λ_L.

Superconductors can be classified further as Type I or Type II depending on their magnetic behaviour. Fig. 2.5 illustrates the magnetic behaviour of these two types of superconductor. For normal Type I superconductors, H_c is the highest magnetic field that the superconductor can expel from its interior upon cooling below T_c. Above this threshold superconductivity is destroyed. High-T_c superconductors do not exhibit this sharp transition between the superconducting state and normal state. Instead, they have two values of critical magnetic field. This is defined as Type II superconductivity. Below the lower threshold, H_{c1}, the field is completely expelled and the Meissner state exists. However, above H_{c1}, the magnetic field penetrates the material slowly up until an upper

threshold, H_{c2}, is exceeded. Beyond this point the material reverts to the normal state. The state between H_{c1} and H_{c2} is called the vortex or mixed state. Here vortices of magnetic flux penetrate the material. The flux penetrates in tiny, precisely quantized units of flux

$$\Phi_0 = \frac{h}{2e} = 2.07 \times 10^{-7}\,\mathrm{T/cm^2} \tag{2.1}$$

where h is Planck's constant, and e is the magnitude of electronic charge. We call these objects flux lines or vortex lines. The motion of these vortices in the presence of electrical currents, dissipate energy, and this reduces the critical current density of the superconductor. Microscopic defects are required to pin these flux lines against energy dispersive motion. H_{c2} is in general much larger that H_{c1} and it is precisely this ability to handle large magnetic fields that makes Type II superconductors useful on a large scale. For YBCO these critical fields are also highly anisotropic, being much larger when parallel to the c-axis.

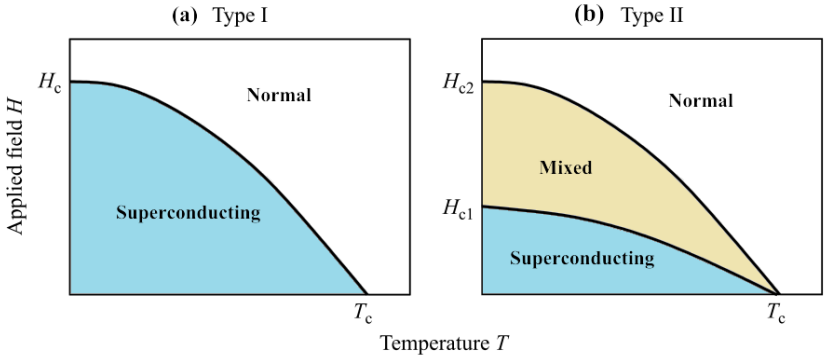

Figure 2.5: Critical magnetic field as a function of temperature for (a) Type I superconductors and (b) Type II superconductors.

A superconductor's critical current density is another important parameter which indicates how much current it can carry before superconductivity is destroyed. A large J_c is required, especially for superconducting thin films. A larger critical current density allows for smaller track line widths and device sizes.

The critical current density and critical magnetic field parameters of a superconductor are inherently dependant on each other as currents induce magnetic fields and vice versa. They should therefore be considered together for design applications.

2.1.2 The Importance of T_C

The further below T_c that a superconductor is cooled, the higher its critical magnetic field and current density become (see Fig. 2.4). Therefore, the superconductor is more robust to operating

conditions, such as carrying high currents and being subjected to large magnetic fields. It is therefore essential for device applications that the thin film produced have a T_c as high as possible to maximize these values for the desired operating temperature (e.g. for YBCO this is 92K, the bulk T_c value [40]). This is especially true for YBCO thin films when liquid nitrogen cooling is desired. In this case the operating temperature is fixed at 77K the boiling point of liquid nitrogen. Any film that is to form part of a practically useful device has to become completely superconducting within the narrow temperature range of 77K to 92K. In addition any further processing that is applied to the thin film, after deposition, to construct the superconducting device, will generally degrade the film quality and T_c. The useful T_c range is therefore even narrower depending on the quality of the fabrication process. Thin film deposition and device fabrication processes must be optimised to produce the best quality epitaxial films possible with maximum T_c. Single crystal YBCO thin films with excellent properties exhibit a critical temperature close to that of the bulk compound [40]. A high T_c is an indication of good crystal structure, high J_c and a smooth surface morphology.

2.2 Superconductor Theory

Only the most important theories and models most relevant to this thesis will be mentioned in this section. Detailed descriptions and in-depth coverage can be found in any superconductivity textbooks (an excellent example being [40]). This section is only an introduction and where further elaboration is required it will be discussed where needed in that specific section.

2.2.1 The Two-Fluid Model

Gorter and Casmir proposed the model that the current flowing in a superconducting material can be seen as a fluid consisting of two components [40]. A normal (ohmic) current due to the flow of normal electrons. These electrons experience resistance as they would in a conventional conductor and a super-current where super-electrons carry current without resistance.

The density of the normal electrons, n_0, compared to super-electrons, n_s, can be expressed as

$$n_s = n_0 \left\{ 1 - \left(\frac{T}{T_c} \right)^4 \right\} \tag{2.2}$$

for temperatures $T \leq T_c$. Above T_c, only normal electrons exist and as the superconductor is cooled below T_c more and more of the normal electrons are converted into super-electrons. At $T = 0K$, all the current is carried by the super-electrons. The BSC theory would later identify these super-electrons as bound pairs of electrons (Cooper pairs) which break apart as the temperature rises [40].

2.2.2 Complex conductivity

By describing the the current in terms of a superconducting and normal part it is possible to model the superconductor in terms of a complex conductivity $\sigma = \sigma_1 - j\sigma_2$, which is known as the two-fluid model [40]. A simple representation of this model is the equivalent electrical circuit shown in Fig. 2.6.

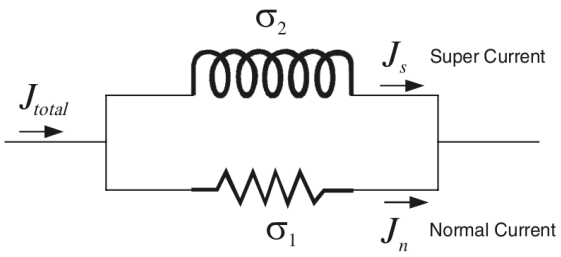

Figure 2.6: Simple circuit representation of complex conductivity of a superconductor.

In the circuit, J_{total} is the total current density that flows in the superconducting material. J_n and J_s denote the current densities carried by the normal and paired electrons respectively. The supercurrent flows through the reactive inductance and the normal current through the resistance, dissipating of energy. As the frequency decreases the reactance part becomes smaller and more of the total current flows through the inductor branch. At DC current (i.e. zero frequency) the resistance is completely shorted out and all the current is carried in the superconducting branch and therefore zero resistance is experienced.

The complex conductivity can be written as

$$\sigma = \sigma_1 - j\sigma_2 = \sigma_n \left(\frac{T}{T_c}\right)^4 - j\frac{1}{\omega\mu\lambda_0^2}\left[1 - \left(\frac{T}{T_c}\right)^4\right], \tag{2.3}$$

where σ_n is the normal state conductivity at T_c and λ_0 is a constant parameter known as the penetration depth (at 0K). Equation (2.3) is not valid close to T_c.

2.2.3 Penetration depth

The penetration depth is given by

$$\lambda = \frac{1}{\sqrt{\omega\mu\sigma_2}}, \tag{2.4}$$

when the approximation $\sigma_2 \gg \sigma_1$ can be made. This approximation is generally valid for good quality superconductors not to close to T_c, where more normal electrons are present. Substituting σ_2 from (2.3) into (2.3) gives

$$\lambda = \frac{\lambda_0}{\sqrt{1 - \left(\frac{T}{T_c}\right)^4}}. \tag{2.5}$$

Therefore, we can see from (2.5) that λ_0 is the penetration depth at zero Kelvin. λ_0 is typically 200nm for good quality high-temperature superconductors.

The penetration depth is a characteristic depth at the surface of the superconductor. It is analogous to the skin depth of normal conductors and represents the depth to which electromagnetic fields penetrate the superconductor. It also defines the depth to which currents can be induced at the superconductor's surface. However, unlike the skin depth of normal conductors, λ is frequency independent.

Another dissimilarity between normal conductors and superconductors is that DC current or fields cannot penetrate fully into them. DC current decays away from the surface of superconductors proportional to e^{-z/λ_L}, where z is the distance into the superconductor and λ_L is known as the London penetration depth. λ_L is a depth where the DC current decays by e^{-1} the magnitude of the current at the surface of the superconductor. In the two-fluid model this depth is the same as the AC penetration λ depth given by (2.5).

2.2.4 Surface Impedance

Surface impedance is an important parameter for superconducting materials. By solving Maxwell's equations for a uniform plane wave in an infinitely thick metal sheet, with conductivity σ, yields the surface impedance, given by

$$Z_s = \frac{E_t}{H_t} = \sqrt{\frac{j\omega\mu}{\sigma}}, \tag{2.6}$$

where E_t and H_t are the electric and magnetic fields tangential to the metals surface. This general definition of the surface impedance is also applicable to superconductors. Setting $\sigma = \sigma_1 - j\sigma_2$ gives

$$Z_s = \sqrt{\frac{j\omega\mu}{\sigma_1 - j\sigma_2}}, \tag{2.7}$$

which can be separated into its real and imaginary parts,

$$Z_s = R_s + jX_s, \tag{2.8}$$

resulting in the surface resistance

$$R_s = \sqrt{\frac{\omega\mu}{2}}\left(\frac{\sqrt{k+\sigma_1}-\sqrt{k-\sigma_1}}{k}\right), \tag{2.9}$$

and the surface reactance

$$X_s = \sqrt{\frac{\omega\mu}{2}}\left(\frac{\sqrt{k-\sigma_1}+\sqrt{k+\sigma_1}}{k}\right), \tag{2.10}$$

where

$$k = \sqrt{\sigma_1^2+\sigma_2^2} = \sigma_2\sqrt{\left(\frac{\sigma_1}{\sigma_2}\right)^2+1}. \tag{2.11}$$

Once again, if we apply the approximation that $\sigma_2 \gg \sigma_1$, we obtain $k \approx \sigma_2$ and $\sqrt{1\pm\frac{\sigma_1}{\sigma_2}} \approx 1\pm\frac{\sigma_1}{2\sigma_2}$. Substituting back into (2.9) and (2.10), we obtain

$$R_s = \sqrt{\frac{\omega\mu\sigma_2}{2}}\left(\frac{\left(1+\frac{\sigma_1}{2\sigma_2}\right)-\left(1-\frac{\sigma_1}{2\sigma_2}\right)}{\sigma_2}\right) = \sqrt{\frac{\omega\mu\sigma_2}{2}}\left(\frac{\sigma_1}{\sigma_2^2}\right) \tag{2.12}$$

and

$$X_s = \sqrt{\frac{\omega\mu\sigma_2}{2}}\left(\frac{\left(1-\frac{\sigma_1}{2\sigma_2}\right)+\left(1+\frac{\sigma_1}{2\sigma_2}\right)}{\sigma_2}\right) = \sqrt{\frac{\omega\mu\sigma_2}{2}}\left(\frac{2}{\sigma_2}\right). \tag{2.13}$$

Furthermore, rewriting (2.4) for σ_2, we get

$$\sigma_2 = \frac{1}{\omega\mu\lambda^2}. \tag{2.14}$$

Substituting (2.14) into (2.12) and (2.13) we finally arrive at

$$R_s = \frac{\omega^2 \mu^2 \lambda^3 \sigma_1}{2} \tag{2.15}$$

and

$$X_s = \omega \mu \lambda. \tag{2.16}$$

Therefore, for the two-fluid model, the surface resistance increases quadratically with frequency. R_s also depends on temperature, due to the temperature dependence of σ_1 and λ, and increases sharply near T_c.

In comparison to the surface resistance of normal conductors, the surface resistance of HTS increases much more rapidly with increasing frequency. The surface resistance and reactance of a normal conductor are given by

$$R_s = X_s = \sqrt{\frac{\omega \mu}{2\sigma_n}}. \tag{2.17}$$

They are equal and only proportional to the square root of frequency. Figure 2.7 shows a typical comparison of the copper's surface resistance with the surface resistance of YBCO at 77K, as a function of frequency. Despite the quadratic dependency on frequencies the surface resistance of superconductors is still far superior to that of normal conductors. We can see that in the region of 2GHz the surface resistance of YBCO is approximately a thousand times smaller than that of copper at 300K. The surface resistance of copper only becomes smaller that that of YBCO at frequencies approaching 100GHz. This is known as the crossover frequency. Considering that the quality factor Q of a conductor is inversely proportional to surface resistance [41], the same device made in superconducting technology can have a significantly higher quality conductor Q.

The surface reactance of the superconductor can be expressed as $X_s = \omega L$. Where inductance term L is called the kinetic inductance and is given by $L = \mu\lambda$. The kinetic inductance is also temperature dependent (due to λ) and this can be a cause of frequency shift in superconducting filters due to temperature fluctuations, if the stability of the cooling system is insufficient.

The surface impedance described above is actually for an infinitely thick film. For finite thickness thin films the surface impedance tends to increase for thinner films [41]. Figure 2.8 shows a plot of how the surface resistance is dependent on the thickness of the film. It shows that in order to minimise the surface resistance the film thickness should be greater than at least three times

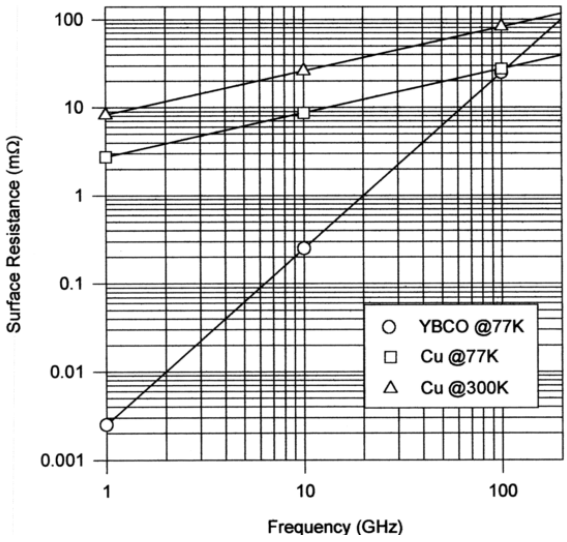

Figure 2.7: Comparison of the surface resistance of YBCO at 77 K with copper as a function of frequency. [41]

the penetration depth. This is similar to the design consideration for the skin depth of a normal conductor film.

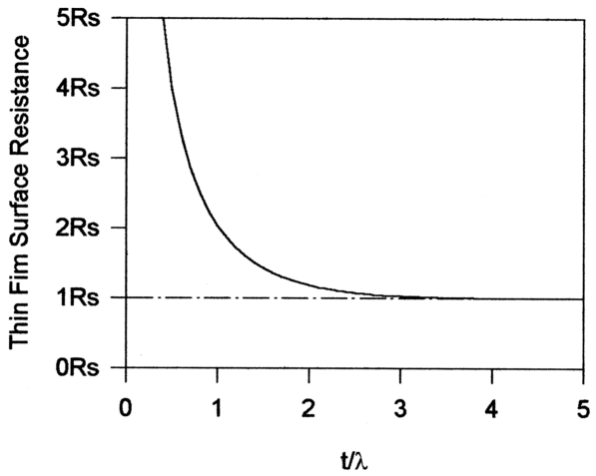

Figure 2.8: Surface resistance of superconducting thin films as a function of thickness. [41]

2.3 HTS Microwave Filters

One of the thin film applications that have been successfully employed commercially have been high-frequency electronics for radio frequency (RF) microwave communications [34]. The RF/microwave spectrum generally of interest, divided into its various frequency bands, is shown in Figure 2.9. Filters play important roles in many RF/microwave applications [41], where they are used for the

separation of different frequencies. Filters are used to select or limit microwave signals to their assigned spectral bands. This is needed due to the limited electromagnetic spectrum that has to be shared between a growing number of many applications and signals. The explosion of wireless communications and signals continues to place increasingly more stringent requirements on RF devices. HTS filters offer capable solutions to these stringent requirements.

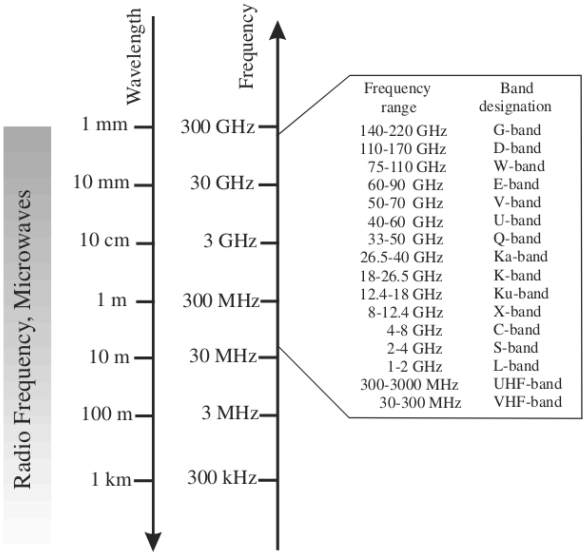

Figure 2.9: The radio frequency and microwave spectrum form 300kHz to 300GHz. [41]

According to Hong [41] *"High-temperature superconductivity is at the forefront of today's filter technology and is changing the way we design communication systems, electronic systems, medical instrumentation, and military microwave systems."*

2.3.1 HTS Microstrip Filters

HTS thin films are very suitable for microwave filter devices due to their very low surface resistance [42]. Their use offers a significant performance advantage over conventional RF/microwave microstrip filters. Most HTS filters are constructed from simple microstrip structures made from superconducting thin films, instead of conventional conductor films [41]. The low surface resistance leads to superior devices with minimal passband insertion loss and extremely high selectivity. They are particularly well suited to applications that require as ultra narrow-band filters.

Due to fabrication difficulties of HTS and the expensive substrates they require, it is often desirable to make the filter devices as compact as possible to make cost-effective use of the materials given the fabrication limitations. Microstrip filters are already quite compact in size compared to waveguide filters. However, more compact designs can be achieved using novel filter configurations such as miniaturized dual-mode filters, multilayer filters and slow-wave resonator filters [41]. Reducing the size of a filter generally leads to increased dissipation losses and reduced performance.

Smaller a microstrip resonators have smaller the radiation losses, but have higher conductor loss. Therefore, the much lower conductor losses offered by HTS materials makes them ideal for these types of devices.

High-T_c superconductors can be prepared in a wide variety of forms, each best suited for its own specific applications. In this research we focus on the fabrication and processing of superconducting thin films for electronic applications. Thin films (classified as less than 1μm thick) are widely employed in microwave devices, optical detectors, and microelectronic circuits. Low-noise devices and passive components generally also use thin films. Whereas, high-power components mostly employ thick films due to their ability to handle higher current densities. However, HTS films are primarily suited to low-power applications due to the non-linearity of the superconducting materials surface resistance [41].

2.4 Conclusion

In this chapter we covered the fundamental properties of superconductors and provided some background on microwave filter HTS devices and technologies. HTS have much lower surface resistances than conventional conductors and therefore exhibit superior performance as passive microwave filter devices. The transition temperature of a superconductor is a very important parameter, that critically effects many of the superconducting properties and device performance. Good quality thin films with maximum Tc are needed in order to be able create superconducting devices with good practical application. The material properties of YBCO and fabrication processes required to produce good quality thin films with high T_c will be presented in the next chapter.

Chapter 3

YBCO and its Deposition

Despite the great promise and excitement surrounding the discovery of high temperature superconductors, it has proven challenging to find practical and commercially profitable applications for superconductors [42]. Numerous problems still have to be overcome at each step of the fabrication process up to the final components. These steps include film preparation and substrate related problems, film patterning, packaging and cryogenic aspects [1]. This chapter aims to introduce the basic material properties of YBCO and the difficulties associated its deposition as high quality epitaxial thin films. Furthermore, possible methods are highlighted from literature that can be used to improve the deposition of YBCO under suboptimal conditions.

3.1 YBCO

High quality epitaxial thin films grown with the correct crystal structure and that exhibit good superconducting properties are required to produce practical devices. Compared to the other HTS materials, epitaxial YBCO films are easier to synthesize and achieve a thin film T_c that is near the bulk value ($\sim$92K). However, HTS thin film deposition and the processing of these brittle ceramic crystal layers is never easy and it remains a significant challenge to produce films suitable for practical technologies. A good understanding of the fundamental material properties of YBCO is required to fabricate devices that are capable of achieving the state-of-the art performance promised by HTS materials.

3.1.1 Crystal Structure

YBCO has an oxygen-deficient perovskite derivative crystal structure [36]. Like many other HTS materials YBCO has a complex multi-element composition and strict control of the stoichiometry of the composition is very important for preparing superconducting thin-films with desirable characteristics. YBCO can be seen as the stacking of three perovskite units: $BaCuO_3$, $YCuO_2$ and

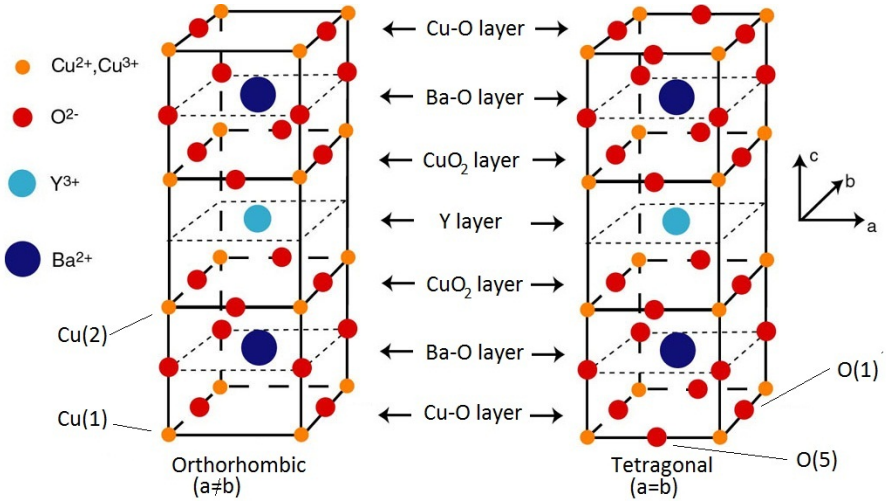

Figure 3.1: Orthorhombic and tetragonal structures of $YBa_2Cu_3O_{7-\delta}$ material, showing the various layers and molecular groupings making up its perovskite derivative crystal structure

$BaCuO_2$. Under closer inspection, the structure can be viewed as the stacking of different layers: CuO / BaO / CuO_2 / Y / CuO_2 / BaO / CuO. Figure 3.1 shows the two CuO_2 layers present in the crystal structure that play an important role in YBCO's superconducting behaviour. For copper oxide perovskites, their transition temperature increases with the number of CuO_2 layers, however the exact mechanisms for this are not yet know [35].

YBCO thin films have to be grown in the correct phase in order to be superconducting. The films grown are very sensitive to oxygen content and impurities present during deposition. Even a small change in the oxygen content or the cation doping level can transform the material from superconductor to semiconductor. The chemical formula for YBCO is usually given as $YBa_2Cu_3O_{7-\delta}$. The δ-factor accounts for the fact that not all the oxygen sites are always filled. $YBa_2Cu_3O_{7-\delta}$ has seven oxygen atoms occupying a possible nine open oxygen positions. Oxygen atoms at the top and bottom planes of the unit cell are missing in the [100] direction, thus giving Cu-O chains in the [010] direction. In YBCO, these Cu-O chains are known to play an important role for superconductivity and the uptake and loss of oxygen is reversible. T_c maximizes near 92K when the oxygen content is near 7 ($\delta \simeq 0$) and the structure is orthorhombic. The lattice constants of the orthorhombic crystal structure are a = 3.83 Å , b = 3.88 Å, and c = 11.68 Å. As oxygen is removed, the T_c decreases until superconductivity disappears at $\delta \simeq 0.6$, where the structure becomes tetragonal (see Fig. 3.1).

Usually, at the time of deposition the semiconducting tetragonal $YBa_2Cu_3O_6$ compound is formed. Slow cooling in an oxygen atmosphere can turn the semiconducting tetragonal YBCO into the superconducting orthorhombic YBCO phase. The correct temperature and oxygen pressure is vital to ensure that the correct orthorhombic superconducting phase is formed. Figure 3.2 shows the Phase stability diagram for YBCO and the dependence on substrate temperature and oxygen pressure (PO_2) [43]. A fully oxidised orthorhombic sample can also be transformed to the tetragonal

phase by heating in a vacuum at high temperatures. The heat and vacuum allow the oxygen to escape and the result is non-superconducting oxygen deficient YBCO. It is therefore extremely important that any fabrication process minimises any high temperature processing steps as this can lead to unwanted degradation of the YBCO thin film layers.

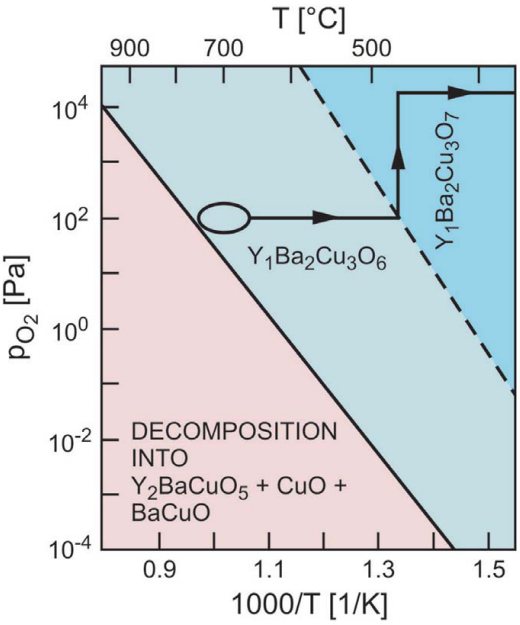

Figure 3.2: Phase stability diagram for YBCO thin film deposition [43].

3.1.2 Anisotropy

A number of additional properties characterize superconductors, including critical magnetic field, penetration depth, coherence length (ξ), critical current density and energy gap (Δ). For HTS these distinctive properties can prove either useful or troublesome for device manufacture. Because of its layered structure, YBCO exhibits strong anisotropy. Therefore, the values of the superconducting properties are different in different directions. For example, the electrical conductivity is much higher parallel to the CuO_2 planes (i.e. the *a-b* plane) and significantly less in the direction perpendicular to this (i.e along the *c*-axis). Similarly, the coherence length is much shorter in the *c*-axis direction (typically, 2-5 Å along the *c* axis and 10-30 Å in the *a-b* plane). Thus, perpendicular to the *a-b* plane the superconducting wave function is essentially confined to a few adjacent unit cells. The low value of coherence length makes YBCO very sensitive to the presence of local defects such as oxygen vacancies, dislocations, and variations in stoichiometry. Generally the properties in the *a-b* plane are far superior to those along the *c*-axis. This presents interesting challenges for device fabrication and processing, especially when making multilayer devices [42]. HTS YBCO devices generally have to be designed to be mostly planar, with minimal inter-planar connects and

crossovers.

Due to the short and highly anisotropic coherence lengths, the J_c is drastically reduced by the presence of weak links in the crystal structure. Weak links are localised regions in the superconductor where various superconducting properties are degraded. Grain boundaries in polycrystalline high-T_c superconductors also act as weak links and severely limit the current density that can flow in the material [44]. In epitaxial thin films, where grain boundaries are reduced, the J_c value is found to be as large as 10^6 A/cm^2 at 77K. It is vital that the YBCO crystal be grown as perfectly as possible to maximise the J_c. Polycrystalline films with large angle grain boundaries have a much lower current carrying ability than single-crystal epitaxial films. Major issues arise when impurities and imperfections from the growth process cause weak links and defects in delicate structures where they are not wanted. Unwanted imperfections limit device performance and can even destroy a circuit's functionality .

A superconducting microwave device designer is primarily interested in the surface resistance, insertion loss, quality factor and critical current density characteristics of the thin films. These characteristics all depend on the transition temperature and more fundamental underlying characteristics such as surface roughness, stoichiometry, penetration depth and coherence length [45].

The overall attenuation or insertion loss in a microwave circuit is the sum of the losses in the conducting material and in the substrate material. The insertion loss of a metallic film is strictly due to its surface resistance. The surface resistance is a strong function of operating temperature and frequency. In HTS thin films, material impurities and surface resistance are the main factors responsible for losses. Dielectric losses are the dominating loss mechanism in the substrate material. Dielectric losses occur in granular substrate materials due to their porosity, whereas the metallic losses are primarily due to chemical non-stoichiometric impurities that are by-products of some film preparation processes.

For HTS thin films to be useful for electronic applications, they have to have high transition temperatures T_c at a comfortable margin above liquid nitrogen's boiling point, 77K. For device fabrication and research purposes; the films must be stable, have smooth surfaces and sharp interfaces. High quality epitaxial thin films are therefore required. The thin films need to have the correct phase and oxygen content to be optimally superconducting.

3.2 Substrates for Superconducting YBCO Films

A crucial starting point in the growth of HTS thin films and multilayers is the selection of the substrate material and its preparation. Substrate influence crucial properties of the thin film they support, with poor substrates leading to poor films [46].

The first task of a substrate is that it should act as a template for the crystal structure of the thin films grown on them [47]. Other factors that need to be considered, include commercial

availability, cost, the potential for integration with other device technologies, thermal expansion coefficient, dielectric constant, and the dielectric loss tangent (tan δ) at microwave frequencies [43, 48]. Additionally, substrates should also provide mechanical strength for the thin films grown. The ideal substrate is both chemically and structurally compatible with the thin film.

It is important for the thermal expansion coefficients of the substrate and HTS film to be well match. The extreme thermal cycling that a sample undergoes from deposition, at temperatures as high as 900°C, to cryogenic testing temperatures can lead to cracking if the substrate and thin film contract and expand at different rates. This is one of the problems that faces the integration of YBCO with silicon and sapphire substrates [49]. Generally buffer layers of MgO, CeO_2 and YSZ are required to reduce the mechanical strain the films experience. These buffer layers are also used to improve lattice match and can act as diffusion barriers to prevent the YBCO from reacting with these substrate at the high deposition temperatures. Any substrate reactions with YBCO tend to degrade and poison its superconducting properties.

For deposition the crystal lattice of the deposited YBCO film and substrate must be well matched for the film to grow epitaxially, with the correct *c*-axis (001) orientation on the substrate [48]. Minimising the lattice mismatch is reduces the strains developed in the thin films. The lattice mismatch, μ, is calculated as

$$\mu = \frac{a_{film} - a_{substrate}}{0.5 \times (a_{film} + a_{substrate})} \times 100\%, \tag{3.1}$$

where a_{film} and $a_{substrate}$ are the lattice constants on the film and substrate respectively.

For microwave devices the substrate should have favourable high frequency properties such as low dielectric constant and low dielectric loss [41]. This is important, as it is often the substrate losses that dominate and limit the device performance rather than the surface resistance of the HTS [50].

Substrates suitable for HTS devices can categorised into two general groups, perovskite oxides (such as $SrTiO_3$, $LaAlO_3$ and $NdGaO_3$) and non-perovskite (MgO and Al_2O_3) oxide materials. Some of the most commonly used substrates and their properties are listed in Table 3.1.

Table 3.1: Properties of various substrates commonly used for YBCO growth.

Substrate Material	MgO	$SrTiO_3$	$LaAlO_3$	LSAT	Al_2O_3
Lattice mismatch	9%	2%	3%	1%	11.2%
tan δ	5×10^{-4}	6×10^{-2}	3×10^{-5}	2×10^{-4}	3×10^{-5}
Dielectric constant	9.65	277	23	22	9.34

Due to the similarity in crystal structures, perovskite substrates are well matched to YBCO [51]. However, perovskite substrates are quite expensive and complicated to produce. $SrTiO_3$ (STO), in particular has been established as a standard substrate material for high-quality YBCO films [47]. However, STO exhibits poor microwave properties. Other perovskite-like substrates like $LaAlO_3$

have better microwave properties but are much more expensive and not available in larger sizes. MgO is an example of a non-perovskite oxide that has been successfully used as a substrate to produce high quality YBCO thin films. Despite its large lattice mismatch, it is a popular substrate material due to its availability, low cost and favourable dielectric properties. Its thermal expansion coefficient also similar to that of YBCO [52]. Its low dielectric constant is practically temperature-independent and it has low dielectric losses [46]. This makes it ideal for high frequency superconducting microwave applications and devices.

$(LaAlO_3)_{0.3}(Sr_2AlTaO_6)_{0.7}$ (LSAT) is a more recently developed single crystal substrate material that has a perovskite structure and is twin-free. LSAT is cheaper to produce and exhibits an excellent lattice match with YBCO, therefore, it is expected to replace $LaAlO_3$ and $SrTiO_3$ as a common single crystal substrate for epitaxial oxide thin films superconductive devices.

For an in-depth review of HTS substrate selection and their properties please refer to [48].

MgO is the substrate choice for this thesis, due to their low cost, high availability and favourable microwave properties. The MgO used were 0.5mm thick, 10×10mm square, with a surface roughness below 1.5nm. These substrates were already pre-cleaned and could be used without any preprocessing. MgO is very sensitive to moisture and therefore were carefully stored in vacuum and had minimum exposure to the atmosphere before being used for deposition.

3.3 Thin Film Deposition

The key to growing high quality ceramic superconductor films lies in controlling film epitaxy and stoichiometry. Of primary importance is the lattice match of the substrate and film, deposition temperature, and deposition gas composition and pressure. Fine tuning these deposition parameters allows one to tailor the films to exhibit specific properties (e.g. smooth films, a targeted J_c, low surface resistance). In a multilayer film process, the requirements for good film growth remain the same, but satisfying them becomes more difficult. This is because the various layers require separate processing steps which can degrade previously formed thin film layers and structures. It is therefore important that any processing steps be compatible with the materials present in the multilayer structure, when that step is applied.

Many different techniques (e.g. sputtering, evaporation, molecular beam epitaxy, laser ablation, chemical vapour deposition [53]) have been successfully employed to fabricate superconducting HTS thin films. These techniques vary in complexity, the types of materials that can be used and the equipment cost [43]. Most of these techniques work in a vacuum environment with an oxygen partial pressure maintained near the substrate. The correct superconducting phase can be achieved in situ (i.e. during deposition without breaking vacuum) or by post-deposition oxygen annealing. In situ techniques typically require high temperatures (650-800°C) in an oxidising environment. These techniques have the advantage of producing smooth film surfaces and can

be used to effectively synthesize multilayer film structures. Ex-situ deposition techniques comprise depositing either amorphous or a polycrystalline YBCO and then later annealing the films at high temperature and oxygen pressure to form the desired superconducting phase [54]. This post-deposition annealing at high temperatures for upper superconducting layers tends to degrade lower layers (which tend to become oxygen deficient) and can cause unwanted material diffusion within the structure [23].

The substrate temperature during deposition is a crucial parameter that determines the micro-structural details such as thin film texturing and the degree of epitaxy of the film. Substrate-film interactions such as inter-diffusion can affect the quality of the films. It is therefore desirable to develop processes that allow low substrate temperatures. Low temperatures make the effects of crystal lattice and thermal expansion coefficient mismatch less severe and the smaller temperature ranges allow more materials to work together.

In general, stringent control of the composition is required during deposition. HTS are complex multi-component oxides with complex crystal structures [43]. The formation of a specific superconducting oxide phases requires an optimisation of both the temperature and the oxygen partial pressure consistent with the thermodynamic phase stability of the compound. The electronic properties of YBCO are strongly dependant on its oxygen content. Practical devices require extremely smooth thin films with excellent superconducting properties. These collective requirements prove challenging for nearly all techniques presently used in thin film fabrication. Pulsed laser deposition is one of the most versatile deposition techniques and it is well suited to the stoichiometric deposition of complex oxide materials such as YBCO. This method has the benefit of being fast, robust and cost effective.

3.4 Pulsed Laser Deposition

3.4.1 Characteristics of PLD

PLD is a versatile and relatively simple technique, capable of producing high quality multi-component thin films under a wide variety of ambient conditions [55]. It is easy to set-up and use, offering a large freedom of choice in target material and deposition characteristics. The film stoichiometry is nearly identical to that of the target material and films can be grown in reactive environments such as oxygen. One of the primary advantages of PLD is that can be used to grow various types of superconducting, semiconducting and insulating films. This technique has been widely used to grow thin films of numerous complex oxides [56], in particular YBCO [19, 32].

PLD is conceptually very simple. It essentially requires only five components: a pulsed laser source, a vacuum chamber, background gas, a substrate heater and a target. The target is made of the desired growth material or a precursor that will react with the background gas in the chamber to form the desired growth material. A pulsed laser beam is focused onto the surface of a solid

target. The strong absorption of the electromagnetic radiation by the solid surface leads to rapid evaporation of the target materials. The evaporated materials consist of highly excited and ionized species. In vacuum this forms a glowing plasma plume immediately in front of the target surface. The plume is ejected and expands forwards, depositing onto the substrate surface. The substrate is heated depending on the type of material deposited and the type of crystal growth desired.

Only a few parameters need to be controlled during the PLD process such as laser energy density and pulse repetition rate, this makes its operation simple [57]. PLD targets are much smaller than other targets required by other sputtering techniques. It is therefore well suited to experimental research where only small amounts of target material may be available. It can be used to produce multi-layered multi-material films by ablating using various different targets in sequence and various different background gasses be used to produce a wide variety of thin films. Furthermore, by controlling the number of pulses, a fine control of film thickness down to atomic mono layer can be achieved. One of the most important features of PLD is the stoichiometric transfer of target material to the deposited films [58]. The extremely high heating rate of the target surface leads to the congruent evaporation of the target material and its constituent elements and compounds. PLD also requires much lower substrate temperature than other film growth technique to deposit crystalline films, due to the high heating rate of ablated materials [59].

In contrast to the simplicity of the technique, the physical processes in PLD are highly complex and interrelated, and depend on the laser pulse parameters and the properties of the target material and substrate. Optimizing any particular deposition system for ideal crystalline film growth can be very tricky and time consuming. Growth of epitaxial, complex oxide superconducting thin films poses a particular challenge, because the demand on crystalline perfection is most stringent.

One of the major problems with PLD is the formation of particulates on the deposited films. The size of particulates may be as large as a few micrometers. Such particulates will greatly affect the growth of the subsequent layers as well as the electrical properties of the films. Another problem of PLD is the narrow angular distribution of the ablated species, which is generated by the adiabatic expansion of laser, produced plasma plume and the pitting on the target surface. These features limit the usefulness of PLD in producing large area uniform thin films, and PLD has not been fully deployed in industry. Recently, remedial measures have been proposed. Inserting a shadow mask is effective to block off the large particulates [60]. Rotating both the target and substrate can help to produce larger uniform films [61]. The nature of the target (i.e. target density, composition and stoichiometry) and its preparation are both very important aspects that influence the formation of particulates. Careful target preparation, cleaning and pre-ablation is needed to ensure a fresh target material surface for good deposition [62].

3.4.2 Perspectives on PLD at Stellenbosch University

Pulsed laser deposition been the most commonly used technique here at Stellenbosch University. It was the only means to deposit YBCO until recently when the inverted DC magnetron sputtering unit was developed [27, 29]. Yet despite its long tenure here amongst the Stellenbosch superconducting researchers, and multiple optimisations performed on the process, most attempts to obtain working devices have failed. This has been largely due to the the multi-user research environment and variability of the experimental setup. When success has been achieved it has been with basic singular devices (Josephson junctions) and films with poor reproducibility [63, 64]. Conradie [65] was the first to optimise the entire PLD deposition process for YBCO. In general he had results that corresponded well with literature in some respects, but, however, was significantly different in others. This is due to the variability of many groups' deposition setup. The work of [60, 66, 67] also confirmed this. In general the recipes that are published in literature give an idea of the parameters that should give good quality films. However, in practice, following these recipes does not guarantee good films. This is because every research group has its own unique deposition system, different size chambers and different quality vacuum pumps. Our PLD system was again thoroughly characterised by Rottier [67] and Maritz [68], who investigated some of the parameter interdependencies. Rottier [67] highlighted that the laser energy, oxygen pressure, target to substrate distance, laser pulse frequency and substrate temperature, are important and interdependent for the PLD setup at Stellenbosch University. For a detailed literature study of some of the parameter sets and their relationships, the reader is referred to [67, 68].

3.4.3 Optimization Problem

Pulsed laser deposition is arguably one of the most versatile deposition techniques that exist to deposit superconducting films [69]. It is not only conceptually simple and easy to operate, but it is also extremely easy to modify and accommodate more exotic deposition configurations. This versatility can be problematic in an environment where multiple users run multiple experiments and have to share the same equipment. This is especially troublesome when these different experiments involve several different deposition materials and experimental configurations. A constantly changing experimental setup can easily lead to cross-contamination, rapid equipment degradation and erratic film quality control. When the system changes the researcher is often limited to work within a certain sub-optimal range of deposition parameters.

Different research groups each have their own unique deposition recipe that is suited to their specific PLD system [70]. Systems vary significantly, because the PLD technique is so versatile. It is easy to modify, adapt, control and run with only a limited number of parameters. Replicating in-house research results is thus relatively easy [60]. However, different research groups' results are more difficult to replicate. The process of finding a new optimal deposition parameter set is expensive and time consuming. Although PLD is only controlled by a small set of parameters, it is

a very complex process. The parameters have multiple interactions and dependencies that effect the resulting film deposited [67]. Furthermore, experiments tend to have multiple local optima with-in a given parameter set [65].

Ideally once a optimal parameter set has been found, re-optimisation should be unnecessary and deposition with sub-optimal parameter sets should never be a problem. If the laser energy is too low, fix the laser so that it produces more energy. Or if the target is starting to get old and degraded, simply replace the target. Through constant monitoring of the manufacturing process it can be maintained and kept at an optimum. However, in practice this is difficult to do as has been shown over the past years of superconductor research here at Stellenbosch University [63, 66, 67, 71]. A large amount of the research here has been dedicated to re-characterising and re-optimising our PLD system. Often promising results have been attained only to be let down by another stage in the fabrication and testing process. Often knowledge of the system has gone missing from researcher to researcher and time and resources have been wasted in repeatedly re-optimising the system that is continually changing due to high usage and poor maintenance of the PLD equipment. It would be helpful if an additional non-essential parameter could be added and adjusted to compensate for the essential parameters that might have changed, and thereby produce better films.

In the research presented here, we investigated the idea of finding a new parameter to improve the existing deposition system, regardless of the current level of optimisation. Rather than repeat another optimisation of this same equipment again, we desire to find an independent parameter that can be adjusted during deposition to help improve the quality of the films produced with PLD.

A possible application would be where the researcher wants to adjust one of the deposition parameters to accommodate a certain substrate material into a deposition process. If this adjustment reduces the quality of the films produced, an additional parameter that can compensate for the sub-optimal parameter is required. A specific example of this is decreasing the substrate temperature during YBCO thin film deposition [72, 73].

Candidates for this non-essential parameter can be found from some novel solutions suggested in literature for improving PLD film quality. The in situ application of electric fields, voltage biasing and plasmas into the deposition process, have been shown to improve the crystallinity of various PLD grown thin films. An overview of some of these hybrid PLD solutions from literature will be presented in the next section.

3.4.4 Lowering YBCO Deposition Temperatures

Being able to reduce the deposition temperatures to below 600°C would make YBCO compatible with a much wider range of substrate and inter-layer materials. Silicon becomes a more viable substrate material at these lower temperatures and this would allow for better integration of HTS with semiconductor technology [15]. Multilayer HTS technology would also benefit. The electrical

characteristics of the superconducting layers are very sensitive processing temperatures. For multilayer fabrication, the health of the bottom layer electrode is highly dependent on the processing used to fabricate and pattern the subsequent upper layers [22]. High deposition temperatures can cause the lower superconducting layers to decompose, loose oxygen content and therefore superconductivity [23]. Deposition conditions for upper superconducting layers should be kept as low as possible to try to preserve the superconducting characteristics of lower layers. Lower processing temperatures also help to minimize inter-facial diffusion between the substrate and the various inter-layers [25, 74].

However, in general, YBCO has to be grown at temperatures in the range of 650-900°C in order to obtain films with good crystallinity and the right superconducting phase [49]. Depositing thin films at lower temperatures is therefore a sub-optimal deposition process. The critical temperature of the films drops off rapidly with decreasing substrate temperature [22]. Films deposited at low substrate temperatures are usually poorly superconducting and have to undergo high temperature anneal treatments to recover superconductivity [16, 75]. Deposition at lower temperatures is challenging because the volume of *a*-axis oriented grains perpendicular to the surface increases with decreasing substrate temperature [26]. YBCO is highly anisotropic and has a short coherence length. If the major (*a*-*b*) planes are not well aligned and parallel to the surface of the film, poor device performance is obtained.

It has therefore been a hot topic to develop methods that allow one to reduce the substrate temperature to as far below optimal as possible [17, 24–26]. The as-deposited films should still retain good superconducting properties without needing any further high temperature annealing to be compatible with multilayer deposition processes [22].

3.4.5 Activated oxygen

The importance of oxygen species near the substrate during the pulsed laser deposition of YBCO, has been shown by a number of researchers [24, 65, 76]. In particular, activated oxygen species are important for improving the in situ low temperature film growth of YBCO [77]. The superconducting properties of YBCO thin films are very sensitive to oxygen content [78] and the substrate temperature greatly influences the amount of oxygen incorporated into the thin-film. It is reported that increased excited oxygen species during deposition, facilitates the formation of the superconducting phase at lower temperatures than normal [72].

Various different deposition configurations have been developed to achieve high concentrations of activated oxygen species near the substrate and improve PLD oxide thin film growth. Techniques that have been used include: the use of oxygen plasma generated by DC- and RF fields [79], the injection of ozone [60, 67] or laser dissociated N_2O [51] near the substrate [72]. Most of them have concluded that atomic or ionic oxygen near the substrate is most important for good film growth. Rottier [67] also showed that replacing molecular oxygen with ozone as a background gas,

during deposition and annealing, has a number of positive effects on the PLD process. His results showed an overall improvement of the oxygenation and T_c of the thin films and a reduction of their surface roughness. The inclusion of ozone also tended to reduce the experiments sensitivity to variations in substrate temperature and background gas pressure. This increased robustness is exactly what is needed to obtain good results with sub-optimum conditions.

Although the films produced using these methods and lower substrate temperatures are generally not as good as those prepared at high substrate temperatures they do offer a significant improvement [77]. Figure 3.3 shows their results and how the superconducting films T_c was enhanced most using activated oxygen gas. These techniques therefore offer a suitable compromise for being able to use lower substrate temperatures and still obtain relatively good superconducting thin films with high T_c. In general, most of these techniques show the biggest improvement of T_c on conditions that produce the poorest film quality and very little to any improvement when the films are close to optimal [80,81]. This is to be expected, as near optimum T_c there is less room for improvement. Films deposited at the lowest substrate temperatures and were not superconducting, often obtain reasonable superconductivity using the adapted parameter sets. For example, [51] managed to achieve superconducting YBCO thin films with a $T_c(0) = 84$K, depositing at 600°C on (100) STO substrates. In comparison to films grown in a similar fashion but without the laser disassociation of N_2O, which where not superconducting at all. Such a technique is therefore of most importance to poorly optimised, deteriorated and sub-optimal deposition conditions.

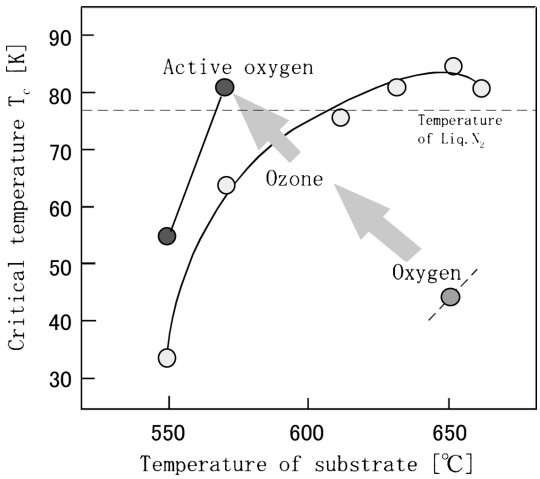

Figure 3.3: Improvement in the T_c of a thin-film high-temperature superconductor deposited by using oxygen, ozone, or active oxygen [77].

Adding DC and RF generated oxygen plasmas (or activated oxygen) to PLD, has shown the most promising results for reducing the substrate temperature. Tanaka et al. [77] found that using activated oxygen during deposition results in better films than using ozone or normal oxygen gas. In addition, De Villiers [63] has shown that using ozone leads to the rapid degradation of the O-rings that seal the vacuum deposition chamber, causing vacuum leaks. Therefore, we do not

employ this technique. The N_2O technique proposed by [51] requires the use of a second laser and the appropriate synchronisation between the two laser pulses. This is therefore a much more expensive and complicated technique to implement. The application of DC- and RF fields are therefore considered more viable solutions. PLD is most commonly enhanced by the addition of a plasma discharge which interacts with the laser ablated plume before it deposits onto the substrate [79, 82–84]. This technique is called plasma-assisted or plasma-enhanced pulsed laser deposition. We will refer to it as plasma-enhanced pulsed laser deposition PE-PLD. PE-PLD comes in two varieties, depending on how the plasma is generated, using either DC or RF power sources.

Using RF to induce plasmas adds a substantial amount of complexity to the setup [84]. RF power sources are more expensive and complicated to control, monitor and apply [85]. Additional RF matching networks are required and suitable RF-blocking filters are needed to protect the equipment and operators from the RF signals [86]. By comparison, DC plasmas and E-fields are simpler to implement and control [85]. DC power sources are less expensive and do not require the complex RF matching networks, filters or shielding that RF plasma generation needs. Although a classical configuration, DC glow discharges are still popular and widely used [87].

3.5 Plasma

Plasma processing technology can be found in nearly every branch of microelectronics and material science [88]. Plasma is used in cleaning and activating surfaces, and thin film deposition. The application of plasmas during deposition is not a new concept. It has been used for many years in conjunction with many different techniques and wide variety of materials to improve the quality of the films deposited [87].

Plasmas are often referred to as the fourth state of matter [87], since it occurs by adding energy to gas [89]. Plasmas are ionized gases consisting of charged ions (positive and negative) and electrons, as well as neutral species (atoms and molecules) [89].

Plasmas that can be generated in the laboratory can be classified into two groups, namely high-temperature (fusion) plasmas and low-temperature plasmas, otherwise known as gas discharges. In this work, we are only concerned with gas discharges.

The important parameters for gas discharge plasmas is the gas pressure ρ and the distance between the electrodes D. The product ρD further classifies the plasmas into plasmas in thermal equilibrium (LTE) and plasmas not in thermal equilibrium (non-LTE). A low gas pressure results in few collisions in the plasma and therefore there are many different temperatures present in the plasma due to inefficient energy transfer mechanisms. Higher pressures imply more collisions and therefore higher plasma temperatures and more uniform plasma temperatures amongst the plasma species. Non-LTE plasmas are used for application where heating is undesirable, such as etching or material

deposition. In these discharges the electrons are at much higher temperatures (energies) than the ions and neutral species. This is due to their small mass and how easily they are accelerated by electromagnetic fields. The electrons are responsible for the high reactivity of the plasma and are the primary agents of the plasma [87]. They are responsible for initiating the responses of the heavier particles. The heavier particles often are responsible for the primary action of the plasma, i.e. sputtering.

3.5.1 DC glow discharges

A gas discharge occurs when a potential difference is applied between two electrodes, in a gas, is sufficiently high to cause the gas to break down into ions and electrons. The mechanisms of gas breakdown are summarised in Fig. 3.4. Initially only a few electrons are emitted from the electrodes. They are emitted from the cathode, the (more) negative electrode, and accelerated toward the anode, the (more) positive electrode. As they are accelerated they collide with the gas molecules present in the gas. Depending on their energy they can either cause elastic or inelastic collisions. Inelastic collisions can lead to excitation or ionisation of the gas. Excitation collisions are followed by de-excitations with the emission of radiation. This is responsible for the glow observed in this discharge. Ionisation generates new electrons and ions, which are then accelerated by the E-field. The ions are accelerated towards the cathode. When they collide with the cathode, new electrons are released (ion induced secondary electron emission). The new electrons are also accelerated and cause new collisions, potentially creating more ions and electrons. This process therefore becomes self-sustaining, with electrons being emitted at the cathode and ionisation in the gas (plasma) [90]. Additionally, the ions bombarding the cathode cause atoms to be knocked out of the cathode. This is known as sputtering and occurs if the voltage applied between the electrodes is high enough. Sputtering forms the basis of many of the applications of DC plasmas, ranging from material deposition to etching.

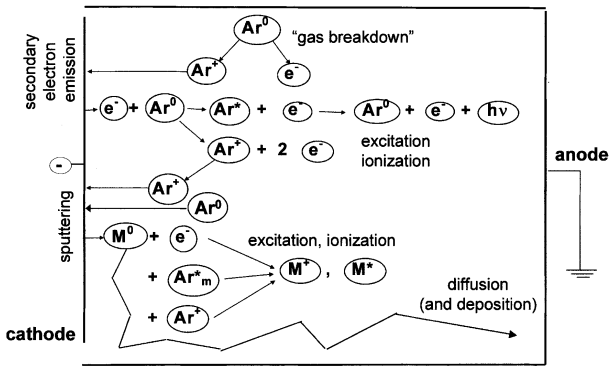

Figure 3.4: The various processes that occur in a DC glow discharge. [87]

The potential difference between the two electrodes is not equally distributed due to the moving gas and ions that redistribute the charge distribution. Fig 3.5 shows how the potential varies in

between the two electrodes of a glow discharge. It drops nearly completely a short distance from the cathode. This small region next to the cathode is known as the "cathode dark space" or "crooks darks space" (CDS). It is characterised by a large E-field and there is very little charge present here, as any charged species are swept away by the strong E-field. It is a relatively dark area due to the lack of charged species. The next region is called the "negative glow" (NG). It is the largest region and it has a slightly positive potential know as the "plasma potential". This is the main region where the gas plasma is contained. It is a bright area the gives the characteristic glow to the process. The E-field in this region is relatively small. The final region is the "anode zone" (AZ). Here the potential drops to zero again. This is also a relatively empty area, due to the small electric field that sweeps the charge out of this region.

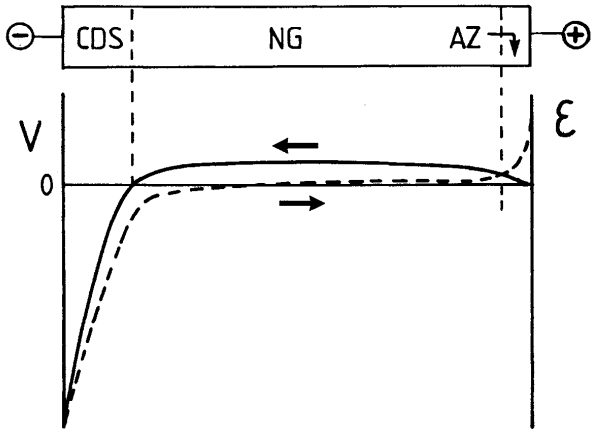

Figure 3.5: The distribution of the potential difference and electric field between the cathode and anode in a DC glow discharge, with a short cathode–anode distance and or low pressure; [87] (CDS = cathode dark space; NG = negative glow; AZ = anode zone). The cathode (left) has a negative potential and anode (right) is at zero potential. The solid line represents the potential distribution, an the dashed line the E-field distribution.

Non-conductive electrodes

In DC glow discharges the electrodes play a very important role of emitting the electrons that feed the discharge process. If they are not conducting they will not be able to sustain the discharge [87]. Initially there will be a short break down, followed by an accumulation of charge on the surface of the electrode. The electrodes gradually become charged up due to the accumulation of charged particles, extinguishing the discharge.

Oxidation

Plasma oxidation or "anodisation" is a process that happens at the anode that is positively biased in a plasma. The positive potential here attracts the electrons and negative ions to the surface of

the electrode, where oxide growth is stimulated [87]. This form of oxidation can be very effective leading oxide layers that are several micrometer thick.

3.5.2 Electric field enhancement of PLD YBCO

A number of researchers have explored using the addition of DC biases and plasmas to enhance PLD of YBCO thin films and many have reported good results. We therefore choose to focus on this technique as a simple and cost effective add-on technique for improving YBCO thin film deposition quality

The method of introducing DC plasmas to enhance the PLD growth of YBCO involves introducing an electrode or electrifying a part of the deposition chamber (e.g. the target or substrate heater), which then acts as an electrode. The electrode is biased with a certain DC voltage to establish an E-field inside the chamber. This E-field influences the laser induced plasma, the ambient gas and the deposited material on the substrate. Under the right conditions (voltage, current and gas pressure) the E-field will set up an DC plasma or glow discharge in the chamber. This plasma gas consists of excited oxygen species, ions and electrons which then interact with the laser induced plasma plume. This interaction enriches the chemical reactions in the plume, between the plume and background gas, and help to energise the growth at the substrate. This is a very simple view of the processes thought to be at work which cause the enhancement of the film growth. However, there are a rich assortment of dynamic interactions at play in this process and it is not easy to say how or what exactly is happening [91].

In the literature, typically four basic configurations are considered for introducing E-fields into the deposition chamber. Figure 3.6 illustrates these four and details the positions of electrode and possible points of electrification inside the chamber. Configurations (a) and (b) are used most often, whereas (c) and (d) are only employed by two specific groups to solve certain issues they have with the process.

In-line triode configuration

The configuration shown in Fig 3.6 (b) was the first reported that could be used to enhance the superconducting properties of YBCO thin films in 1988 [25]. In this configuration a bare metal ring electrode is introduced into the deposition chamber and a potential is applied to it. The ring is placed in between the target and substrate, and aligned so that the plume passes directly through the electrode ring. The substrate and target are either electrically grounded or left at a floating potential. We will refer to this configuration as the in-line triode configuration. Witanachchi et al. [25] used this configuration successfully, biasing the electrode at +300V and grounding the target, leaving the substrate heater at a floating potential. The electrode was placed exactly half-way between the target and substrate, which were placed 75mm apart. They report being able

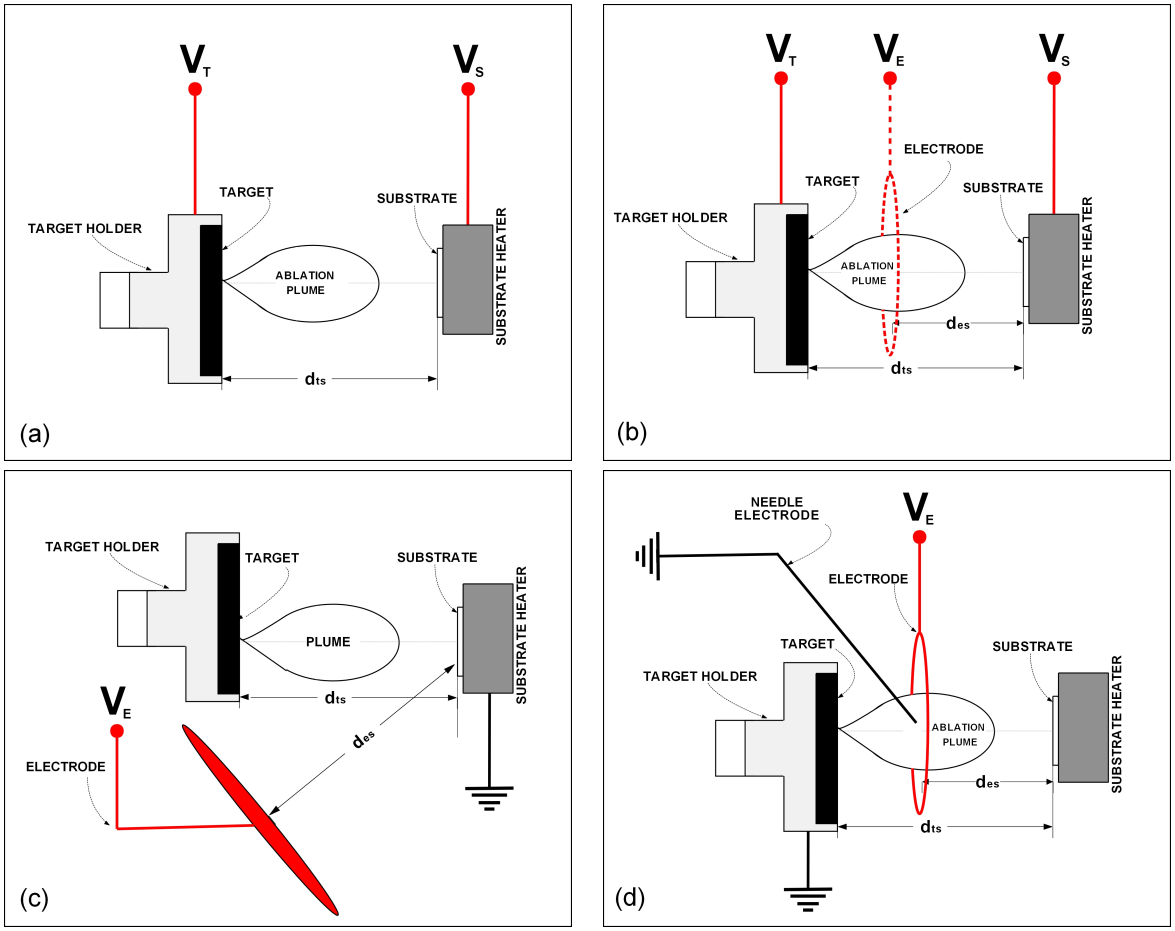

Figure 3.6: Four standard configurations used in literature for introducing DC bias fields and DC glow discharge plasmas into the PLD chamber during deposition: (a) direct biasing of target or electrode, (b) in-line triode configuration, (c) off-axis disc triode configuration and (d) auxiliary needle triode configuration.

to deposit good quality ($T_c(0) = 85$K, $\triangle T_c = 5$K) YBCO thin films on (100) STO substrates using deposition temperatures as low as 400°C. It should be noted that they report the estimated temperature of the substrate. The standard convention from literature is however to report the temperature of the substrate holder, as this temperature can be accurately measured. The temperatures therefore seems 100-150°C cooler than reported by similar literature. Furthermore, they report the presence of a low pressure oxygen discharge (glow) is triggered by the first laser pulse and sustained in the region between the target and electrode. They did not know the exact reason for the enhanced YBCO growth at the low temperatures. However, they attribute the improvement in YBCO superconducting properties to the generation of O_2+ ions which are repelled from the target region, enhancing the region near the substrate. Witanachchi et al. [92] also reported the improvement has on both buffered and unbuffered sapphire substrates. The buffer layers investigated included 50nm of MgO, $BaTiO_3$ and Ag. The unbuffered substrate deposited with their technique at 450°C showed a $T_c(0) = 75$K, which was comparable to that achieved with the buffer

layers [93]. They maintain that the main effect of the DC bias is to preferentially bombard the substrate with positive and negative ions from plume and DC glow discharge and that the gas is in an enticed state in the region between the electrode and substrate, oxygenating the thin film. We should note that the deposition pressures reported are very low below 0.02mbar and they did not anneal their samples after deposition. They again repeated the technique on silicon substrates [17], achieving a $T_c(0) = 45$K of unbuffered substrates using deposition temperatures of 400°C. On a MgO buffered silicon substrate the films were improved to have a $T_c(0) = 70$K and $\triangle T_c = 10$K. In 1991, Kwok et al. [74] showed how the same in-line triode configuration reported by Witanachchi et al. [25] with the ring electrode biased at +300V could be used to decrease the substrate temperature by 50-70°C and still obtain similar quality films. Fig. 3.7 shows their results. They report that at any substrate temperature, the films produced with the plasma are always better than those without. However, the improvement is more noticeable at low temperatures. They also measured the ions present in the plume with and without the bias voltage applied and conclude that there is definitely a higher concentration of excited ionic species present in the plume, and that it is this ion enrichment that somehow improves the film quality. The complex dynamics of the plume and the plasma's tendency to maintain neutrality make it hard to say with any certainty what the exact mechanisms are. The work of Kwok et al. [74] shows compelling evidence as to why this is such a valuable technique. Using this technique they were able to make their deposition process more robust against temperature variations. In all the experiments reported by this group they make no mention of the electrode size nor do they specify the power supply that is used to bias the electrode.

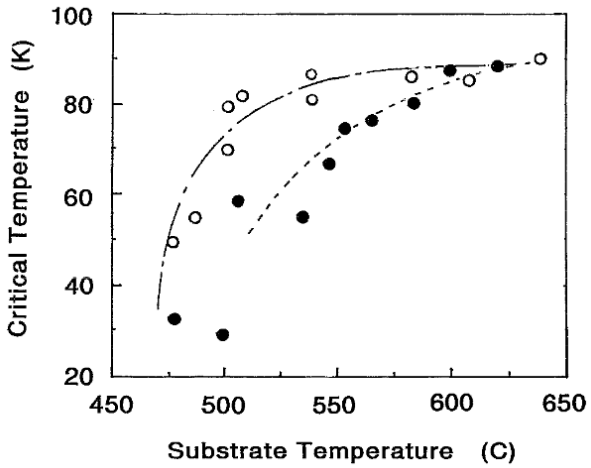

Figure 3.7: The results of [74], showing the T_c's of YBCO films as a function of the deposition temperature for no bias voltage applied (solid circles) and for a in-line triode configuration with a +300V bias voltage (open circles).

Singh et al. [94] report similar results using the same in-line triode configuration. They experiment using the same voltage of +300V, however the electrode to target spacing is reduced to 8mm

and the target-substrate distance is reduced to 50mm. They made use of higher oxygen pressure in the chamber $\sim 2.6 \times 10^{-1}$ mbar. Interestingly, they mention mention that no DC plasma glow is present in the chamber. This is most probably due to the close proximity of the target and electrode. They do not mention of the electrode size. They report achieving a $T_c(0)$ of 88K ($\triangle T_c = 2$K) at a deposition temperature of 550°C on (100) YSZ. Of importance here is how the oxygen is introduced into the chamber. They use a nozzle to direct a jet of oxygen at the substrate or the target. The best results are always achieved if the oxygen jet is directed at the substrate during deposition. In a similar experimental study, Singh et al. [94] report being able to drop the deposition temperature of YBCO on (100)STO and (100) YSZ to 500°C and 550°C, respectively. The best $T_c(0)$ they achieve at these lower temperatures is $T_c(0) = 77$K ($\triangle T_c = 5$K) and $T_c(0) = 88$K ($\triangle T_c = 1.3$K) for STO and YSZ substrates respectively. In the unbiased configuration, the YSZ sample degraded to $T_c(0) = 80$K ($\triangle T_c = 7$K). They show that the *c*-axis crystallinity of the samples was improved using the technique. Singh et al. [95] again used the technique to deposit YBCO through physical masks to produce as-deposited patterned films. The films therefore required no further lithography or patterning. They propose that it is the modification of the kinetic energies of the charged species in the plume that is responsible for the improvement in film quality.

Various spectroscopic studies have been attempted to analyse the content of the plasma plume with and without a DC bias applied to the ring electrode [74,91,96–98]. They all observe that there is an enhancement of the excited species in the plume. However, they conclude that spectroscopy cannot fully explain the behaviour observed. Not all species can be observed due to spectral overlapping and this technique only provides a picture of the excited species in the plume (i.e those that radiate) not the neutrals or reactions that do not radiate energy. Ying et al. [96] report that it does increase the plasma temperature at the substrate, improving film growth by supplementing the energy deficit created by lower substrate temperatures. The substrate temperature supplies energy to increase the surface mobility of the atoms and to promote the formation of the correct crystalline phase [74]. Thermal activation from the substrate is therefore substituted supplying a higher temperature plasma. [98] maintain that it is the enhanced formation of diatomic molecules such as YO, CuO, and BaO (due to enhanced reaction in the plume) that arrive at the substrate that leads to lowering of the substrate temperature under the biasing conditions. The most recent study, performed by Miu [91], made a study of both positive and negative biases, showing that there is are complex interactions between all the irradiation parameters. Their study used more typical deposition parameters for YBCO thin films, however the laser energy densities used were relatively low (0.6–0.75 J/cm^2). They used a copper ring electrode with a diameter of 2.5cm placed 2cm from the target and no substrate was used. Investigations were made for vacuum (10^{-5} mbar) and 2.6×10^{-1} mbar oxygen. They also investigated a range of bias voltages: 0V, $\pm 240V$, and $\pm 450V$. In vacuum, all voltages could be tested, however at the higher oxygen pressure, there were continuous discharges (arcing) for voltages greater with magnitudes greater than 240V and they could only test using $\pm 240V$. This is an interesting observation as most of the other studies

did not note this due to the low pressures they employed. This also hints at an instability that might be present for this technique. The plasma shock-front was observed at the leading edge of the plasma plume, caused by the slowing of emitted target species through collision with the ambient gas. These species accumulate into the region behind the shock-front. Furthermore they observed a discharge current when the plume reached the electrode. In the 2.6×10^{-1} mbar oxygen environment they found that the -240V leads to higher emissions than the +240V. They presumed that the increased emission intensity was due to species excitation produced by electron collisions with the plasma species. They thought that the negative bias voltage strongly repelled the electrons into the region between the target and electrode, leading to enhanced excitation of the oxide species. What is interesting to note is that only positive bias voltages have been reported to work with this in-line triode configuration. Ying et al. [96] reported that a negative bias voltage does not lead to superconducting YBCO thin films. It would therefore seem that some other interaction results in the improved film quality. The electrical properties of the YBCO thin films are strongly dependent on the oxygen content in the films, and therefore the amount of oxides and reactive species is important. However, the complex interactions necessary for good film growth cannot be identified by emission spectroscopy alone, complementary analysis of non-emitting species is also necessary to provide a complete picture.

Direct Biasing

Direct biasing refers to the configuration shown in Fig 3.6 (a). In this configuration, either the target or substrate heater are biased, with the other grounded. Izumi et al [81] found that this configuration could also be used to improve the quality of YBCO thin films produced at lower deposition temperatures. In their experiments they biased the substrate and grounded the target. This required a special radiative heater that could isolate the substrate heater. Once again this group did not directly measure the substrate heater temperature, rather they made calibrated approximations as to what the substrate temperature was. They also made use of an oxygen nozzle jet pointed at the substrate. They tested the following voltages: 0V, $\pm$300V, and $\pm$500V. MgO substrates where used and substrate temperatures in the range of 630-670°C degrees were tested. The substrate and target were separated by 50mm. Figure 3.8 summarises their results for films deposited at various temperatures.

They found that a positive substrate bias led to the best results. The films had better superconducting properties and their crystal properties were also better. Hiromi et al. [99] showed that for these +300V biased substrates, highly *c*-axis oriented YBCO grains grew directly from the substrate surface. The biasing showed little effect on the composition of the films and did not effect the deposition rate. There results were interesting because they are the first to note an improvement for both polarities of bias voltage. A negative bias is much less effective than a positive bias. Izumi et al [81] conclude that, because the laser plume is filled with positive and negative particles and emmisive species, it is expected that the application of an electric field will have an

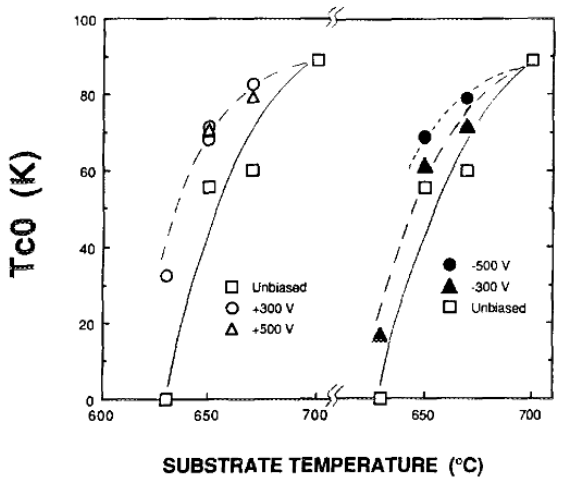

Figure 3.8: The results reported by [81] for various substrate bias voltages and PLD depositions performed at different substrate temperatures.

effect. However, they cannot give a complete explanation of the complex dynamics at play. Using a high-speed camera, they observed that for a negative bias there was no observed no change to speed of plume and and emission when the plume reached substrate, most likely to electrons being emitted and accelerated by the E-field. For the positive substrate bias voltage they observed a bright flash at the laser strike and species travelling to the substrate at different velocities.

The work of Fried et al. [100] confirm the observation of this different timing in emissions at the substrate and target. They did not focus on the films produced, but rather the effect the applied E-field has on the plume generated during the laser ablation of YBCO in an oxygen environment. The discharge current characteristics were dependant on the polarity and magnitude of the applied voltage and the background oxygen pressure. They found that, under the right circumstances, two successive plumes (discharges) where observed. The first plume originated due to the impact of the laser pulse, and was classified as neutral, because the capacitor (biasing the electrode) did not discharge during this period. Instead, the capacitor discharged a number of microseconds later, resulting in the second plume (re-entrant plume). The second plume was considered charged as it was accompanied by a discharge current, or in other-words a net transfer of charge. The phenomenon of two plumes is only observed for the parallel field with sufficiently high background gas pressure, and the delay between the two plumes varies as a function of the ambient oxygen pressure. The double discharge case results in higher intensity emissions from the excited species for a longer period of time. Interestingly, in literature it is the experimental configurations that are most similar to the single discharge configuration that are reported in literature as giving the best improvement in the superconducting properties of YBCO thin films. This is similar to the finding of Izumi et al [81], where an emission was observed together with the laser strike for the positive bias condition that showed the best improvement. For the negative bias as second emission (the plume being the first) is observed when the plume reaches the substrate. Fried et al. [100] offer a plausible

explanation for what is occurring during deposition with the addition of bias voltages. Figure 3.9 shows an illustration of their explanation of the plume dynamics at work. Their explanation is given purely in terms of the discharge currents observed. This is not very helpful from the point of view of film growth. We will therefore give our opinion of what is occurring to improve the film growth of YBCO, based on their explanation of the electron dynamics. We can define the E-field as parallel, in the same direction of the laser plume, and anti-parallel, in the opposite direction to the plume. The effect of the E-field on the light and highly mobile electrons in the plume results in a change in the charge neutrality of the plume [101]. In the parallel case the electrons are attracted back into the plume (the direction of the electric field is the direction a positive charge would move, therefore negatively charged electrons move in the opposite direction of the electric field). Once the plume material strikes the material and electrons generated are accelerated back to the target, through the low density region is left behind the piston of the plasma plume, causing the second discharge. In the anti-parallel case, the E-field accelerates the electrons away from the plume, causing the plume to loose neutrality making it more reactive. The electrons cascading collisions with ambient oxygen in from of the plume excites the oxygen species in this region and promotes the reaction with the more positively charged plasma material. Therefore more oxygen can be incorporated into the plasma plume and the active oxygen at the target surface most probably improves the oxygen absorption of the thin film. In our opinion, this model is most successful in qualitatively explaining many of the results reported in literature.

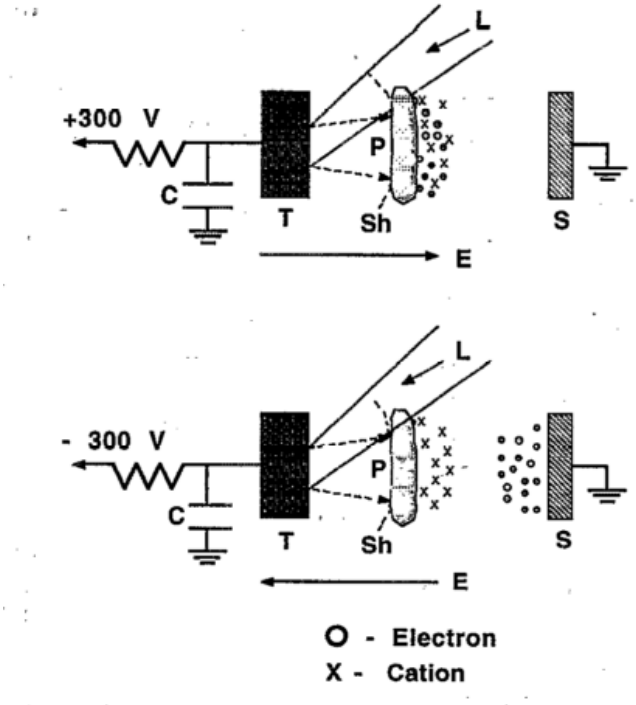

Figure 3.9: Possible laser plume interactions with applied E-fields and its affect on the plume constituents. [100]

Off-axis disc triode configuration

Mirsa and Palmer [102] report how the in-line triode configuration used by Singh et al. [80] was unsuccessful for their experiments. They therefore attempted a new electrode configuration, shown in Fig 3.6 (c). This off-axis disc triode configuration uses a disc electrode position off-axis out of the plume to generate a DC discharge plasma. The electrode was negatively biased at -300V and they report that it improved the films that they were able to deposit with a Nd:YAG laser ($\lambda = 1060$nm). The distance between the electrode and the grounded substrate was 35mm and the target-substrate distance was 25mm. The best film that they were able to deposit using this configuration, on a (100) STO substrate, at a deposition temperature of 540°C, was $T_c(0) = 92$K, $\Delta T_c = 8$K. A possible reason why the configuration of Singh et al. [80] proved ineffective, was that they used a bias voltage of -300V. Singh et al. [80] used a positive bias voltage of +300V. Ying et al. [96] also reported that a negative bias voltage does not lead to superconducting YBCO thin films. These results were again reported in [103].

Auxiliary needle triode configuration

The final configuration considered is shown in Fig 3.6 (d). This configuration was used by Atanasov et al. [38] to deposit YBCO on STO, ZrO_2 and MgO substrates at temperatures as low as 450-550°C. This configuration was used to try to obtain a more stable plasma than those produced by the in-line triode configuration. They report problems maintaining a stable discharge from the standard in-line triode configuration. By adding an auxiliary needle electrode, they confine the electric field into the region of the plasma plume. The electrode was biased at $\pm 300V$ and placed between the target and substrate ($d_{ts} = 50$mm). They annealed the films for 30 minutes at 400°C at 1 bar oxygen pressure. The best results that they obtained for this configuration on STO at a substrate temperature of 450°C were $T_c(0) = 86$K, $\Delta T_c = 9$K. For the ZrO_2 substrate at 450°C, $T_c(0) = 88$K, $\Delta T_c = 9$K, and for the MgO substrate $T_c(0) = 89$K, $\Delta T_c = 7$K at 550°C. The films all showed good c-axis crystallinity. Furthermore, they report that using a negative bias voltage produced films that were not superconducting. They attribute this to partial re-sputtering of the YBCO film by O_2^+ ions generated in the DC plasma discharge. This is unlikely due to the configuration and the behaviour of DC plasma discharges.

Table 3.2 summarises some of the results found in the literature. A quick glance shows that the most common bias voltage is 300V and the presence of a DC glow discharge is not a prerequisite for the technique to work. This suggests that it is the effect of the electric field on the plasma plume that could be the cause for the improved deposition reported.

Table 3.2: Summary of literature results for DC PE-PLD

Ref	Config Fig 3.6	d_{ts} [mm]	d_{es} [mm]	P_{O_2} [mbar]	T_s [$^\circ C$]	Substrate	$T_c(0)$ [K]	$\triangle T_c$ [K]	DC glow discharge?
[25]	(b) +300V	75	37.5	1.3×10^{-4}	400	STO	85	5	Yes
[94]	(b) +300V	50	8	2.6×10^{-1}	550	YSZ	88	2	No
[80]	(b) +400V	50	8	2.6×10^{-1}	500	STO	77	5	No
[92]	(b) +400V	75	37.5	6×10^{-3}	450	Al_2O_3	75		Yes
[17]	(b) +300V	75	37.5	1.3×10^{-4}	400	Si	45		Yes
[102]	(c) -300V	25	35	2.4×10^{-1}	540	STO	82	8	Yes
[81]	(a) +300V	50	-	1.3×10^{-2}	670	MgO	82.6		No
[38]	(d) +300V	50	25	6.7×10^{-2}	450	STO	86	9	Yes
[38]	(d) +300V	50	25	2.6×10^{-1}	550	MgO	89	7	Yes

3.5.3 Other materials

In situ applied static E-fields, bias voltages and DC plasmas, have also been shown to improve the quality of a wide variety of thin films deposited using PLD [104–108]. In certain cases, for example ZnO, it seems that the improvement occurs because the material's unit crystal structure has a distinct polarity along a certain axis and this tends to align with the applied electric field [105, 109]. One would therefore expect oppositely directed fields to have a similar effect, as the unit crystal structure would still be aligned along the same axis. However, there is a drastic difference in the effect of oppositely polarised applied E-fields. This contradicts the idea that it is only the E-field alignment of the unit crystal structure that is responsible for the improvement, and tends to indicate that other processes are also at play. The exact mechanisms for this improvement are not clear or completely understood [91]. Another plausible explanation might be that the E-field's enrichment of energetic ionic species in the plume improves the crystal film growth [72, 106, 110]. This is one of the most common assertions in the literature. The high reactivity of the excited oxygen species results in enhanced oxygen absorption and therefore improved films growth. Jones et al. [108] suggested that it is the moderate acceleration of the ions in the plume that provides surface ion bombardment and film reconstruction, similar to that obtained by ion beam assisted PLD [55].

3.5.4 Arcing and plasma instability

Arc handling is one of the biggest concerns in both DC and RF plasmas. Arcs are localized discharges of extremely high current density. If left unhandled, these arcs can cause major damage to substrates and equipment [85]. The most common way of handling them is by quickly shutting down the power source and thereby extinguishing the arc and avoiding its destructive effects. For low current sources this is less of a problem, as the arc tends to extinguish itself because the voltage drops when the current becomes to high. However random discharges will lead to variable deposition conditions and limit the repeatability of experiments. Stable operation is desired so that the same results can always be expected from applying the same parameters [85].

According to Safi [85], the destructive effects of arcs can be summarised as:

1. driving a process to become unstable,
2. reducing the target lifetime, and
3. creating defects in the sputtered films.

The effect of the sudden highly localised avalanche stream of electrons results in a high current and temperature at one spot. This can result in outgassing of the area and sudden melting and evaporation of the material in that region. If it occurs at the target, this can damage the target and lead to the deposition of molten drops of target material that could ruin the surface of the film. If it occurs at the substrate it can lead to damage of the thin film. If it occurs at some other region in the chamber it can lead to contamination of the target and deposited thin film.

There is some evidence from literature that there are issues with instability for the DC PE-PLD technique, particularly where there is a DC plasma discharge. Izumi et al. [81] report using lower gas pressures to avoid a continuous gas discharge in the chamber. Atanasov et al. [38] created a new electrode geometry to stabilise the plasma discharge and confine it to the region between target and substrate. Mui [91] reports that voltages over 240V in magnitude could not be used due to continuous discharge in the chamber. Mirsa and Palmer [102] also report that their modified geometry resulted in a more stable plasma. Furthermore, the low deposition pressures used by the group of Witanachchi et al. [17, 25, 92] and Kwok et al. [74], seem to suggest unstable discharges at higher pressures.

Finally, despite the initial very positive results reported for this techniques in the early 1990's, it never became a standard deposition technique for YBCO. This would suggest that there were problems with this method that were not reported. Also, as better substrate heaters became available, deposition at higher temperatures became more convenient and this technique was abandoned [74]. Other issues that exist with the reported results are that the electrodes' exact size is rarely reported [17, 25, 92], the power source characteristics are also omitted and there are discrepancies with how the substrate temperature is measured. Despite these concerns, it remains a very promising technique. Multiple groups, using a variety of configurations and substrates, have reported its efficacy and potential for improving the superconducting properties of PLD deposited YBCO thin films. We therefore decided to investigate the application of this technique, to try to identify its problems and attempt to find possible solutions.

3.6 Conclusion

The superior properties of HTS thin films make them extremely good candidates for electronics applications. However, growing these brittle ceramic layers in the correct fashion proves very

challenging. Pulsed laser deposition is one of the most versatile deposition techniques and it is well suited to the stoichiometric deposition of complex oxide materials such as YBCO.

A promising technique is the addition of DC biases and plasmas to enhance the superconducting properties of the YBCO films. A number of researchers have reported good results. However, there is still no complete understanding of what the exact mechanisms are for the observed improvement. Although promising, these techniques have inherent stability issues due to the high voltages, combined with the low pressure deposition environment. We therefore choose to focus on this technique as a simple and cost effective add-on technique for improving YBCO thin film deposition quality.

In the next chapter we will investigate applying the technique to try to recreate the results reported in literature and develop an understanding for the process and its possible problems.

Chapter 4

Experimental Methods

This chapter describes how the thin films in this thesis where grown, characterised, patterned and fashioned into basic microwave filter devices. We will also present how the final filter device was tested. All steps were performed in-house.

4.1 Process Overview

The entire process of film deposition, characterisation, patterning and device testing, employed in this research, can be briefly summarised as follows:

- The superconducting YBCO thin films were deposited on (100) MgO single crystal substrates, using PLD. The substrates were heated to achieve well formed *c*-axis orientated YBCO thin films. The deposition was carried out in an oxygen ambient environment and was followed by a short in situ anneal at a higher oxygen pressure and lower temperature, to improve the superconducting properties of the thin films.
- The film surfaces were examined with optical microscopy and Atomic Force Microscopy (AFM). Optical microscopy provided a macroscopic overview of the thin film quality and showed the number and size of particulates present on the the films. AFM was used to get a closer view of the films, providing a measure of the surface roughness, and was also used to determine the film thickness. The crystal quality of the superconducting films was measured using X-Ray Diffraction (XRD). Furthermore, the superconducting characteristics of the films where determined using susceptibility measurements, performed in our 35K cryocooler.
- Standard photolithography techniques were used to define the filter device structures in photoresist on top of the superconducting films. A wet etching process, using a dilute citric acid solution, was used to pattern the films; etching away any areas of YBCO left exposed after photolithography. Electrical contact was made by depositing gold contact pads onto

the thin films and wire-bonding them to the test circuit boards. The final filter devices were tested and characterised using a vector network analyser. The filters were tested at 77K, by cooling them in liquid nitrogen.

The facilities, fabrication equipment and processes involved have be detailed on numerous occasions by the various researchers here at Stellenbosch University [27, 60, 63–67, 71, 111–114]. Most of the preceding research conducted within our research group has focused on the characterisation and optimisation of the micro-fabrication steps required to manufacture simple superconducting devices . Therefore, a basic set of working procedures and parameters have been established for the available equipment. These were used as much as possible so that this research could be focused on investigating the effect of adding high voltage and E-fields to the PLD process. For in-depth coverage of the optimisation of the equipment and working procedures, the reader is referred to the work conducted by previous researchers. The following sections will only cover the main aspects and parameters specifically used within this project. Schenke [115] gives an excellent account of the history and current status of our microelectronics laboratory.

4.2 Film Deposition

Thin film deposition consists of a number of steps, that need to be strictly adhered to, to ensure good quality superconducting films. The entire process for depositing each YBCO film is lengthy and can take a number of hours to complete. Therefore, mistakes are costly, both in terms of materials and time wasted. It is important to work carefully and methodically to ensure that mistakes are eliminated as far as possible. The most important aspects to be aware of, will be highlighted in the next section.

4.2.1 Pulsed Laser Deposition

YBCO films were prepared on (100) MgO single crystalline substrates using PLD. For a detailed account of the PLD system, please refer to the work of Rottier [67] and Maritz [68].

Fig. 4.1 shows the PLD system used here at Stellenbosch University and a schematic representation of the typical deposition setup. The system consist of a few critical components, namely the the laser source (with optics), the vacuum chamber (with vacuum pumps), the target holder, the substrate heater and a source of ambient gas. We will discuss each of these components and their relevant parameters.

Laser Source

The laser source used was a Lambda Physik EMG-203MSC pulsed XeCl excimer laser. It had a wavelength of 308nm and a pulse width of approximately 30ns. The pulse repetition rate could be

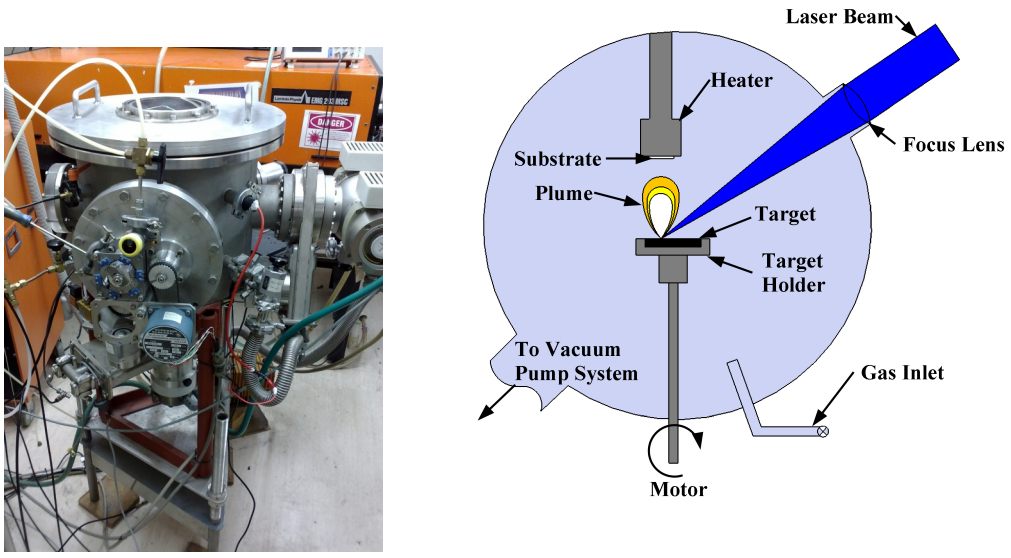

(a) (b)

Figure 4.1: (a) PLD system at Physics Department Stellenbosch University (b) Schematic representation of the PLD experimental setup, with the important components labelled

adjusted from 1-100Hz. A rate of below 10Hz was most frequently used. The energy per laser shot could be controlled by adjusting the voltage applied to the laser. Fig. 4.2 shows the measured pulse output energy as a function of the applied voltage. For this research, the applied voltage was adjusted to obtain an output energy of approximately 220 mJ per pulse.

Laser energy per pulse output of the laser was measured with a pyro-electric detector. The detector produces a voltage pulse proportional to the energy of the laser pulse incident on the detectors surface. The conversion ratio is 1.8 V/J.

Laser Optics

The laser beam is steered toward the chamber via a dielectric multilayer mirror optimised for a 45° incidence angle of the laser beam. The beam is focused, at an angle of 45°, onto the target through a focussing lens and a flat window. All optics are UV-grade fused silica and the total loss through the optics is at least 26% [68]. It is important to keep all optics clean and properly aligned to ensure maximum energy transfer to the target. A dirty lens can also be damaged by localised heating of any contaminated regions.

The position of the focussing lens can be adjusted, to adjust the focus and thus spot size of the laser beam on the target. Fig. 4.3 shows the calibration of the spot size as a function of the distance that the focal lens is from its most focused position. The best fit approximation of the

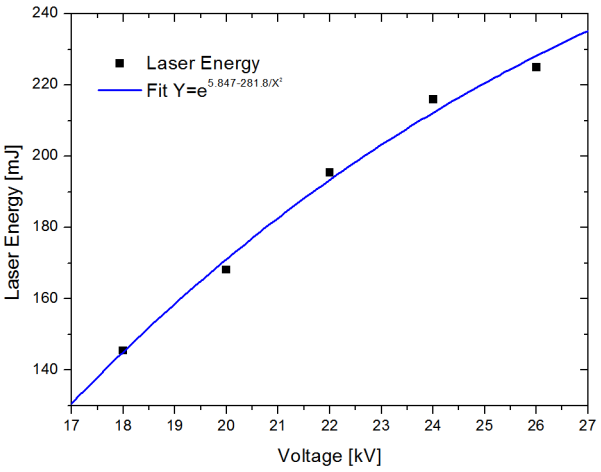

Figure 4.2: Calibration of the laser energy of the beam as a function of voltage applied to the laser

data is given by

$$A_{spot} = \frac{0.31\, e^{(l_{focus}/17.458)} + 4.391}{1000}, \tag{4.1}$$

where A_{spot} is the spot area in cm^2 and l_{focus} is the distance from the most focused position in millimetre. The lens has a total range of movement of approximately 90mm, therefore the spot size can be varied from about $0.005cm^2$ to $0.07cm^2$.

In our experiment, the rectangular laser beam (22mm×8mm) was focussed onto an spot area of approximately $0.01cm^2$ (2mm×5mm) of a rotating stoichiometric YBCO target (50mm diameter, 99.999% purity). The beam was aligned so that it hit the target at least 10mm off-centre, to ensure that the target is evenly used during target rotation. The laser then ablates material from a circular track of the target, rather than a single one spot.

The fluence of the laser beam can be calculated as

$$\text{Fluence}\left[\frac{\text{Joules}}{cm^2}\right] = \frac{\text{Laser Spot Energy [J]}}{\text{Effective Spot Area [cm}^2\text{]}} \tag{4.2}$$

The average laser fluence ranged from 2-3 J/cm^2 depending on the excimer laser energy on the day.

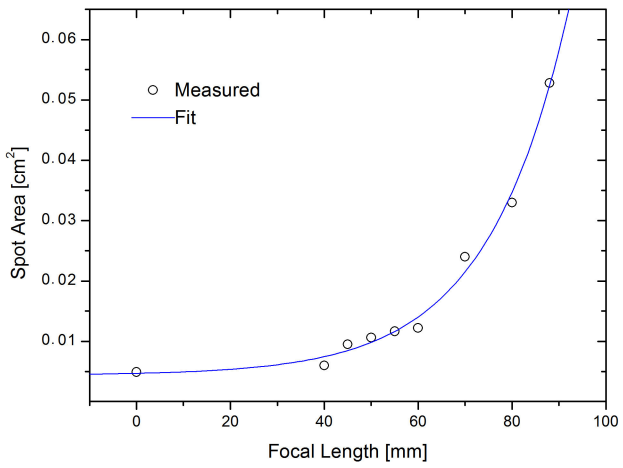

Figure 4.3: Calibration of the laser spot size on the target as a function of the distance that the focal lens is adjusted. (distance from most focused position)

Target holder

The PLD chamber is fitted with a rotational multi-target carousel, shown in Fig. 4.4, that allows up to 6 target materials to be loaded into the chamber at once [68]. Although in principle this should work well, material from one target easily deposits onto neighbouring targets leading to cross-contamination. Therefore, more than one target is rarely used.

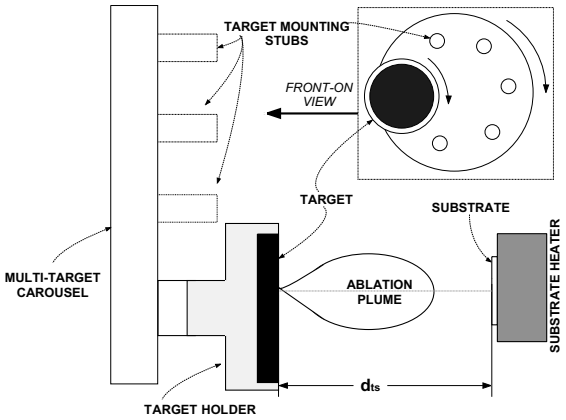

Figure 4.4: Schematic of the standard PLD deposition setup employed here at Stellenbosch University.

The target holder slowly rotates via a stepper motor to facilitate even ablation of target material.

The distance between the target and substrate d_{ts} was was adjusted during our experiments. This was necessary to accommodate various electrode geometries in the deposition chamber. It was

also varied depending on the laser energy, in order to keep the substrate approximately in the tip of the plume if possible.

Xu et al. [116] calculated an empirical relationship between energy density and target-substrate separation as

$$\frac{(E_J - E_{th})}{d_{ts}^2} = 0.14\,\mathrm{J/cm^4}, \tag{4.3}$$

where E_J is the optimum laser energy density, E_{th} is the threshold energy above which any ablation can occur (for YBCO, 1 J/cm^2) and d_{ts} is the target-substrate separation distance. d_{ts} is therefore a significant factor due to its quadratic dependence.

Plume dynamics and interactions of the particles are highly energetic near the target, but drop off significantly in energy and velocity near the substrate. Large particles, such as barium atoms with large velocities can cause sputtering effects on the substrate if to close. On the other hand, if the substrate is too far away there will be hardly any deposition, there is therefore an optimum target-substrate separation distance. As a general rule of thumb the substrate should be positioned at the tip or slightly inside the visible plume (see Fig. 4.5).

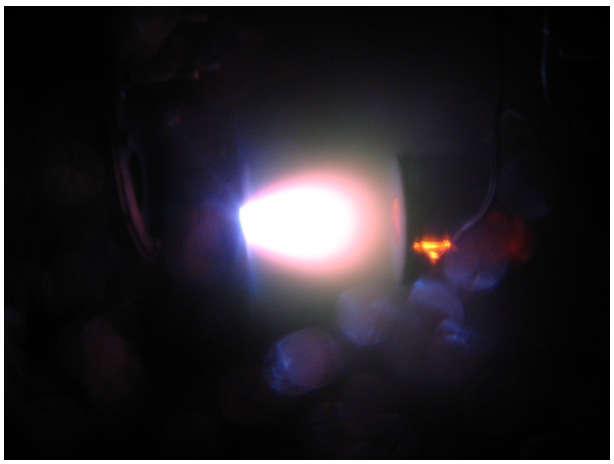

Figure 4.5: Laser ablated plasma plume from a stoichiometric YBCO target in a 0.08mbar oxygen ambient environment.

Conradie [65] also found that the ratios between the various elements forming YBCO vary from the centre to the edges, indicating localised changes in the composition of the different sections of film. Therefore, it is vital that the film be correctly aligned with the plume. Resurfacing of the target after every deposition is extremely important as the plume is pulled off-centre by as much as 20° if it is allowed to etch trenches and grooves in the target, due to excessive deposition from the same track.

Substrate Heater

The substrate heater is a vital part of the YBCO PLD system. The ablated species from the plume condense on the substrate, which needs to be controlled at the correct temperature to ensure proper crystal growth of the superconducting film. For all our experiments a substrate temperature of 723°C was used. The substrate heater was designed and built by [29]. It is a compact and cost effective design that is capable of rapidly heating up to 800°C within 30min. The design makes use of a high wattage halogen bulb to rapidly heat the stainless steel heater block body.

Figure 4.6: Photo of the custom built substrate heater [29], with four samples mounted with conductive silver paint. The temperature probe enters through the heat shield (bottom middle).

The substrates were mounted onto the heater with conductive silver paste[1] to ensure good thermal contact between the heater and the substrate. Fig. 4.6 shows a photo of the heater. Note that the four samples mounted to the heater were not properly glued to the heater. If not enough silver paint is used, uneven heating of the substrate can lead to poor film growth.

The temperature is monitored using a type-K chromel/alumel thermocouple connected to an programmable PID-type temperature controller. The temperature could be controlled to within ±5°C. The temperature probe is connected to the heater body, approximately 1mm below where the substrate is mounted. Fig. 4.7 shows a typical heating profile used for deposition and annealing.

Vacuum Chamber

Establishing a good base vacuum in the PLD chamber accounts for most of the time required to complete a deposition run. A good base pressure ensures that most contaminant gas molecules and water vapour have been extracted, so that the ambient conditions can be precisely controlled to specification. Fewer contaminants mixing with the reactive gas during the deposition helps to

[1] http://uk.rs-online.com/web/p/conductive-adhesives/1863593/

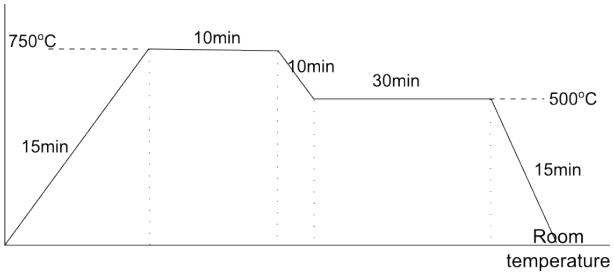

Figure 4.7: A typical substrate heating profile used during deposition and annealing

ensure that reliable results can be attained. Our system has two turbo molecular pumps that allow a base pressure of approximately 3×10^{-6} to be reached.

The PLD deposition chamber is very large, 410mm and 360mm in height (see Fig. 4.1). This makes it ideal for accommodating various experimental configuration and adaptations to the system. However this also makes the system very slow to pump down to high vacuum. The time needed to reach a base pressure of 2×10^{-5} mbar, is nearly four hours. To reach 3×10^{-6} mbar, the system needs to be pumped down over night. This can be very time consuming when trying to characterize a new process where multiple parameter changes are required. In this work, a base pressure of 2×10^{-5} mbar was used for each deposition run.

Oxygen content plays a critical role in the properties of YBCO thin films. Ultra high purity oxygen is fed to the vacuum chamber through a needle valve. This allows accurate control of the chamber's pressure during deposition. A deposition pressure of 8×10^{-2} mbar oxygen was used for all deposition runs in this thesis.

After deposition, the films were annealed at 500°C for 30min in a 1 bar oxygen environment and then allowed to cool down naturally to room temperature. This helps to fully oxygenate the crystal structure of the YBCO thin film.

Sample Preparation

All substrate samples came pre-cleaned and individually sealed from the suppliers. Therefore, they where used as is, without any cleaning procedures. The researcher needs to work carefully to ensure that the substrate samples remain clean and are not left outside for prolong periods of time as MgO and YBCO are both sensitive to moisture and can degrade rapidly if not handled properly.

Deposition Procedure

The target needs to be properly aligned and positioned in the deposition chamber. The surface of the target also needs to be resurfaced periodically and cleaned with acetone and ethanol. The substrates are mounted onto the substrate heater with silver paste. Enough silver paint must be

used to ensure an even coverage of the back of the substrate to ensure good thermal contact is made to the heater. The chamber can be sealed and pumped down to base pressure of 2×10^{-5} mbar. This takes approximately 4 hours, and therefore care should be taken that proper contact is made between the heater and the thermocouple to the temperature controller. The target should be pre-ablated for about a minute to ensure that a fresh surface of YBCO is available for deposition. The target rotator should always be on when the laser is firing, otherwise the laser could fire a hole through the target and cause uneven deposition. The substrate needs to be mechanically shielded from the ablation plume. Once the base pressure is reached the chamber is filled to deposition pressure (8×10^{-2} mbar) with oxygen and the heater controller is turned on to run the heating profile (see Fig. 4.7). Once the substrate reaches the deposition temperature (725°C), the laser can be turned on and deposition can start. It is very important that all the deposition parameters are stabilised and at the correct values before deposition is started. They also need to be continuously monitored to ensure that the deposition is successful. Once the required deposition time has passed, the laser can be turned off. The ambient pressure is raised 1bar and the temperature of the substrate is allowed to cool to the annealing temperature of 500°C. After a 30 minute anneal the heater is switched off and the sample is allowed to cool naturally to room temperature. Once the sample is cool, the chamber is vented with nitrogen and the sample is carefully removed from the substrate.

The parameters used for deposition are summarised in Table 4.1. These parameters are not optimized, but rather chosen close to those regularly used by our research group. As mentioned previously it was not our intention to optimise the deposition parameters for the system. We rather investigated finding a method that could improve the superconducting film quality of films deposited using PLD regardless of the specific deposition parameters. Where needed the parameters in Table 4.1 were adjusted to obtain better films if necessary. This would be for example when the films produced were to thin or attempts to reduce a-axis texturing in the YBCO films.

Table 4.1: PLD parameters used

Deposition temperature	T_{dep}	725°C
Base pressure	ρ_{base}	2×10^{-5} mbar
Oxygen pressure	ρ_{O_2}	8×10^{-2} mbar
Laser pulse frequency	f_{dep}	5-10Hz
Laser fluence		2.3 J/cm^2
Target-substrate distance	d_{ts}	60mm
Deposition time	t_{dep}	30min
Annealing temperature	T_{ann}	500°C
Annealing time	t_{ann}	30min

4.2.2 Deposition Parameter Optimisation

The parameters generally reported to characterise a deposition process are substrate-target separation distance, substrate temperature, base vacuum pressure, background gas pressure, laser fluence and laser firing rate. It has been suggested that this parameter set is insufficient to describe a PLD system completely when comparing it to different systems [70]. This is mostly due to differences in the exact positioning of the various sub-components and where measurements are taken. For example the substrate temperature is often reported without exactly specifying whether it is the temperature measure on the substrate or the substrate heater temperature. The actual substrate temperature could be 60 to 100°C lower than the measured substrate heater temperature. Where the pressure of the chamber is measured in the chamber and the position where the background gas is introduced into the chamber also have significant effects on the quality of the films produced. The size of the deposition chamber, the quality of the vacuum system and the rate at which the gas is cycled through the system is also of significance. Beam homogeneity, and where the laser energy is measured, also have an effect [67]. Where exactly the beam strikes the target and the composition and density of the target are also important. However, despite the importance of these additional parameters they are rarely specified. These other additional parameters are often intrinsic to a specific system and harder to adjust once the deposition system has been established. Most often only the basic controllable parameters are specified and focused on at the expense of universal reproducibility. However, certain universal trends exist in the relationships between the various parameters and what effect adjusting certain parameters have [78,117]. These relationships are useful in optimising and comparing non-identical pieces of equipment.

Researchers initially need to optimise deposition conditions in order to obtain the most ideal controllable parameter set that will produce the best quality films possible. Two of the most commonly used optimisation techniques are *design of experiment* (DOE) [118] and *one-parameter-at-a-time* (OPAT). DOE focuses on characterising the system first and then choosing an optimum from the system's known characteristics. On the other hand, OPAT is a brute force method more focussed on finding an optimum parameter set, and in doing so disovering certain characteristics. Both these techniques require numerous deposition runs to characterise the deposition process and find an optimum parameter set.

OPAT Optimisation

OPAT is the most commonly optimisation technique used here at Stellenbosch [29,60,63,66,111–113,119] and more generally in literature [117,120–122]. This method basically entails optimising one controllable parameter at a time until the best results are achieved. Each parameter is considered individually, keeping the other parameters fixed. Each individual parameter is adjusted over its controllable range. Parameters are then fixed at their optimal values as they are discovered, until all the parameters have been optimised. The premise is that the global optimal is the parameter

set containing all the optimal parameters determined. However, this is not guaranteed (especially for PLD) and further rounds of optimisation may be required. This OPAT method ignores certain two-parameter interactions and can require a large number of experiments to fully characterise a certain process. However, this technique remains popular, because it easy to perform and can deliver good results. This technique also provides the researcher with valuable understanding and intuition of the different effects and sensitivities of each of the control parameters.

DOE Optimisation

DOE uses statistical theory to analyse a whole collection of experimental runs. In doing so a whole system can be characterised for a certain number of key parameters and measurable responses. The resulting mathematical model of the system's behaviour can then be used to choose optimum parameter values. Being able to mathematically model a complex system makes this method very powerful. DOE provides more information per experiment than the OPAT, and it can be used to optimise for multi-parameter interactions. This makes it highly suited to complex processes such as PLD [123, 124]. Rottier [67] employed this DOE method with success, obtaining reasonably good quality YBCO thin films with $T_c(onset) = 91\text{K}$, $\triangle T_c \simeq 5\text{K}$.

Despite Rottier's good results, his optimisation required a very large amount of experimental runs and characterisations per sample. Additionally, the entire PLD system was not be completely characterised. The entire process yielded a single optimum parameter set and a few broadly specified parameter interactions where determined. These relationships are fairly obvious to any system operator with a reasonable amount of experience in using the PLD system. Rottier [67] also hinted at some of the shortcomings of this technique, particularly for our research environment. All the runs have to be performed in a large group, analysed completely and then correctly modelled before this technique can deliver any results. This becomes especially problematic when equipment fails or changes during the course of a group of runs, or during the analysis of the data. Particularly a problem when equipment is constantly being upgraded or modified. Changing the system can invalidate initial experimental runs and require numerous repeat experimental runs. Another difficulty associated with this method is that each of the responses of the system have to be converted into a single numerical quantity. This can sometimes be difficult (for example in the case of XRD or AFM scans) and if performed incorrectly, can lead to misleading results (e.g. with Rottier's surface roughness results). It also negates other more intuitive observations, such as how the film looks to the trained eye (film colour, roughness, etc.), which can be used as a quick acid test as to whether an experimental run was successful. Early recognition of whether a sample film is superconducting can save a lot of time, avoiding the fruitless testing of inferior films (for example, cryocooler testing for superconductivity can take more than half a day to perform correctly).

In our research OPAT was employed due to its simplicity and adaptability to a variable deposition environment. However, it should be emphasised that we did not try to optimise the entire PLD

system again or determine its characteristics. Rather, we attempted to optimise the application of E-fields in the current PLD process to find the best configuration for its reliable application.

4.2.3 Initial System Measurements and Characterisations

The first task we set out to complete, was to determine the effect the many deposition parameters have on the deposition rate our the YBCO material. By doing this we can roughly determine the correct deposition we want to use and what effect any deviation from our desire operating point is. We used a Quartz Crystal Microbalance (QCM) sensor to monitor deposition rate. The QCM sensor works by measuring the change in resonant frequency of the quartz crystal resonator as material is deposited onto its surface. The crystal monitor was calibrated for YBCO as is detailed by [115]. The sensor allowed us to accurately determine the deposition rate while varying the parameters: target-substrate separation distance (d_{ts}), the background oxygen pressure (ρ_{O_2}) and the laser pulse-frequency (f_{dep}). The laser fluence was kept constant at 2.3 J/cm^2 per shot. The sensor was positioned in an on-axis configuration directly in front of the expanding plasma plume. Fig. 4.8 b), c) and d) summarise these results.

The results have all been plotted on the same scale so that one can clearly see the difference d_{ts} has. The further the substrate (or in this case sensor) is placed from the target the lower the deposition rate observed is. The results also show that the deposition rate is directly proportional to the laser pulse frequency. This constant of proportionality varies according to the background O_2 gas pressure in the chamber, the lower the pressure the less the gas molecules disperses the plume material and the higher the deposition frequency.

Although these results offer a reasonable indication of the effect of ρ_{O_2}, d_{ts} and f_{dep}, they do not accurately model the thin film growth on a hot substrate completely. It only gives the rate at which the target material arrives at the substrate. There are a number of competing processes that determine the rate of growth of a film, namely the rate of material arriving, the rate that deposited material is re-sputtered by the incoming target material, and the rate that the target material evaporates when coming into contact with the heated substrate. This experiment only considered the amount of material on the substrate and not the percentage of that material that actually forms part of the thin film. PLD is notorious for large particulates and droplets being ejected from the target, and these appear on top of the growing thin film as large boulders and outgrowths adding to the mass of material deposited but are completely undesired and not part of the thin film. The correct substrate conditions (temperature and background pressure) must be maintained to ensure that the desired thin film crystallises. Furthermore the measurement only considers the deposition rate over the small area of the sensor. The deposition rate for a larger area substrate will be different, due to the limited size of the plume and its dispersion in the chamber.

Each data point collected represents approximately one minute's deposition, so as to minimize the effect of target roughening. This could explain the jagged dependence of deposition rate with

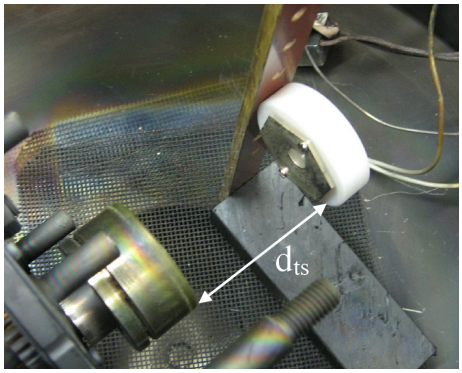

(a)

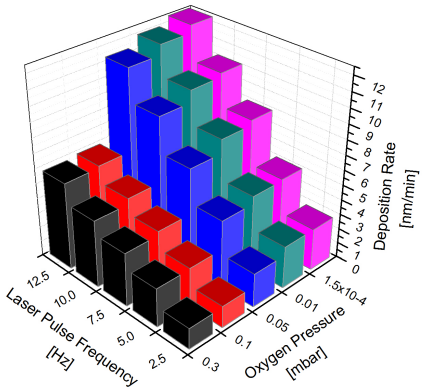

(b) $d_{ts} = 40$mm

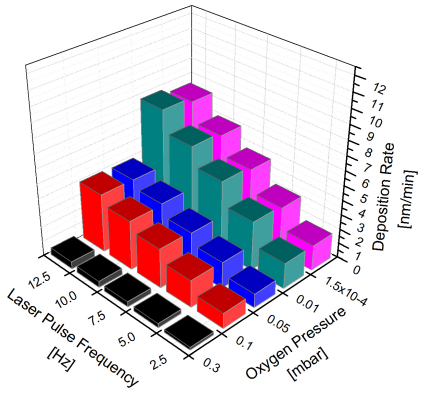

(c) $d_{ts} = 60$mm

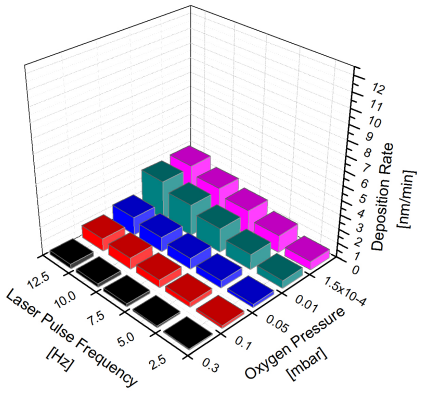

(d) $d_{ts} = 90$mm

Figure 4.8: (a) The experimental setup used to determine the deposition rate with the laser fluence held constant at 2.3 J/cm^2. The QCM film thickness sensor is placed directly in-front of the plasma plume. (b-d) Shows how the deposition rate varies with laser pulse frequency and background oxygen pressure when the sensor and target are separated by (b) 40mm, (c) 60mm and (d) 80mm.

change in oxygen pressure.

The results confirm why PLD is a useful deposition technique. By controlling the laser pulsing frequency, the deposition rate can be precisely controlled with ease. Furthermore, we see that at the deposition parameters most commonly used within our research group ($\rho_{O_2} \simeq 8 \times 10^{-2}$ mbar, $d_{ts} = 40 - 60$mm and $f_{dep} = 10$Hz) we can expect deposition rates in the range of 6-10nm per minute. This will give approximately 300nm thick films in 30-50 minutes, which is what we have come to expect.

4.3 Film Characterisation

The YBCO thin films deposited need to be thoroughly characterised to determine their superconducting and crystalline qualities and surface morphology. This section gives an overview of the equipment and techniques used to characterise the film quality. Three parameters were chosen to assess the quality of the thin films grown, namely surface roughness, crystallinity and superconducting transition temperature.

The superconducting transition temperature (T_c) and superconducting transition width (ΔT_c) were measured by performing non-destructive susceptibility measurements. The crystalline phase and structural characterization were determined by X-ray diffraction (XRD) θ-2θ scans from monochromated Cu$K_{\alpha 1}$ radiation. Atomic force microscopy (AFM) was used to observe the thin film surface morphology. Standard light microscopy was also used as a quick test of film quality and the intermediate results of the fabrication process.

4.3.1 Atomic Force Microscopy

AFM is a very sensitive technique that is capable of producing atomic resolution 3d scans of material surfaces. These scans are used to determine the surface morphology of thin films, providing an indication of the surface roughness, number and size of particulates present on the surface and even provide material characteristics of the thin film. It can also be used to scan devices fabricated on the surface of a film for imaging and quality control purposes. AFM is also a useful tool for determining the thickness of thin films, if a step-edge can be defined and the film is not too thick.

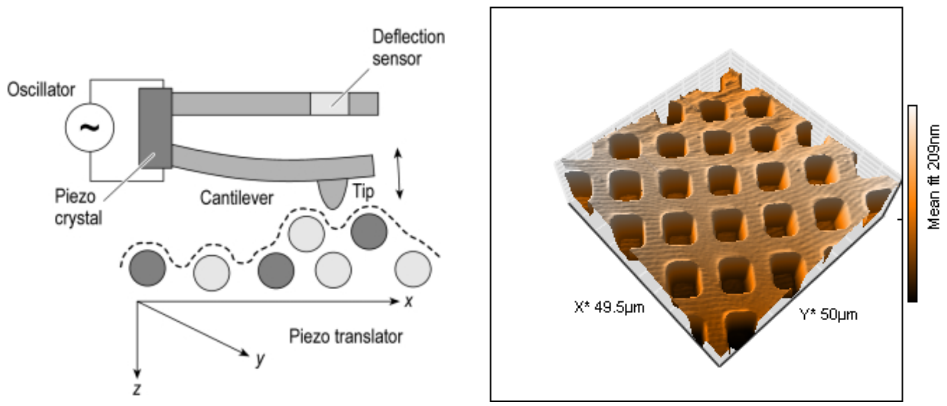

(a) (b)

Figure 4.9: (a) The basic operating principle of an AFM. The deflection of a sharp tip in close contact to a surface is measured. [125] (b) An AFM image of the calibration sample. The structure consists 10μm×10μm square holes that are 100nm deep.

The main sensing element of an AFM is miniature cantilever with a sharp tip at its end. This tip, is scanned over the samples surface, while the deflection of the cantilever are monitored and

recorded (see Fig. 4.9 (a)). The cantilever is flexible and bends easily in response to the interacting forces between the tip and the sample surface [125]. Sample surface features deflect the cantilever and this is recorded as a 3d surface map. These images contain direct depth information of the samples surface features. AFM measurements can provide height (or depth) and lateral resolution down to atomic resolution [126] This technique's analytical potential lies in the fact that imaging can be performed over larger areas up to $100\mu m$ and then zoom into details of interest [125]. Furthermore, both conducting and insulating materials can be analysed without sample special sample preparation [126].

The average surface roughness R_a of a film is defined as [126]

$$R_a = \frac{1}{N}\sum_{i=1}^{N} |z_i - \bar{z}|\,, \tag{4.4}$$

where z_i is the height measured for at N sample points, and $\bar{z}$ is the average height of all the sample.

In general the surface roughness of thin films intended for microelectronic application needs to be extremely smooth. This is important for so that small device structures can be well defined. For example, high quality superconducting films need an average surface roughness less than 15nm to be acceptable for practical applications. If large particulates are present on the film, they can cause unwanted shorts or completely ruin smaller features.

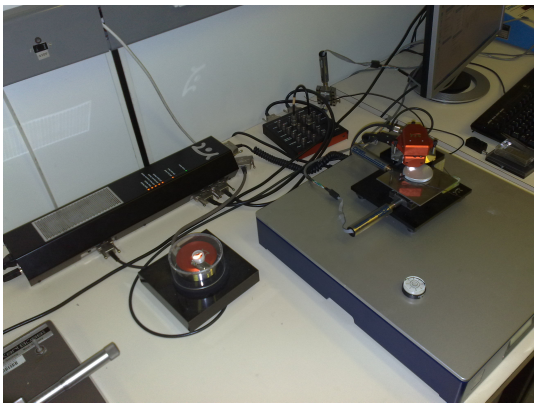

Figure 4.10: The *Nanosurf Easyscan2* compact AFM measurement unit, standing on its stabilization table, with the controller behind it.

In this research, we used the *Nanosurf EasyScan2 AFM*[2], shown in Fig. 4.10. It was mounted on a stabilization stable table to isolate it from the laboratory environment vibrations. This AFM is highly compact, easy to operate and does not require a vacuum environment to operate. It was used extensively to analyse the surface roughness of the thin films deposited and also helped

[2]http://www.nanosurf.com/?content=0402

to determine their thickness. It was used exclusively in non-contact mode as the tips lasted the longest and this mode provided the most accurate measurements. The AFM was calibrated using standard micro-structures provided with the equipment, as shown in Fig. 4.9 (b).

4.3.2 X-Ray Diffraction

XRD is widely used throughout to provide detailed knowledge of the composition of solids [127]. It is generally used to characterise the crystal structure of materials. XRD is based on the principle that the regular spacing of atoms in a crystal structure act like diffraction gratings to X-rays [127]. This is possible, because the wavelength of the X-rays are of the same order of magnitude as the atomic spacing of atoms in the crystal lattice. Furthermore, parallel planes of atoms reflect the incident X-rays according to Bragg's diffraction law,

$$\sin\theta = \frac{n\lambda}{2d}, \tag{4.5}$$

where d is the interlayer spacing, θ is the X-rays' incidence angle and λ is the X-ray wavelength, as is illustrated in Fig. 4.11. If the indecent X-ray waves are slightly out of phase then destructive interference occurs therefore, n is usually chosen to be one and monochromatic beams are used [127].

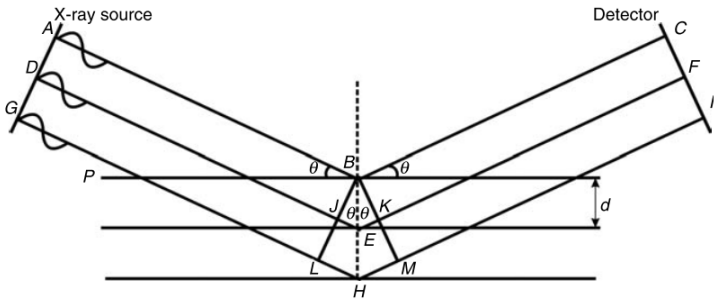

Figure 4.11: Bragg X-ray reflection from a set of parallel atomic planes. [127]

By scanning an incident X-ray beam over a sample, measuring the angle of incidence and the intensity of the reflected beam, it becomes possible to recover the interlayer spacings of the atoms, using

$$d = \frac{n\lambda}{2\sin\theta}, \tag{4.6}$$

where θ is the position of strong intensity peaks in the X-ray diffraction pattern. A powder diffraction pattern of measured intensities is plotted against 2θ. The measured pattern of peaks acts as a

fingerprint that identifies a particular crystal structure. If we know what the crystal structure should be, then we can recover the lattice parameters using the measured d-spacings, the corresponding Miller indices [127], and the following equation that relates the two, for the orthorhombic phase [63]:

$$\frac{1}{d^2} = \frac{h^2}{a^2} + \frac{k^2}{b^2} + \frac{l^2}{c^2}. \tag{4.7}$$

XRD was used to characterise the crystal structure of the YBCO thin films. The presence of the proper c-axis peaks confirms the c-axis growth of the thin films, and the specific position of these peaks can be used to determine the oxygen content of the films. Fig. 4.12 shows a typical XRD pattern for a c-axis orientated YBCO thin film with $T_c = 89$K, grown by PLD. The appearance of the appropriate peaks and in the appropriate ratios give an indication of film quality. Furthermore, the c-lattice constant of YBCO tends to shrink with increasing oxygen content. Therefore, the calculated lattice constant can used as a measure of the quality of the superconducting crystal grown.

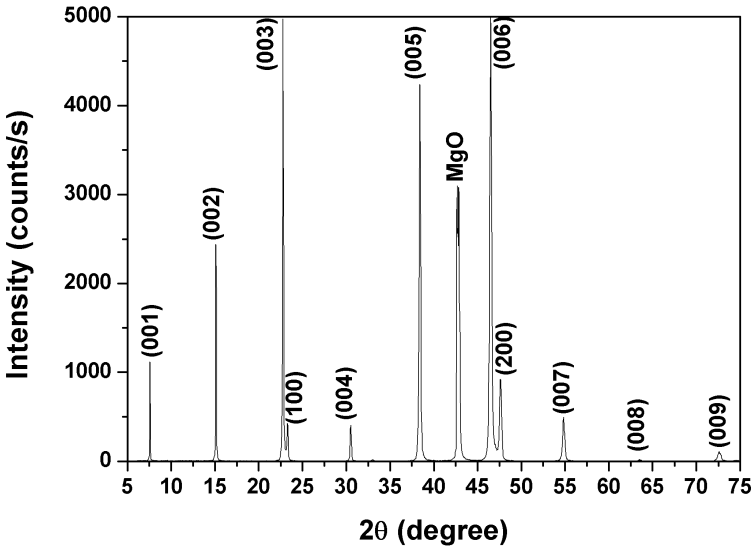

Figure 4.12: A typical XRD pattern for a good c-axis orientated PLD grown YBCO thin film (T_c=89K)

A X'Pert Powder PANalytical X-ray diffractometer[3] was used to measure the XRD patterns of the films deposited in this thesis. This system uses a monochromated Cu $K_{\alpha 1}$ radiation source with a wavelength of λ = 1.54 Å. The machine uses a θ-θ vertical measurement configuration [127], and gives information on the phase, orientation and lattice parameters of the films.

For fully oxygenated orthorhombic YBCO the c-axis (001) peak 2θ positions can be calculated, using (4.7). Table 4.2 summarises the values for the first seven peaks.

[3] http://www.panalytical.com/XPert-Powder.htm

Table 4.2: YBCO c-axis XRD peak 2θ positions

Peak	(001)	(002)	(003)	(004)	(005)	(006)	(007)
2θ [°]	7.57	15.17	22.84	30.61	38.54	46.66	54.36

4.3.3 Susceptibility Measurements

Susceptibility tests were performed to characterize the superconducting properties, the critical temperature (T_c) and superconducting transition width (ΔT_c) of the films. In this way the characteristics of freshly deposited films, without any further processing steps, could be determined. Additionaly, this measurement yields results that are more representative of the entire film, rather than one patterned region (as is the case with resistivity measurements).

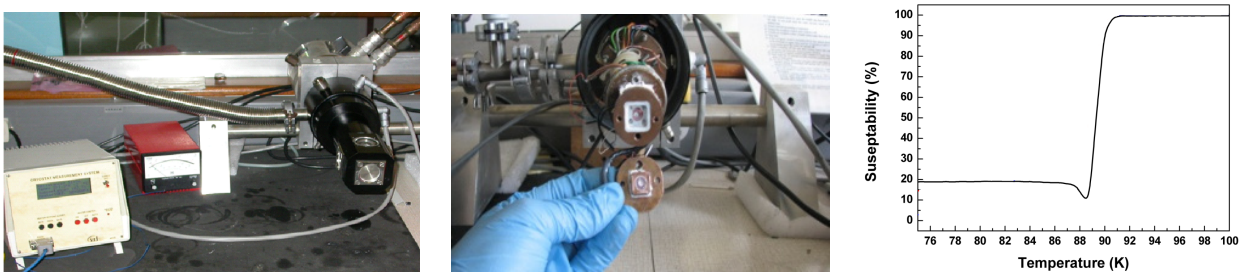

(a) (b) (c)

Figure 4.13: (a) The 35K cryocooler, vacuum pump and data acquisition unit. (b) The susceptibility sample mount on the cryocooler coldfinger. (c) Typical susceptibility measurement for a YBCO sample (T_c=89K).

The cryocooler used for the susceptibility test is shown in Fig. 4.13(a). The sample is mounted between two planar coils situated inside the cold finger (see Fig. 4.13(b)). The primary coil is used to generate a magnetic field perpendicular to the films surface, coupling to the secondary coil that acts as a pick-up coil. The primary is driven with a 1V peak-peak 1MHz sinusoidal signal. The percentage of the signal coupled to the secondary coil is measured. Above T_c nearly all of the signal is transmitted through the sample. Below T_c, the Meissner effect causes the superconductor to expel all magnetic fields from it interior, effectively blocking the signal through the sample and the measured signal drops close to zero. Fig. 4.13(c) shows a typical superconducting transition captured for an YBCO sample. The signal never goes completely to zero, due to coupling through other sources in the laboratory. The measurements are captured to computer for display and data storage.

4.4 Device Fabrication

Micro-fabrication is essential in the process of turning thin films into functional devices. Good quality films are useless unless practical devices can be fashioned from them. High temperature

superconductors such as YBCO are highly sensitive to any processing and deteriorate easily with excessive handling [114]. It is therefore important to keep the number of processing steps to a minimum. Processes should also be as non-invasive as possible to the superconducting layers or parts thereof that make up the device. The first step of the process is patterning the film.

4.4.1 Photolithography

Photolithography can be described as the process wherein an image or pattern is transferred from a mask onto a thin film. In this way devices can be patterned and defined in the thin films. The steps involved consisted of resist application, exposure, development, etching and resist removal. The first steps up to etching are shown in Fig. 4.14. This has become a very standard process in our laboratory and our group is able to routinely define up to 4 micron sized features. For a more in depth review of the photolithography process employed here at Stellenbosch University, please see [27, 60, 112].

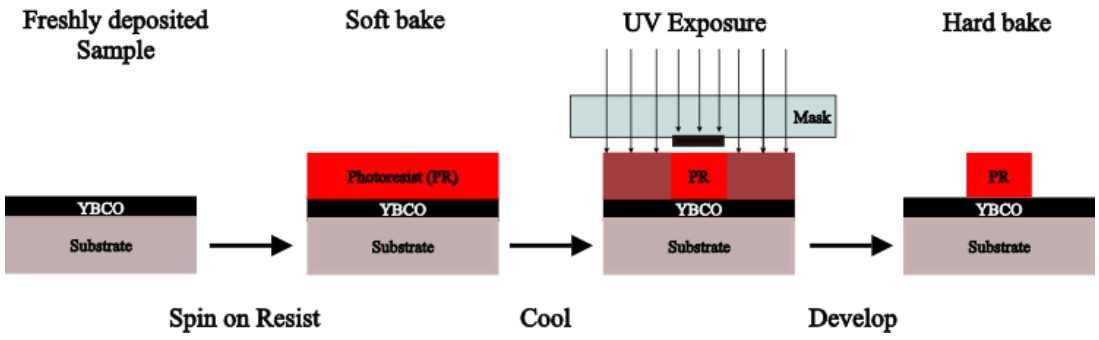

Figure 4.14: Steps involved in the photolithography process.

In this process a light-sensitive film (photoresist) are applied to the sample's surface. A mask with a suitable pattern used to shield certain areas of this photoresist from exposure to the light source. The exposure to the light causes the photoresist to either be strengthened (negative photoresist) or weakened (positive photoresist) through certain polymer cross-linking reactions. The area that are left weak can be washed away (developed) and this leaves a copy of the pattern on top of the sample (see Fig. 4.14), defined in the photoresist material. The copy could be a positive or negative copy of the origonal pattern depending on the type of photoresist used. This remaining photoresist is usually hardened further and then it acts as the shield to the physical etching away of the sample material.

For our research we use ultraviolet (UV) light to expose a positive photoresist ma-P 1225[4] (see Appendix A.A.1 for the datasheet). UV lithography is a simple and effective method way of patterning line widths greater than 1μm. UV light is used rather than visible light due to its shorter

[4] http://www.microresist.de/products/positive_photoresists/overview_pos_en.html

wavelength and therefore ability to define higher resolution structures. The UV alignment and exposure unit is shown in Fig. 4.15.

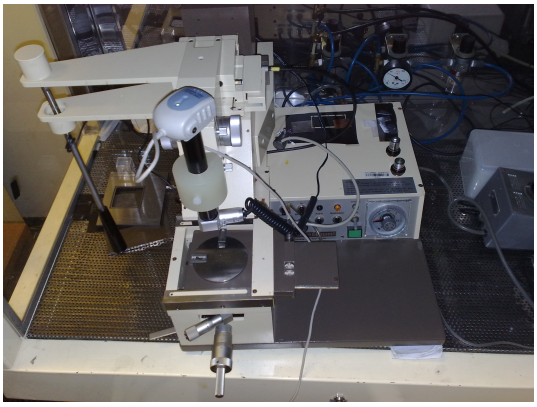

Figure 4.15: The UV photolithography alignment and exposure unit.

It is extremely important that the cleanliness of the sample is maintained through all of the processing steps, as en small pieces of dust or remnants of old photoresist can ruin the whole process. The sample was first ultrasonically cleaned in acetone and then ethanol, and finally rinsed with deionised water and dried using a burst of nitrogen gas. Proper cleaning of the sample is essential to obtain a uniform layer of photoresist on the sample. The samples need to be inspected for cleanliness using the optical microscope.

The photoresist was then spun onto the sample at 4500rpm for one minute to obtain a uniform coating of the sample surface that is of approximately 2.5μm thick (see Appendix A.A.1). The sample then needs to be pre-baked before UV exposure, to help activate the photoresist. This soft bake helps to evapourate the solvent from the photoresist. This is a critical step that needs to be consistently applied as it affects all subsequent exposure and development steps. The sample needs to be allowed to cool to room temperature before proceeding steps. This is due to the chemical nature of the exposure step and that any variations in photoresist temperature will lead to varying results.

Next, the samples were aligned to the mask [60] and then exposed to UV light. The exposed regions become softer and can be washed away using the appropriate developer, ma-D 331[5]. The samples were exposed for 1 minute and then developed for 30 seconds. A post-bake (hard bake) is required after development to improve the photoresist adhesion and chemical resistance. The temperature is typically the same or slightly higher than that of the pre-bake, but, however, needs to be performed for a longer period.

The finer the details and resolution of the mask, the more expensive it is to manufacture and the more stringent the processing steps become to pattern the photoresist properly. The standard masks used for the contact UV lithography are usually chrome masks, produced professionally

[5] http://www.microresist.de/products/positive_photoresists/overview_pos_en.htm

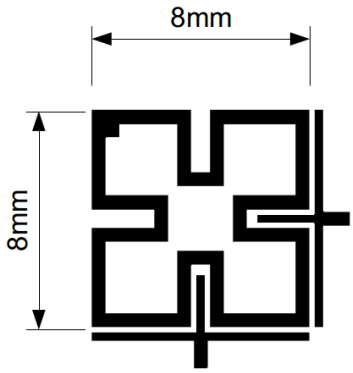

Figure 4.16: The compact dual-mode filter mask pattern.

produced on 4" plates. The chrome masks consists of a thin layer of patterned chrome on a glass plate. Features up at about 3μm can be designed and implement in the masks. These masks are very expensive and take some time to have manufactured. However, they produce excellent results and have a long lifetime, if handled properly. The filter pattern of the microwave filter device that we constructed is shown in Fig. 4.16. Due to time constraints and the lack of an appropriate chrome mask, we used a normal acetate overhead transparency to define the mask. Schenke [115] reviewed the merits of these different options, noting how the loosely packed toner on the transparency films results in edges that are not as well defined (see Fig. 4.17). This type of mask is only acceptable for features down to 60μm. The filter device that we manufactured in this thesis was relatively large, with a smallest feature size of 200μm (the gap between the main resonator and the feedlines, see Fig. 4.16). This mask was therefore considered acceptable considering the constraints of funds and time, and the advantage that the mask could be manufactured in house inexpensively.

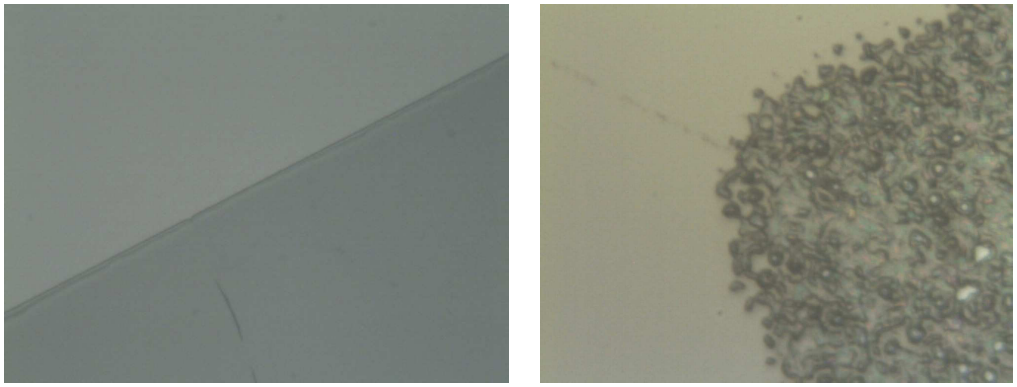

(a) (b)

Figure 4.17: The photoresist edge profile made using (a) a chrome mask and (b) a mask printed on transparency. [115]

The processing parameters of the whole process usually need to be optimized regularly due to ageing of the photoresist and developers. Table 4.3 details the optimised photolithography processing parameters used in this project.

Table 4.3: The used UV Photolithography parameters

Resist	ma-P 1225
Spin	4500 rpm for 35 sec
Pre-bake	115°C for 60 sec
UV exposure	90 sec
Developer	ma-D 331
Develop	90 sec
Post-bake	115°C for 5 min

4.4.2 Thin Film Patterning

Patterning is a process of selectively removing sections of a thin film, transforming it into functional patterns and ultimately a device. Once the photoresist layer has been successfully patterned onto the surface of the thin film, the film needs to be selectively etched way in the exposed regions. A wet etching technique used by [64, 112, 114] was employed to remove the unwanted YBCO regions of the thin film.

The wet etching process involves chemically etching the unwanted parts of the film by washing it dilute solution of citric acid. A 0.1mol solution of citric acid was made by dissolving 10.4g of citric acid in 900ml of deionized water. The samples were etched by immersion into the citric acid solution and applying gentle agitation. The samples were completely etched in 45 seconds. The samples need to be rinsed in deionized water directly afterwards to prevent any further etching. Visual inspections are needed to ensure that all the YBCO had been etched away, and if not, the sample can be etched further. When the process was complete, the excess resist was removed by rinsing the sample in acetone or photoresist remover (mr-Rem660 Photoresist remover). Fig. 4.18 shows a photo of the YBCO sample on MgO, after etching. The optical microscope inspection of the sample showed that there was no significant reduction of the YBCO lines in widths ($\pm 10\mu$m).

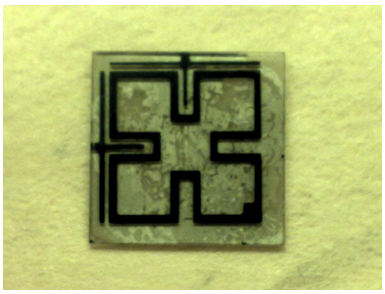

Figure 4.18: YBCO thin film etched into a filter structure.

4.4.3 Making Electrical Contact

One of the final and most important steps in the fabrication process is making electrical contact to the device. In order to connect the sample to external test equipment, electrical contacts must

be provided. The device is rendered useless if electrical signals cannot be transferred in and out via low contact resistance electrical connections. The devices would not be able to be used in conjunction with other electronic equipment. Good low resistivity contacts are required which have good adhesion to the superconducting layers. The contacts must also be able to retain their good adhesion down at cryogenic temperatures.

The ceramic nature of HTS crystal layers makes it inherently difficult to make good contact to them using conventional methods such a soldering. Soldering poisons the YBCO layers, making them lose superconductivity. Sticking anything to the superconductor is also very difficult, as most glues loose their stickiness down at cryogenic temperatures.

Wirebonding is the standard connection method used in our research group [27, 60, 112, 114]. In order to bond the extremely thin gold wires to the surface of the superconductor, thick contact pads have to be deposited. Historically this has been one of the biggest stumbling blocks to the research carried out here. Wirebonding often fails, because the contact pads are either too thin or do not have enough adhesion to the surface of the superconductor, and simply flake off. The pressure of the wirebonding needle forces it straight through the soft metal contacts, damaging the underlying YBCO layers.

Wirebonding could not be performed at the time of the filter device manufacture, due to the wirebonder being broken. Therefore, an alternative method of making contact to the films was sought. Silver contact paint has been tried in the past as a conductive adhesive for metal wires, but with limited success [66]. The wires were pasted onto the surface of the superconductor to make electrical contact. At room temperature the silver paint adheres well and seems mechanically sound. However, it has never been reliable enough, working only occasionally. The extreme cooling to cryogenic temperatures and the mismatch in thermal expansion between the silver paint, the superconducting film and the contact wire, lead to the silver paint coming loose and breaking contact mid-way through measurement.

We tried an alternative procedure, whereby a small piece of aluminium shielding metal tape [6] was used to connect the test board to the delicate feedlines of the YBCO filter. Silver paint was then used to paint a connection between the test board (Rogers 4003 board with copper tracks, a ground plane and standard SMA connectors). The aluminium tape provided a flexible substrate for the silver paint to rest on (particularly in the small gap between the test board and sample substrate) so that, at extreme temperatures, the cracking of the paste can be avoided. This proved to be relatively successful if care was taken to slowly cool the sample and test structure. Fig. 4.19 shows the completed filter, attached to test board.

The method was tested on a YBCO sample to measure resistivity as the temperature was lowered below T_c. The result is shown in Fig. 4.20. The measurement shows that there is a residual resistivity of about 15Ω due to the silver paint contacts. Although this was not ideal, it was the only means available at the time of filter testing.

[6] http://uk.rs-online.com/web/p/aluminium-tapes/7362207/

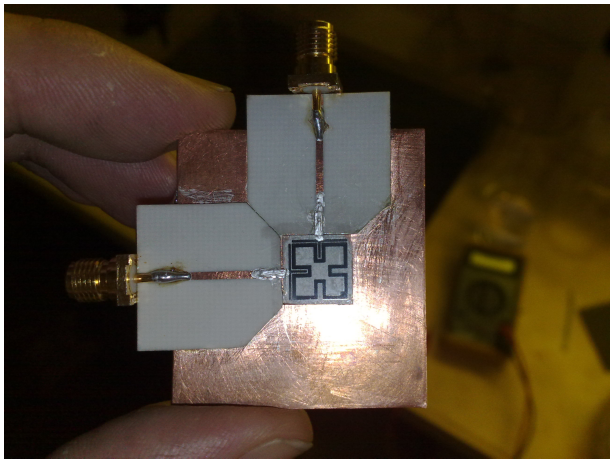

Figure 4.19: The completed filter and test structure. Note the silver paint contacts made between the YBCO filter and the test structures.

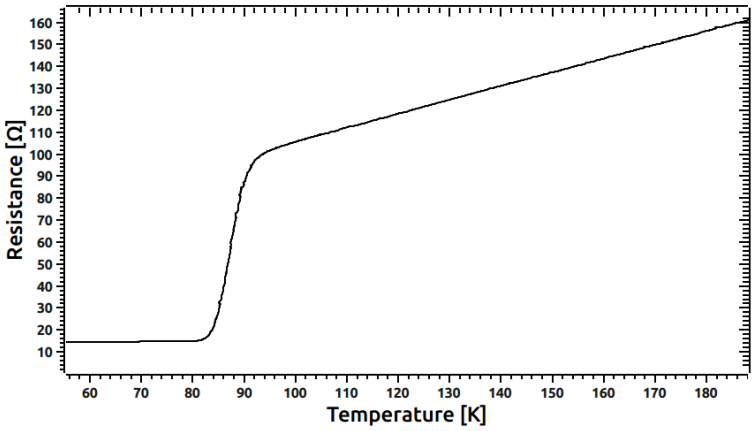

Figure 4.20: Superconducting transition measured with the makeshift silver paste connections. ($T_c(onset) = 91$K, $\triangle Tc = 7$K)

4.5 Conclusion

The basic thin film deposition, fabrication and characterisation process were presented here. Each processing step was highlighted so that this work can be accurately repeated in the future. A number of small fabrication problems, such as no suitable chrome exposure mask, or the wirebonder not working, were overcome by adapting the process as best we could to deliver a working device. The thin film fabrication and analysis techniques presented in this chapter, formed the basis of the experimentation that will be presented in the the next chapters. In the following chapters, the effect of adding static E-fields inside the PLD chamber during deposition are investigated. Here the focus was on finding the best solution that enhanced the superconducting properties of the films produced. A wide variety of electrodes and setup geometries were considered. However, the basic deposition parameters were kept as constant as possible to provide a baseline with which

to compare the results. The various experimental runs were also performed as close together as possible. Experimental runs were preferably all run on the same day to ensure that the same deposition conditions were kept. The final filter structures testing will be discussed in Chapter 7

Chapter 5

DC Plasma Enhanced PLD of YBCO

The potential advantages of adding electric fields and electric potentials into the PLD chamber during deposition, have been highlighted in Chapter 3. Particularly the work of [17, 25, 38, 74, 80, 92, 94, 102] showed that it could be used for improving the quality of YBCO films deposited at lower temperatures. However, we also identified a number of gaps that exist in the literature regarding this phenomena, including the following:

1. Are there any instability issues associated with the plasma discharge as reported by various researchers [38, 81, 91, 102]?
   (a) Can this be avoided?
   (b) Is a plasma discharge required?
2. A limited range of voltages have been studied, with +300V being the most prevalent (see Table 3.2)
   (a) To what extent does this effect work with different values?
   (b) Why are not larger values reported?
3. There is little understanding as to why this method works.
   (a) Why does one potential work better than others?
   (b) Why does the opposite voltage not work?
4. Why is the use of this technique not so widespread?
   (a) How could the method be changed to improve its adoption?

In this chapter we attempt to answer some of these questions. We report on how we recreated some of the results from literature and highlight our experiences and the challenges experienced using this method. We will also suggest a number of improvements, which served as the foundation for the novel research presented in the next chapter.

5.1 Target Electrification

5.1.1 Setup and initial testing

The first approach that was investigated was applying a voltage directly to the target holder during deposition. This configuration is most similar to those considered by [100] and [81]. This configuration was considered the most simple to implement as no additional electrode needed to be introduced into the chamber. Figure 5.1 shows a schematic representation of the experimental setup inside the deposition chamber. The schematic shows that the standard PLD positioning of the target and substrate were used. The substrate was positioned directly in front of the ablation plume. In our configuration, only the target was electrified by touching a high-voltage cable to the bare metal target holder (see Fig. 5.3 (a)). The target holder was insulated from the target carousel and the rest of the chamber using a specially made Teflon insulating stub. The rest of the chamber, including the substrate heater, was electrically grounded. We decided to bias the target rather than the substrate, due to our lack of a special substrate heater that Izumi et al. used [81]. It is difficult to bias the substrate heater due to its very high temperature. Standard insulation materials will melt making it difficult to isolate the HV wire from the deposition chamber. There is also the danger that the high applied voltage will damage the thermocouple used to measure the substrate temperature. Therefore, biasing the target was considered the best choice available.

The experimental setup for generating and introducing HV into the deposition chamber is shown in Fig. 5.2. Two custom built HV power packs were used to generate voltages ranging from -6kV up to +6kV (see Fig. 5.2 (a)). The positive and negative power supplies were rated up to 5mA. The voltage on the electrode was monitored using a HV probe connected to a standard multimeter. The HV was fed into the vacuum deposition chamber using high tension cables via a custom made Teflon feed-through (see Fig. 5.2 (b), (c) and (d)).

Figures 5.2 (e) and (f) show the ablation plume when applying -400V and +400V, respectively, to the target during deposition. The background oxygen pressure was 8×10^{-2} mbar and the target-to-substrate distance (d_{ts}) was 60mm. No significant difference was evident from the appearance of the plume. A maximum voltage of 400V, could be applied to the target before unwanted electrical discharge and arcing occurred using this oxygen pressure. Applying a negative voltage was far more problematic and was more likely to cause arcing than applying a positive voltage.

The voltage measured (400V) when no background gas was present in the chamber, dropped as soon as oxygen was introduced (350V). This indicated that a small current was being drawn from

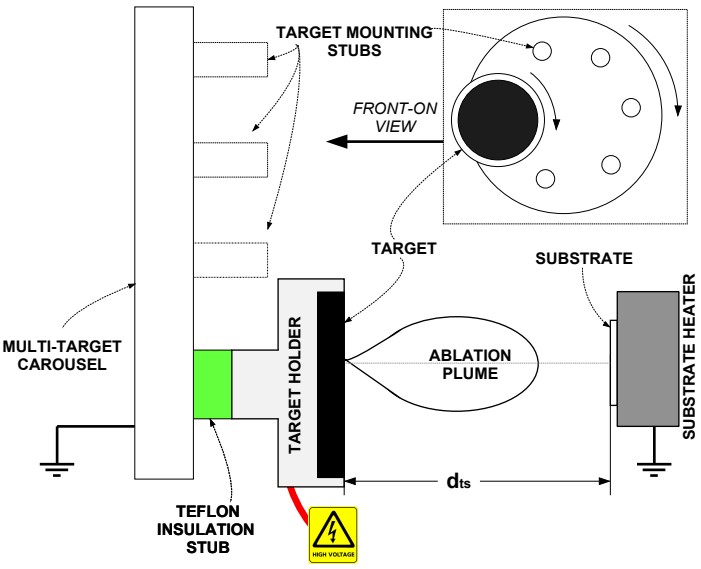

Figure 5.1: Schematic of the initial experimental setup. Only the target is electrified. The entire chamber and substrate heater are grounded.

the electrode to charge the gas present in the chamber. As soon as the laser started pulsing the voltage dropped further to 185V. This would indicate the periodic discharging of the target during each laser pulse. The target was assumed to discharge through the highly conductive plasma plume. This was also verified on an oscilloscope.

Fig. 5.3 (b) and (c), show the effect of background gas pressure. The background oxygen pressure was lower ($\rho_{O_2} = 2 \times 10^{-2}$ mbar) for (b) and higher ($\rho_{O_2} = 1 \times 10^{-1}$ mbar) in (c). The top images show the faint DC glow discharge present when the laser was off, and the bottom two images show the plume during deposition. The plume is much brighter in (c) due to the higher ambient oxygen pressure.

For a lower background pressure the glow is much fainter as there are fewer gas molecules present. The higher background pressure showed more arcing (bright spots in image) and the glow is brighter and concentrated around the target and target carousel (the nearest grounded object in chamber). This can be explained by the number of charge carriers present in the chamber. For a higher pressure more gas molecules and therefore charge carriers are present and can be excited by the charged electrode.

Discussion

The arcing (i.e. the random discharging of the electrode) is unwanted, because it causes instability in the depostion conditions and can cause unwanted contamination and damage in the high vacuum chamber [85]. Arc currents, although brief, can have very high temperatures and under vacuum cause the evaporation of unwanted residual materials from previous depositions as well as

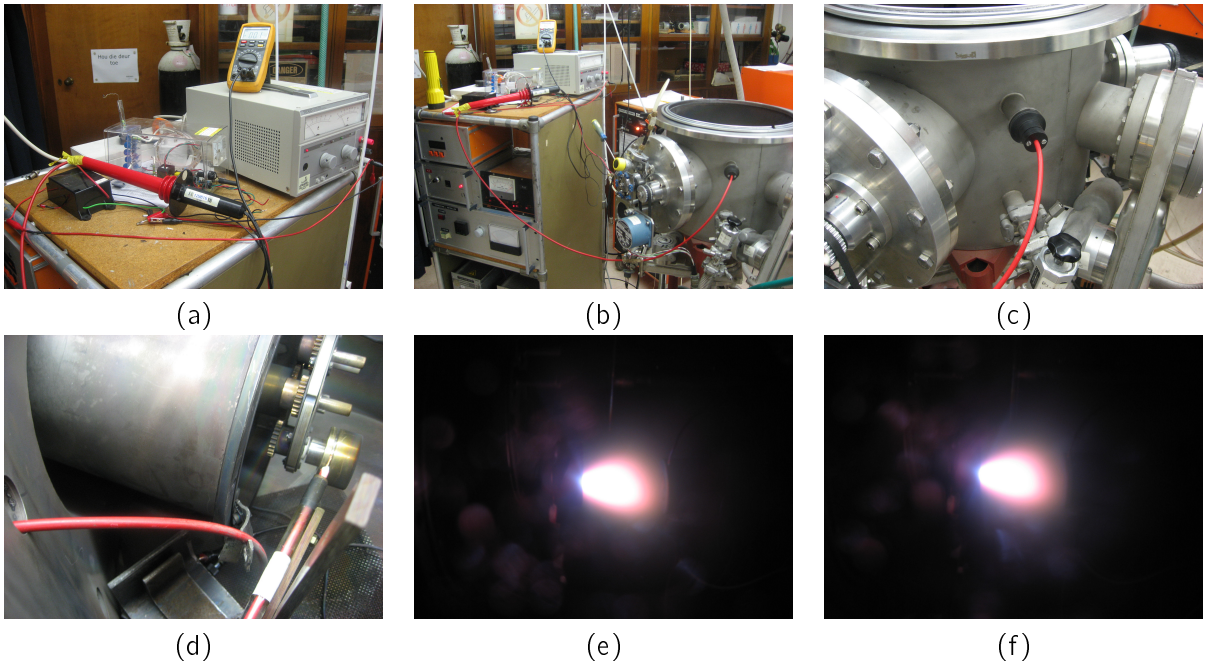

Figure 5.2: Experimental setup for electrifying and measuring the target potential (a-d). (a) HV power supplies connected to the HV probe. (b) A wider view showing how the HV wire is run from the HV probe into the chamber. (c) A closer view of the custom made feed-through port on deposition chamber. (d) Inside the chamber the HV wire is touched to the target, which is free to rotate. Photos of the plume when applying (e) -400V and (f) +400V to the target during deposition ($\rho_{O_2} = 8 \times 10^{-2}$ mbar, $d_{ts} = 60$mm).

the equipment itself. These contaminants can react with the plume during deposition. YBCO is very sensitive to any contamination, requiring nearly perfect stoichiometry to obtain good superconducting films. Additionally, arcing can cause uncontrolled drops in the potential that exists on the electrode. We desire controllable parameters to be able to produce repeatable results. Therefore, this technique requires that we run the deposition at voltages below the limits that cause arcing. We determined the maximum and minimum voltages to be +400V and -400V. These were for the standard deposition parameters shown in Table 5.1.

Table 5.1: Standard YBCO deposition parameters

Target-Substrate Distance	60mm
Laser Fluence	2.37 J.cm^{-2}
Laser Frequency	5Hz
Deposition Temperature	723°C
O_2 Deposition Pressure	7×10^{-2} mbar
Deposition Time	20min
Anneal Temperature	500°C
O_2 Anneal Pressure	1 bar
Anneal Time	30min

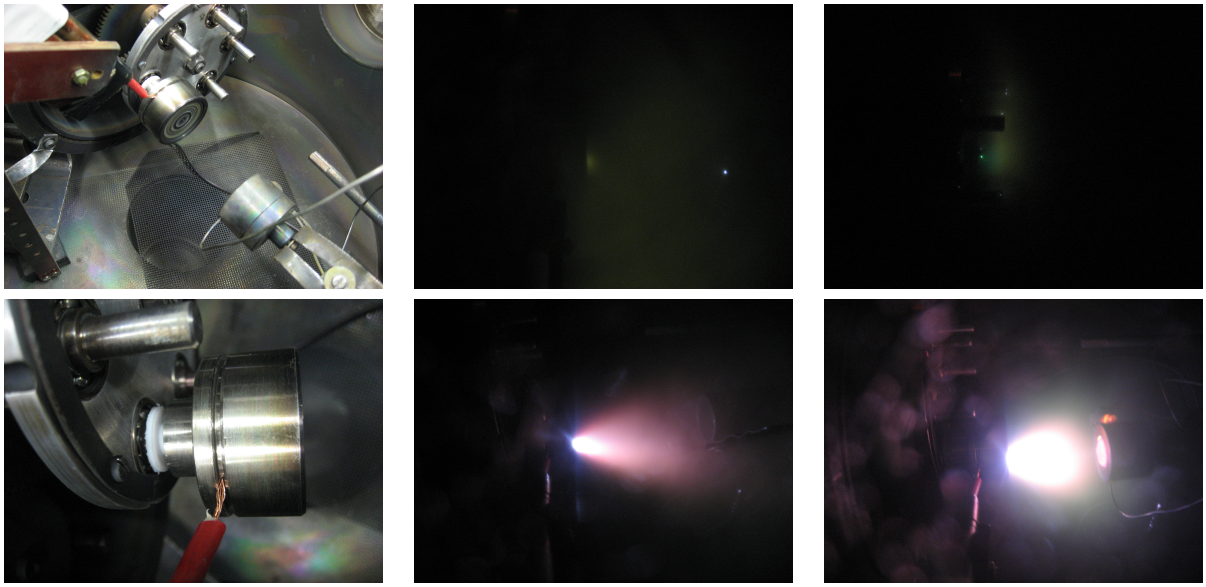

(a) (b) (c)

Figure 5.3: (a) First attempts at applying a potential directly to the target. The target is insulated from the rest of the chamber and that target rotator by a Teflon stub (seen more clearly in the lower image) to which it is mounted. Photos of the electrified target in action with +400V applied are shown in (b) with the background oxygen pressure, $\rho_{O_2} = 2 \times 10^{-2}$ mbar and (c) $\rho_{O_2} = 1 \times 10^{-1}$ mbar, respectively. The bottom images show the plume created during a laser pulse.

Having determined the initial working parameters of the setup, we set out to test the technique for the deposition of YBCO on MgO (100) single crystal substrates.

5.1.2 YBCO Deposition on MgO Substrates

MgO (001) was the first substrate material we attempted deposition on with the electrified target. The deposition parameters are listed in Table. 5.1. Three bias voltages were investigated: -400V, 0V and +400V. These represented the extreme values that could be used before arcing occurred.

Figure 5.4 shows the optical microscope images of the three films deposited. The +400V film seemed to have the roughest surface, containing the most particulates. The -400V film appeared the smoothest. These results were confirmed by the AFM analysis shown in Fig. 5.5. The three films had a surface roughness of 26nm, 6nm and 7nm respectively (+400V, 0V, -400V), determined from 5μm×5μm square scans of the samples on the smoothest sections. Interestingly, the -400V samples was not the smoothest. However, the 0V sample showed the largest number of micrometer sized particulates.

XRD scans of the samples showed that they all exhibited predominantly *c*-axis growth (see Fig 5.6). However, the -400V sample showed the highest intensity peaks, indicating better crystallinity, as is shown in Fig. 5.7 (a). The -400V sample also showed a very small amount of *a*-axis texturing,

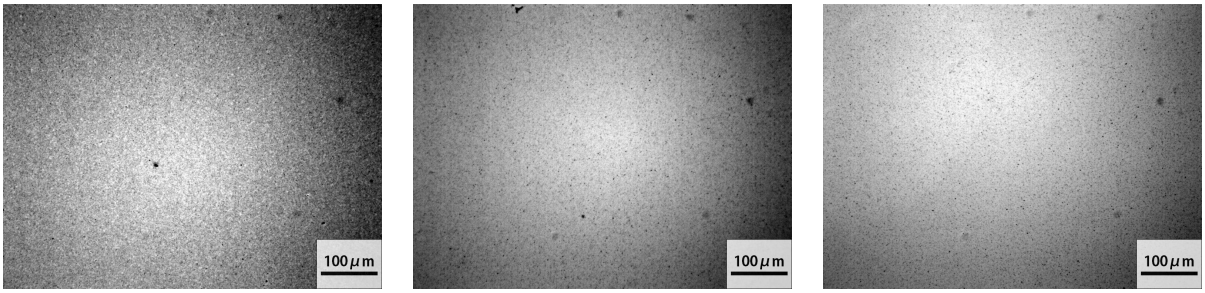

(a) (b) (c)

Figure 5.4: Microscope images of the films deposited with (a) +400V, (b) 0V, (c) -400V applied directly to the target.

as indicated by the presence of a small (100) and (112) peak. However, this texturing may also be present in the other samples, but not visible due to their poorer crystallinity. These results were confirmed by the susceptibility measurements of the three samples, shown in Fig. 5.7 (b). The -400V sample showed the best superconducting transition, with a $T_c(0)$ of 77.2K and $\triangle T_c$ of 6.7K. The +400V sample showed the poorest crystallinity and did not exhibit superconducting properties above 50K. The results are summarised in Table 5.2.

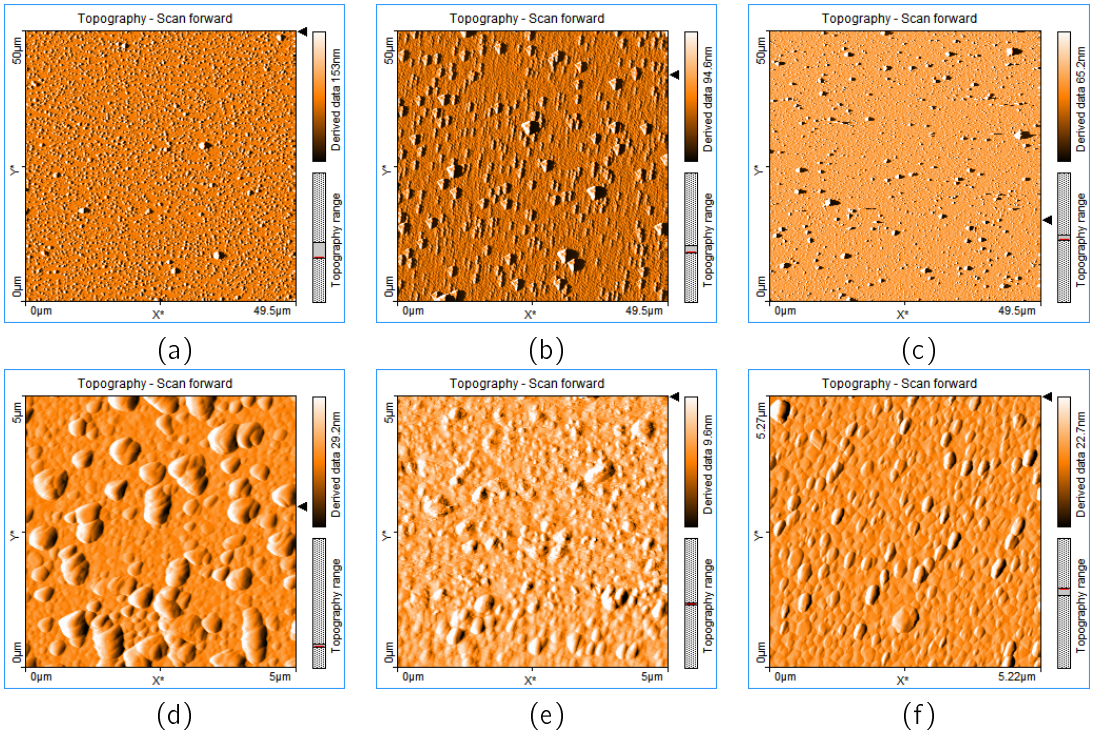

Figure 5.5: AFM results using the three target potentials (a) & (d) +400V, (b) & (e) 0V, (c) & (f) -400V. (a-c) Show 50μm×50μm sample scans and (d-f) show 5μm×5μm scans.

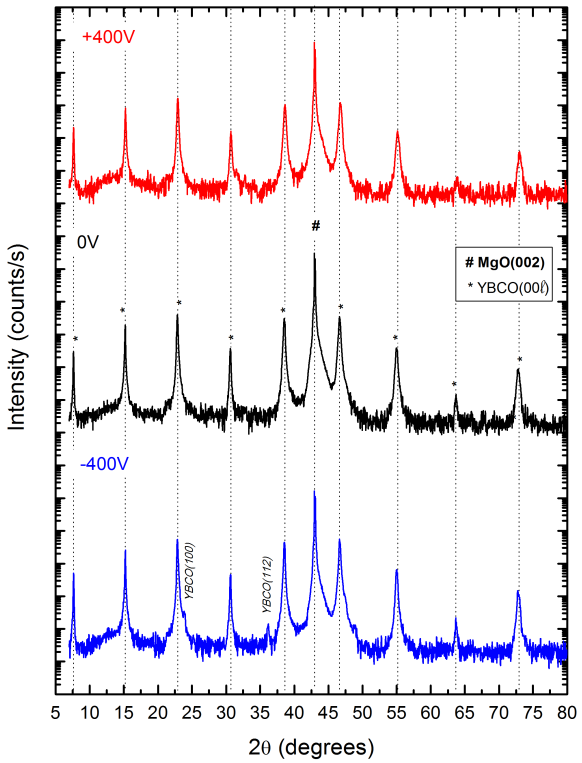

Figure 5.6: XRD patterns of the θ-2θ scan from YBCO thin film deposited on MgO (001) substrate for various applied voltages: +400V, 0V and -400V. The star symbols indicate the YBCO (00l) *c*-axis peaks. The hash symbol indicates the MgO substrate (002) peak.

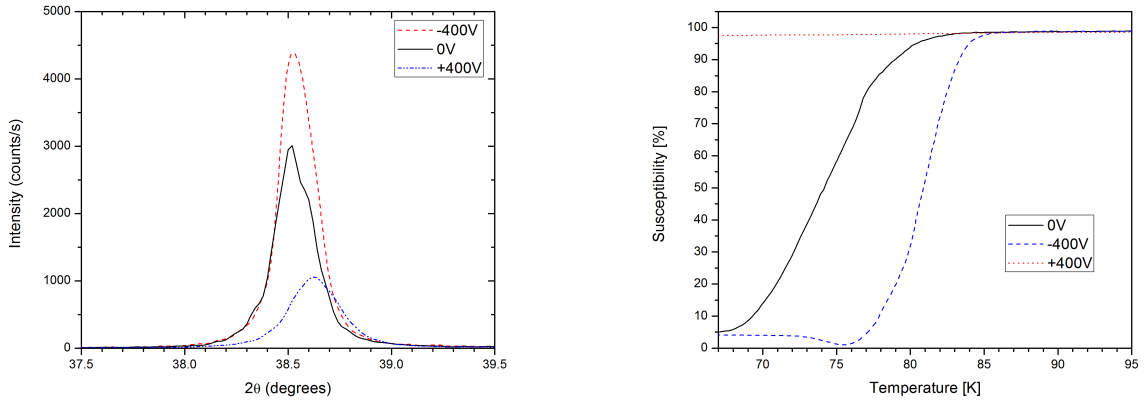

(a) (b)

Figure 5.7: (a) XRD θ-2θ scan showing a zoomed view of the (005) YBCO peak. (b) Susceptibility measurements of the three samples deposited with various target voltages applied

Table 5.2: Summary of AFM, XRD and superconducting results for the electrified target experiment

Applied Voltage [V]	$T_c(0)$ [K]	$\triangle T_c$ [K]	(005) peak Center [°]	FWHM (005) peak [°]	R_a [nm]	$\triangle z_{max}$ [nm]
+400	-	-	38.63	0.279	26	557
0	67.7	12.5	38.53	0.219	6	610
-400	77.2	6.7	38.51	0.201	7	502

Discussion

These results were very promising and they showed that applying a bias voltage to the target during deposition could be an effective way to modify the superconducting and crystal properties of PLD thin films. The results are similar to those reported by Izumi et al. [81], if we consider that a negative target bias voltage (used in this case) sets up the same electric field as a positive substrate bias voltage would (used by Izumi et al.). A negative applied voltage tended to improve the superconducting transition temperature by 10K and decrease the transition width by half compare to the no voltage case (i.e. standard deposition). This improvement was also reflected in the crystallinity of the sample as measured by XRD. The sample produced with a negative bias voltage had larger, more well defined *c*-axis peaks, than those produced without a bias voltage. Interestingly, a positive target bias voltage tended to have the opposite effect, deteriorating the crystallinity, roughness and superconducting properties of the films produced this way. This result confirms reports by [96, 102] that the opposite bias voltage does not enhance the superconducting properties of the films deposited.

We experienced a number of difficulties implementing this technique. At times persistent arcing between the target and target carousel resulted in contamination problems. Because the target holder and the metal target carousel (and other target stubs) needed to be so closely positioned, it was a prime location for arcs and discharges to occur (see Fig. 5.3 (c), top image). Due to this instability, it proved difficult to reproduce results with this technique. We therefore designed and implemented a different electrification configuration to continue experimentation.

5.1.3 New insulated target carousel

In order to overcome the random discharges between the target and target carousel during deposition, a new target carousel was designed and fabricated in-house. It was an exact replica of the previous target carousel [68], but fashioned entirely from Teflon. Teflon was chosen as it is hard wearing and can withstand the relatively high temperatures and high vacuum very well without the danger of additional contamination in the chamber[1]. It was also relatively easy to machine into the desired shape and form required. Fig. 5.8 shows a schematic diagram of how the new target carousel was positioned inside the PLD chamber, and Fig. 5.9 shows how it was implemented inside the deposition chamber. With the new carousel it also became possible to move the electrifying HV wire to the opposite side of the target. Once again, only the target was electrified and the rest of the chamber (including the substrate heater) was kept at ground potential.

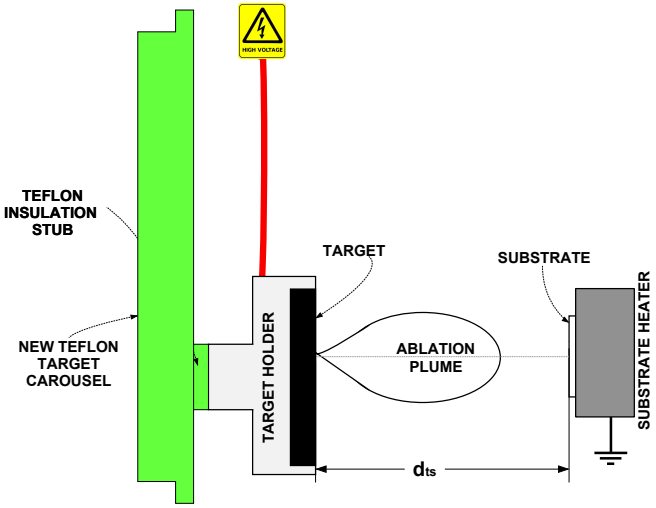

Figure 5.8: The modified experimental setup inside the PLD chamber used for electrifying the target, using the new Teflon target carousel

Fig. 5.10 (a) shows the glow discharge that is visible in the chamber when -400V is applied to the target at deposition pressure. The DC glow discharge was much more visible than before and seemed to be confined to the region in front of the target. We could clearly see the separate

[1] http://www.worldofmolecules.com/materials/teflon.htm

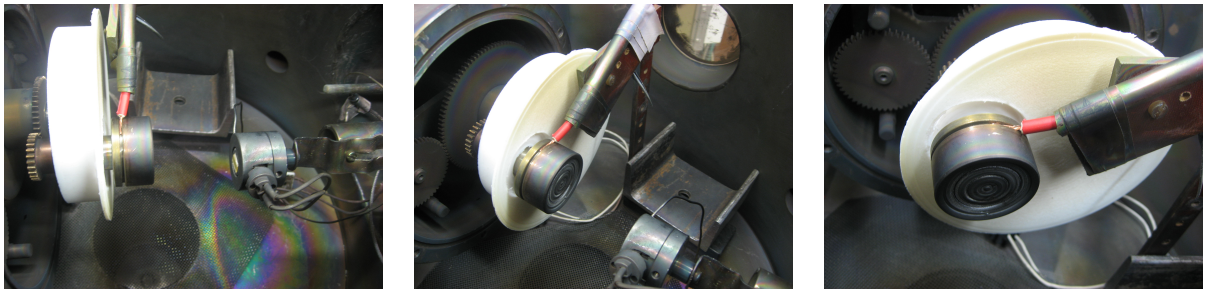

(a) (b) (c)

Figure 5.9: Various views of the new target carousel installed inside the PLD deposition chamber

regions of the glow discharge (discussed in the previous chapter). This would indicate that the new target carousel worked well as an insulator. Additionally, there were no arcs evident near the target (compare to Fig. 5.3 (c) top image). Fig. 5.10 (b) shows the target discharging through the plasma plume to the grounded substrate heater. This was not visible before.

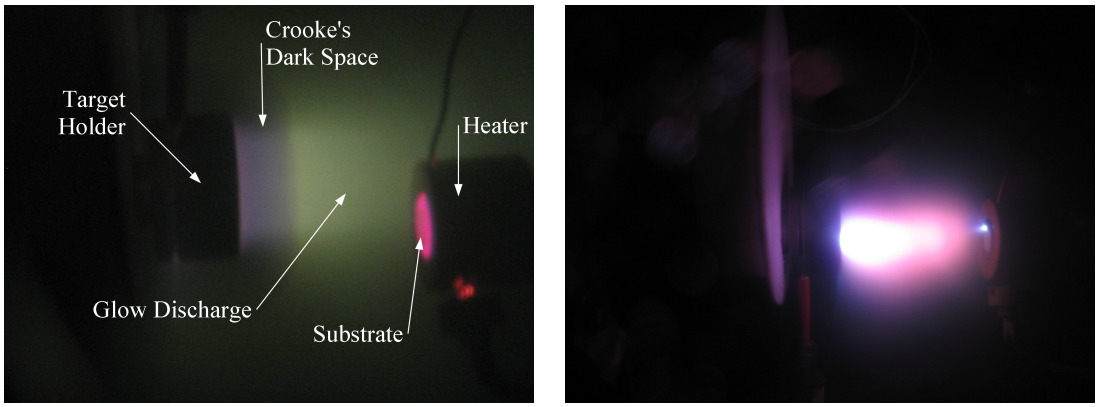

(a) (b)

Figure 5.10: (a) Photo of the glow discharge present when -400V is applied to the target (ambient oxygen pressure of 0.3 mbar). (b) Photo of the target discharging through the conductive plasma plume when the laser pulse strikes (similar conditions to (a))

It should be emphasised that this DC plasma discharge was as visible at the standard deposition pressures used in this study ($\rho_{O_2} = 7 \times 10^{-2}$ mbar). It is only strongly evident at higher ambient oxygen pressures (about 0.3 mbar and higher). However, this gives a good indication of the processes that may be happening that cause the modification of the superconducting film properties.

Discussion

These initial results indicated that the new configuration was behaving similarly to a DC diode sputtering system [128]. As can be seen in Fig. 5.10 (a), a dark space is visible near the target (the cathode) with a glow discharge extending in front of it towards the substrate heater (the anode). The free electrons present in the chamber are accelerated by the electric field generated between

the target and substrate. These energetic free electrons inelastically collide with the oxygen gas molecules. This excites the oxygen molecules causing them to glow. It can also lead to ionisation of the oxygen atoms. During ionisation, secondary electrons are emitted, which in turn repeat the above process and sustains the plasma glow discharge. Near the cathode (target), electrons move much faster than the ions due to their smaller mass. Positive charge builds ups here, raising the potential of the plasma. The few highly energetic electrons cause mostly ionisation rather than excitation collisions. This dark region near the target is more commonly known as Crooke's Dark Space [87]. The electric field is mainly concentrated to within the dark space, which acts as an shield. The electrical field in the surrounding regions is significantly reduced by the screening effect in front of the cathode (target). Positive oxygen ions which enter the dark space are accelerated toward the target, bombarding the target.

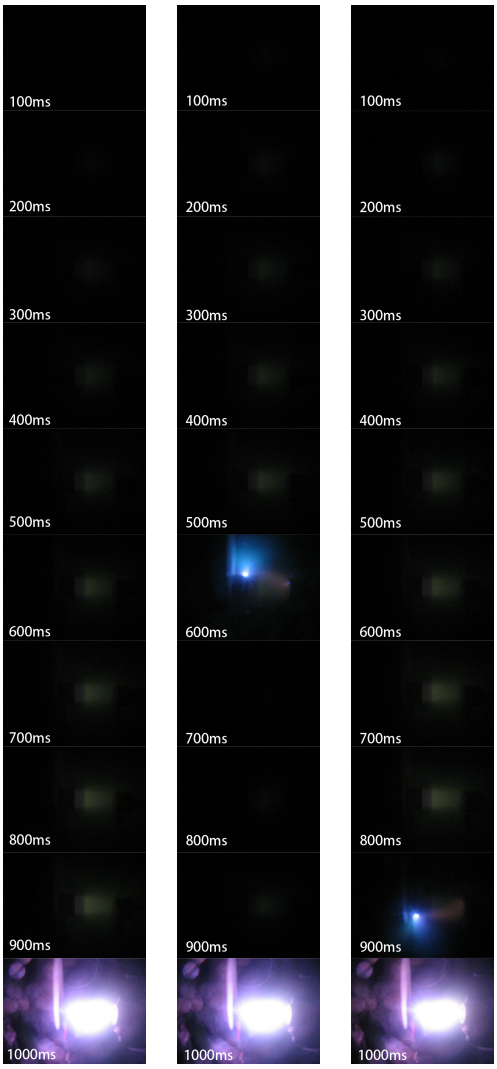

Figure 5.11: Series of photos taken at 100ms intervals during PLD depostion. (a) Shows a normal discharge occuring when the laser strikes, (b) and (c) show random discharge events that occur before the laser can fire.

The new Teflon target carousel worked well at insulating the target and seemed to eliminate most

of the random arcing present before. The discharge mostly occurred through the conducting laser plasma discharge (see Fig. 5.10 (b)). However, random discharge events were still present. Fig. 5.11 shows a series of photos that indicate the evolution of the ambient gas charging in the region of the electrode during deposition. As the charge builds up the gas glows brighter. Fig. 5.11 (a) shows a complete charging cycle, followed by the discharge that occurs through the plasma plume when the laser strikes the target. Fig. 5.11 (b) and (c), show random discharge events happening at 500ms and 900ms, respectively. The charge on the electrode (and gas region) is depleted and does not have time to recuperate before the next laser strike. This is a possible source of inconsistency, as we loose control over the charge on the electrode. As mentioned before, this could hamper the techniques repeatability and could also be the source of contamination to the thin films.

5.1.4 Retesting YBCO Deposition on MgO Substrates

The previous films deposited were very thin (approximately 100nm). Therefore, the deposition parameters were adjusted from those used for the previous experimental setup (with old target carousel), so as to increase the amount of material deposited. The distance between the target and substrate was also decreased to 50mm and the deposition time was tripled to 60 minutes. The changed deposition parameters are shown in Table 5.4. The laser had also been newly refilled, therefore, it achieved a much higher fluence of 3.2 J.cm^{-2}. Due to a shortage of MgO (100) substrates, only two voltages could be tested: 0V and -400V.

Table 5.4: Changed deposition parameters used with the new Teflon target carousel

Target-Substrate Distance	50mm
Laser Fluence	3.2 J.cm^{-2}
Deposition Time	60min

For this experiment, applying -400V resulted in a slightly more textured film than not applying a voltage. This was measured with optical microscopy (see Fig 5.12) and AFM (see Fig. 5.13). The surface roughness of the -400V sample was 26nm, more than double that of the 0V sample (R_a =10nm). However, the -400V sample had smaller particulates (approximate 100nm difference in height). The XRD scans of the samples showed once again that both samples were predominately *c*-axis orientated, with the -400V sample having slightly stronger peaks. Both samples also showed some *a*-axis texturing as indicated in Fig. 5.14. The a-axis texturing can be attributed to the new deposition parameters used, rather than the new Teflon target carousel.

Once again, the -400V sample showed better superconducting properties (see Fig. 5.15). It exhibited a $T_c(0)$ of 88K, 3K higher than that of the 0V sample. Both samples exhibited similar transition widths of approximately 4.5K, with the $\triangle T_c$ of the -400V sample being marginally better.

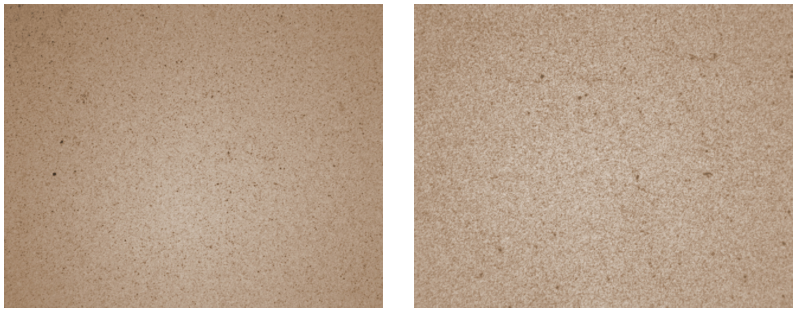

(a) (b)

Figure 5.12: Optical microscope images of the YBCO thin films deposited with (a) 0V applied, and (b) -400V applied to the target.

Discussion

This set of results confirmed our first results, indicating that a negative target bias voltage of -400V can improve the superconducting properties of YBCO thin films deposited using PLD. However, this method did not seem to enhance *c*-axis crystal growth, as is evident from the presence of *a*-axis growth in all samples fabricated. This *a*-axis growth was attributed to the deposition parameters used rather than the technique itself, as it was present in all samples deposited. An important observation that can be made, is that the improvement seems to be less when the technique is used with deposition parameters that already produce good films (without any voltage applied to the target).

As a final experiment using this setup, the technique was applied for depositing YBCO on LSAT (100) single crystal substrates. This served to verify if the method would work when depositing on another substrate material.

5.1.5 Electrified target deposition on (100) LSAT substrates

For this set of experiments, we decided to decrease the deposition time to 45min and double the laser pulse frequency to 10Hz. This was done to see if parameter change would decrease the amount of *a*-axis texturing present in the films. Table 5.5 summarises the changed parameters. The laser fluence changed due to normal usage fluctuations. The same three applied voltages (0V, -400V and +400V) were used in these experiments again.

Table 5.5: Changed deposition parameters used for the YBCO deposition on the LSAT substrates

Laser Frequency	10Hz
Laser Fluence	2.6 J.cm^{-2}
Deposition Time	45min

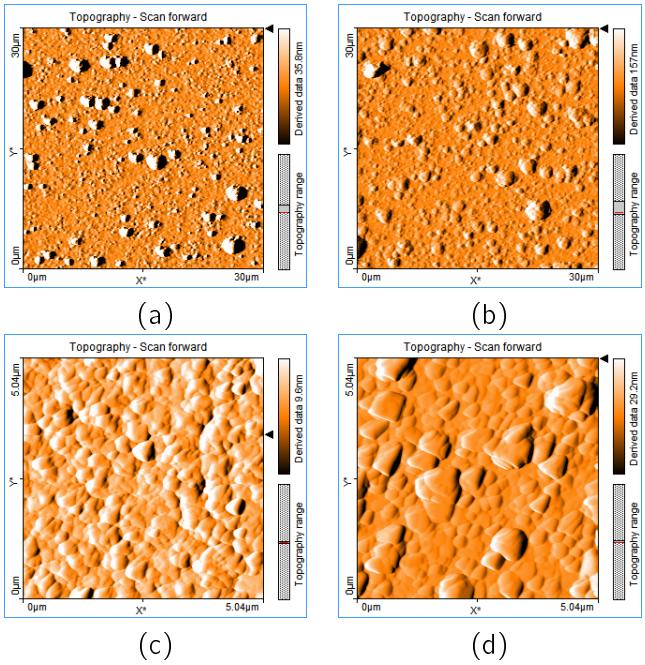

Figure 5.13: AFM scans of the YBCO samples produced by applying (a) & (c) 0V, (b) & (d) -400V. (a-b) show 30μm×30μm sample scans and (c-d) show 5μm×5μm scans.

Similar results were obtained compared to the films deposited on MgO substrates. Fig. 5.16 shows the measured difference in crystallinity and superconducting properties of the three films. Once again, applying -400V resulted in the best superconducting films, with a $T_c(0) = 86$K, $\triangle T_c = 5.5$K. Applying +400V to the target, produced the worst film with $T_c(0) = 64$K, $\triangle T_c = 20.5$K. The XRD data (Fig. 5.16 (a)) also shows that applying the negative voltage tends to increase the quality of the peaks observed. A positive applied voltage reduces the quality of the *c*-axis peaks.

Fig. 5.17 shows the complete XRD scans of the YBCO thin films deposited. All three samples show clear *c*-axis (00l) peaks. The samples also show mixed *a*-axis YBCO (110) and (220) peaks. All three films grown on LSAT show this same type of growth structure. This *a*-axis texturing can clearly be seen in the AFM scans of the sample surfaces (see Fig. 5.18). The -400V sample showed the highest surface roughness, however, the 0V sample had the largest protruding particulates again. Table 5.6 summarises these results.

Table 5.6: Summary of AFM, XRD and superconducting results for the electrified target experiment on LSAT substrates

Applied Voltage [V]	$T_c(0)$ [K]	$\triangle T_c$ [K]	(005) peak Center [degrees]	FWHM (005) peak [degrees]	R_a [nm]	$\triangle z_{max}$ [nm]
+400	64	20.5	38.29	0.553	6	871
0	82.9	9.2	38.33	0.614	9.5	1590
-400	86	5.5	38.38	0.438	12	1273

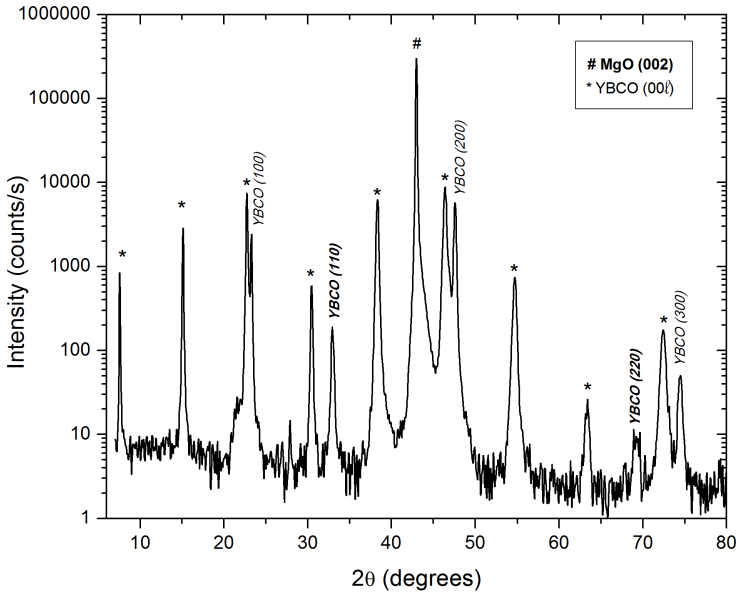

Figure 5.14: XRD θ-2θ scans of the YBCO thin films deposited with -400V applied to the target. The star symbols indicate the YBCO (00l) c-axis peaks. The hash symbol indicates the MgO substrate (002) peak.

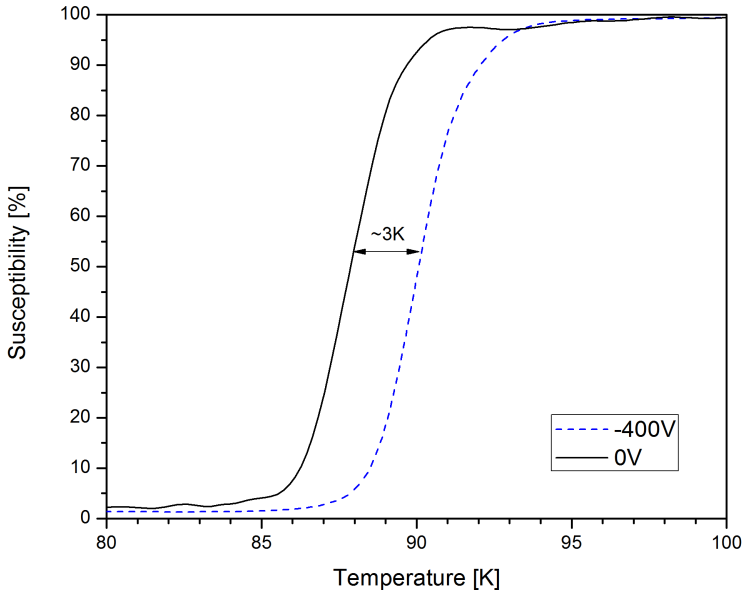

Figure 5.15: Susceptibility measurements for the -400V sample ($T_c(0) = 88$K, $\triangle T_c = 4.4$K) and 0V sample ($T_c(0) = 85$K, $\triangle T_c = 4.6$K) on MgO.

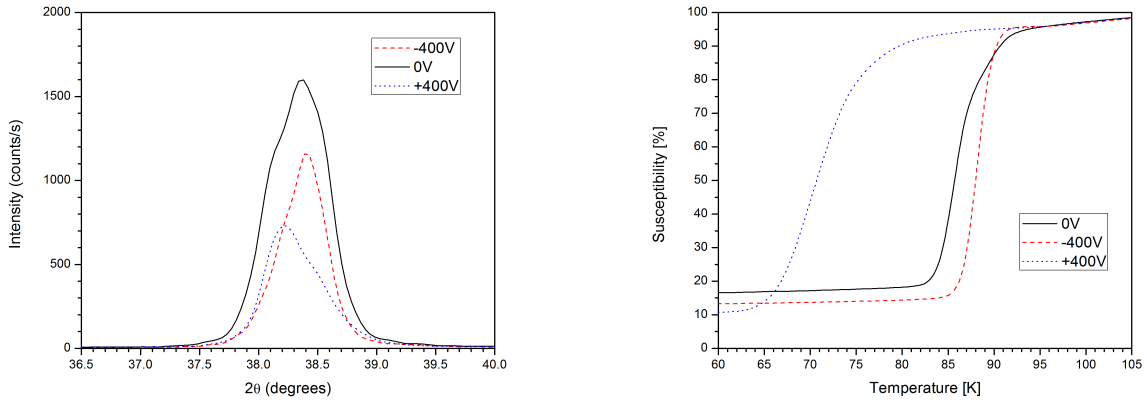

(a) (b)

Figure 5.16: (a) XRD 2θ-scan showing a zoomed view of the (005) YBCO peak and (b) the susceptibility measurements of the three samples deposited on LSAT substrates for -400V, 0V and +400V applied voltages.

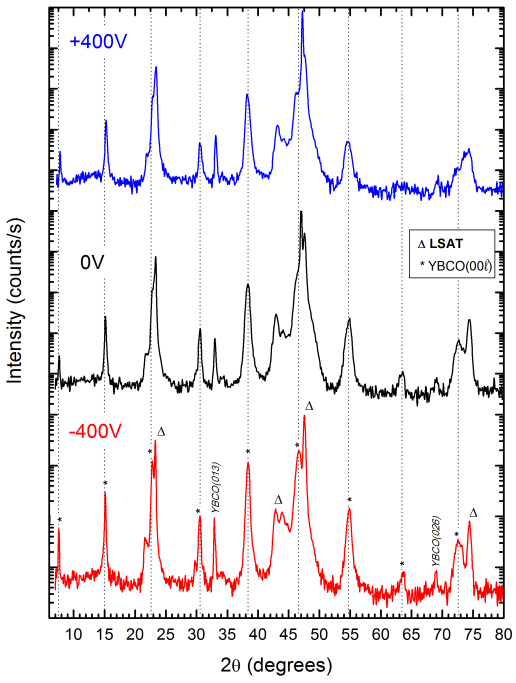

Figure 5.17: XRD patterns of the θ-2θ scan from YBCO thin film deposited on LSAT (001) substrate for various applied voltages: (a) +400V, (b) -400V and (c) 0V. The star symbols indicate the YBCO (00l) *c*-axis peaks. The triangle symbol marks the YBCO mixed a-axis peaks (110) and (220) respectively. The diamond symbols indicate the LSAT substrate peak contributions.

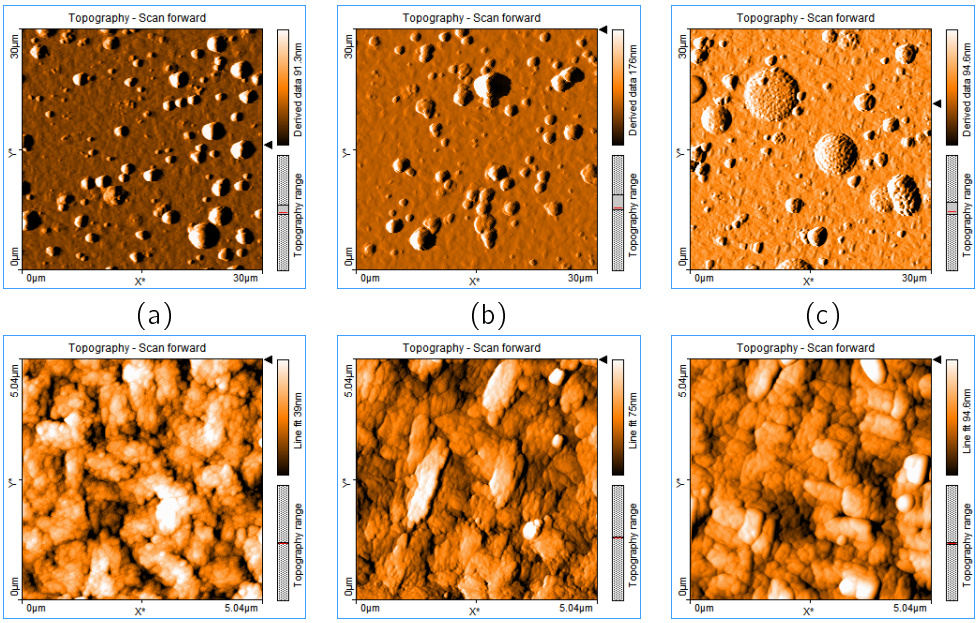

Figure 5.18: AFM scans of YBCO thin films grown with (a) & (d) +400V, (b) & (e) 0V, and (c) & (f) -400V applied during PLD on LSAT substrates.

Discussion

These results again confirmed that applying a negative target bias voltage of -400V can improve the superconducting properties (3K improvement in T_c) of YBCO thin films deposited by PLD. The results also confirmed that applying a positive bias voltage deteriorates the quality of the superconducting films produced. As was seen before, *a*-axis growth was not reduced by the technique. Rather, applying a negative voltage seemed to improve the crystallinity of any phases present in the 0V samples. The method does not only work on MgO substrates but also LSAT substrates.

5.2 Grid Deposition

We also briefly considered one alternate configuration used to introduce electric fields into the PLD chamber. Fig. 5.19(a) shows the experiment run to test the feasibility of depositing YBCO through a wire mesh grid as is done in [107]. A stainless steel mesh grid was placed half-way between the target and substrate which where separated by 60mm from each other. The mesh is made of 0.15 mm thick wire and the weave of the mesh is approximately 2 holes/mm. Unlike Hu et al. [107], no voltage was applied to the mesh as we first wanted to see the mechanical shielding effect it has on the deposited films. It was hoped that the wire mesh would act like a sieve and filter out the larger particulates and droplets from the plume allowing for smoother films to be grown and provide an easy way to apply the electric field uniformly during deposition. The same deposition parameters from the previous section where used.

The photo in Fig. 5.19(a) shows how the plume material is filtered and appears much finer after the grid than in front of it. The resulting film deposited is shown in Fig. 5.19(b) and the grid pattern is clearly visible as a shadow on the film surface. Fig. 5.19(c) shows that two distinctly different regions, a smooth region with nearly no particulates and a rougher region. The film showed reasonably good superconducting properties a $T_c(0) = 84.9$K and had a $\triangle T_c = 5.7$K. XRD measurements confirmed that the sample was *c*-axis oriented. The AFM scans of the two regions indicated that the average surface roughness of the smoother region of the film was 9.8nm and in the rougher region approximately 30nm.

It was also attempted to attach the mesh to an agitator that would slightly adjust its position so that the grid's shadow would not appear on the film. This did not prove successful and at best the shadow was only slightly less distinct, because the pulse rate of the laser and plume was much lower than the agitation frequency possible. An additional problem experienced with this configuration, was that at standard deposition conditions, the electrode tended to arc and discharge to the substrate heater. This was due to the close proximity of the electrode to the heater. This configuration is too complicated to allow for easy application of voltages in the chamber, as was our intention.

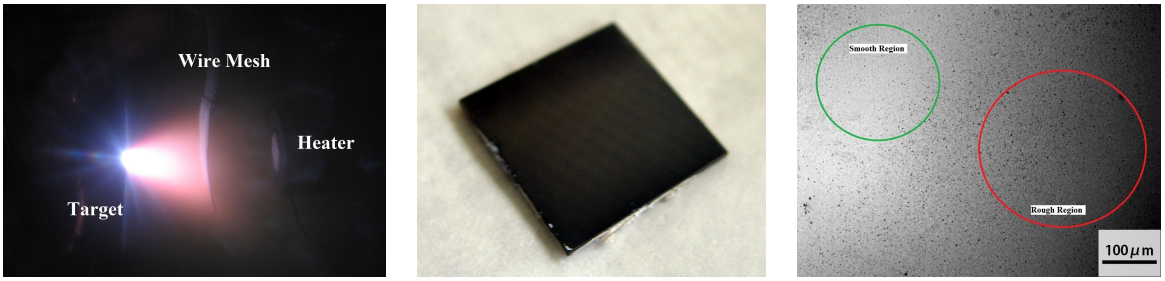

(a) (b) (c)

Figure 5.19: Depositing YBCO through a stainless-steel grid. (a) During deposition and (b) the resulting film that was grown showing the faint grid pattern that is reproduced in the layer. (c) Optical microscope images showing the smooth and rough regions on the films surface.

The only way such a technique would work correctly, would be to rotate the substrate during deposition as done by [107]. This is very difficult, as the heater is by design very hot (especially for the +700°C needed for YBCO growth) and attaching it to any type of actuator device requires very careful thermal insulation and design consideration. A rotating pocket black body heater such as the one used by [129] would be the best solution. This type of heater allows the mechanisms of motion and heating to be kept relatively separate. We do not have this type of heater at our disposal and therefore abandoned the idea of using a grid to introduce the electric field into the chamber.

5.3 Discussion

The results achieved are in excellent agreement to those presented in the literature. By applying a suitable negative bias voltage to the target holder, we can improve the quality of superconducting properties of PLD YBCO thin films deposited. Applying a positive voltage to the target holder during deposition degraded the superconducting quality of the thin films produced. This result is not reported in literature and could possibly be another potential application for this technique. By adjusting the applied voltage during deposition, one might be able to tune the superconducting properties of the thin films produced, yet still maintaining good crystal and material match with superconducting YBCO layers.

We observed that applying the negative voltage is accompanied by a DC glow discharge similar to that present in DC sputtering systems [89]. For high background pressures this discharge is clearly visible. This glow discharge is advantageous for two reasons. Firstly, the energetic oxygen ions bombarding the surface of the target will enrich and improve the oxygen content of the YBCO target material. Secondly, the excited gas plasma outside the sheath is more reactive with the laser ablated plasma plume. It is unlikely that this low energy ion bombardment is strong enough to result in the sputtering of the target or contributes greatly to the amount of target material deposited at the substrate [89]. DC sputtering typically has low deposition rates and this process should be

dominated by the laser ablation. Explaining the degradation of the superconducting films for a positive bias voltage is much more difficult, as the excited oxygen species should also be present in the region between the target and substrate, yet the films exhibit poorer superconductivity. A sputtering effect at the substrate is also unlikely, due to a lack of a cathode dark space.

The explanation proposed in the previous chapter, based on the work of Fried et al. [100], is possibly the reason for the different effects observed for the different biasing condition. As described in the previous chapter, the direction of the electric field may be accelerating electrons towards or away from the expanding plume front. When the electrons are accelerated away from the plume (for the negative bias condition) then the plume tends to loose neutrality and the gas region in front of the plume becomes more excited due to the collisions of the electrons with the gas between the plume and substrate. Therefore, both the plume and the ambient gas become more reactive and this may be more conducive to produce good quality well oxygenated YBCO thin films. When the electrons are attracted back into the plume front (positive bias voltage) they tend to neutralise the plume and could cause it to become less reactive, resulting in poorer films.

One of the main problems with this technique is the use of bare metal electrodes, and their propensity to arcing and discharging. Not only is this a possible source of contamination, it also reduces the reliability and repeatability of these experiments. Arc discharges can be highly destructive and damage sensitive equipment, targets and even the thin films and substrates. Bare electrodes are also a potential safety hazard to the researcher and research environment.

A possible solution to this problem of arcing is the use of an insulated electrode in the deposition chamber [87]. In this way the glow discharge will not be initiated and in this way, the constant propensity of the metal electrodes to discharge would be avoided. If the explanation of the electric fields effect on the electrons in the plume is correct then a DC plasma discharge may not be necessary to observe an improvement in film quality. [80, 81, 94] have all reported cases where the discharge is not present (and purposefully avoided), yet the improved superconducting film quality is observed.

Introducing a separate insulated electrode into the deposition chamber could add more flexibility to this method and allow a wider variety of voltages and deposition parameters to be tested. Researching a novel insulating electrode, is the topic of the next chapter.

5.4 Conclusion

We have demonstrated a simple technique that can be used to improve the quality of superconducting YBCO thin films grown by PLD. By applying a voltage to the target during deposition, the quality of the resulting films can be modulated depending on the polarity of the applied voltage. A positive applied voltage reduces the films quality. A negative applied voltage improves the superconducting characteristics of the films. A glow discharge and dark space, resembling a DC sputtering

process, was observed inside the chamber for this case. We speculate that this DC sputtering effect significantly enriches the oxygen content of the YBCO target material and thereby improves films grown in this manner. We however also propose a new explanation based on the effect the E-fields have on the electrons in the plume. Our qualitative explanation successfully describes the enhancement and degradation effects observed. We have highlighted that the difficulties associated with this method are the regular arcing and discharging of the metal electrodes. We have also proposed an alternative approach that involves an insulated electrode.

Chapter 6

Novel Insulated E-Field Enhanced PLD of YBCO

This chapter describes the development of a novel method to improve the crystallinity and superconducting properties of PLD YBCO thin films, deposited using sub-optimal deposition conditions.

In this work, we extend out previous efforts of applying potentials to PLD targets and the effect thereof. Rather than biasing the target or substrate directly, we investigated the effect of using a nearby insulated electrode to induce a build-up of charge inside the PLD chamber during deposition. This configuration was more flexible, as it allowed for a wider range of potentials to be applied to the electrode. We discuss the setup design and observed experimental results, offering possible explanations for these results.

6.1 Initial Insulated Electrode Design and Testing

6.1.1 Parallel Plate Insulated Electrodes

In the previous chapter, we saw that applying a negative voltage to the target tended to set up an electric field and subsequent glow discharge between the target and substrate heater. Furthermore, we speculated that the improvement observed in superconducting film quality was due to the presence of this charged region of gas that enriched the target material and plasma plume. As a first attempt to recreate the electric field in the region between the target and substrate, the configurations shown in Fig. 6.1 were tested. These configuration are similar to those reported by Mirsa and Palmer [102], except that the electrode was insulated in our experimental setup.

It was decided to start with a very basic electrode. The first prototype was a flat copper disc, insulated with an epoxy resin, connected by a HV cable to the external HV power source (see

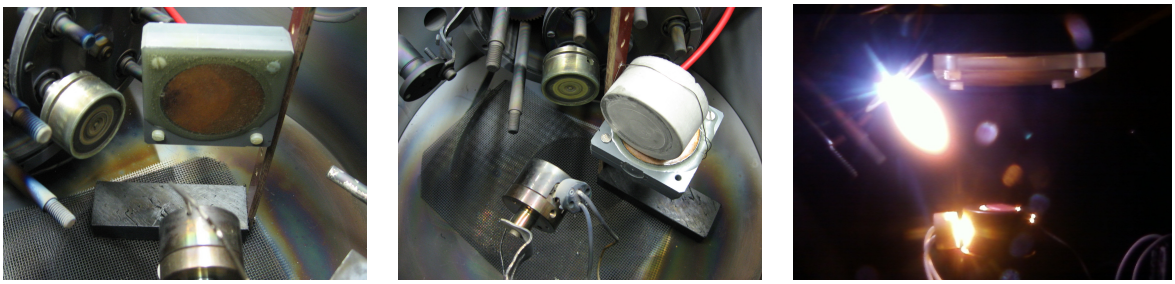

(a) (b) (c)

Figure 6.1: Photos of the initial prototype electrodes used to test the effect that an insulating electrode might have. (a) Shows the first type of electrode tried, encased in perspex. (b) The second electrode tested was encapsulated with a cement type ceramic. (c) Photo taken during deposition showing one of the perspex electrodes warping due to the high temperatures inside the chamber.

Fig. 6.1 (a)). The same sources and measurement setup that were reported in Chapter 5, were used again.

Fig. 6.2 shows the schematic diagram of the experimental setup used inside the PLD chamber. The substrate and electrode were orientated to directly face each other. The ablation plume, substrate and electrode centres are all in the same horizontal plane. The substrate was positioned directly in front of the ablation plume. The potential was applied to the electrode during deposition and annealing. Voltages in the range of -6 kV to +6 kV were tested. The entire PLD chamber, target-holder and substrate-heater were grounded.

YBCO films were deposited on (100) MgO single crystalline substrates using the PLD parameters shown in Table 6.1. The distances between the target and substrate (d_{ts}) and the electrode and substrate (d_{es}) were kept fixed at 60mm, with the substrate rotated 45° off-axis to the plume (Φ_c) (see Fig. 6.2).

Table 6.1: Insulated parallel plate YBCO deposition parameters

Target-Substrate Distance	60mm
Electrode-Substrate Distance	60mm
Laser Fluence	2.7 J.cm^{-2}
Laser Frequency	10Hz
Deposition Temperature	723°C
O_2 Deposition Pressure	7×10^{-2} mbar
Deposition Time	20min
Anneal Temperature	500°C
O_2 Anneal Pressure	1 bar
Anneal Time	30min

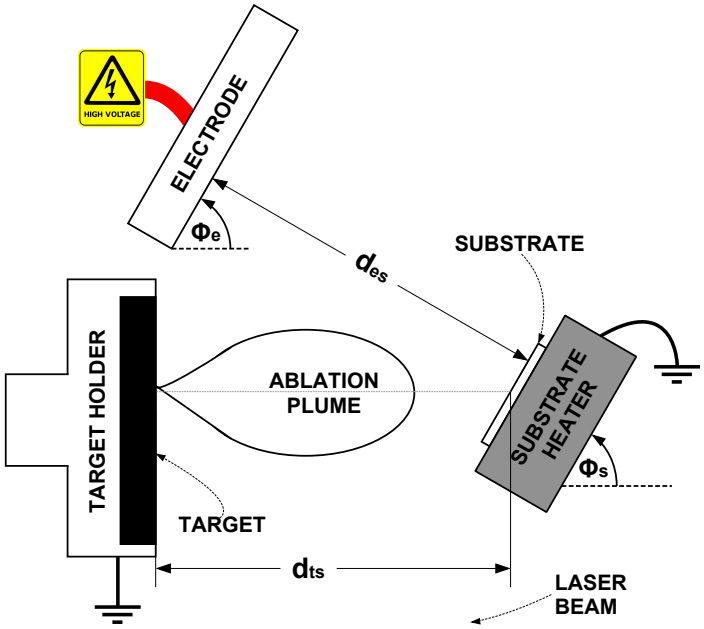

Figure 6.2: The initial experimental setup using the flat insulated electrode. The schematic details the positioning of the target, substrate and electrode relative to each other.

Discussion

The biggest challenge experienced with this setup was the electrode's electrical insulation. Proper electrical insulation is essential to prevent arc discharges from occurring during deposition. The high temperatures and vacuum conditions make it extremely difficult to insulate the electrode properly. The epoxy resin used to insulate the electrode could not withstand the high deposition temperatures and failed regularly leading to arc discharge. It softened after approximately 20 minutes, resulting in the high voltage breaking through the insulation and electrode failure. The electrode had to be placed as far from the substrate heater as possible otherwise the breakdown of the insulation was almost immediate. The discharge always occurred at the edge nearest to the target, as the fields are the highest here. Fig. 6.1 (c) shows how the electrode started to melt and warp during a deposition run. Various insulating materials were tested, such as the cement type ceramic (similar to that used for high-voltage power line ceramic disc-spacers) shown in Fig. 6.1 (b). However, they all tended to fail after a small number of deposition runs. Once again the breakdown occurred where the insulation was weakest and the fields were highest (i.e. where the HV cable was attached to the electrode).

This breakdown is not only problematic in the sense that a regulated voltage cannot be maintained on the electrode due to the arcing current (and the limited power output capabilities of the power source). The arcing current causes extreme localized heating of the insulation material and can lead to its vaporisation and contamination of the the vacuum deposition environment. As mentioned previously, YBCO is very sensitive to contamination.

Another problem with this off-axis configuration, was the uneven film thickness produced due to the 45° slant of the substrate with respect to the plume. The variation in film thickness was so severe that it could be directly observed with the naked eye, as a gradient in the colour of the film.

The constant failure of electrode insulation made this process unreliable and ruined entire deposition runs. This was expensive in terms of both time and money. It would waste more than four hours per deposition run (approximately, three hours to reach vacuum and one hour to cool down to room temperature) and also waste the expensive single crystal substrates required to grow YBCO. Failed runs also produce extra wear and tear on the expensive YBCO target and wasted laser time. In general we had to limit the deposition time to approximately 20 minutes to avoid failure and arcing. This produced much thinner films. However, we did manage to get one set of interesting results on an occasion when the insulation did not fail. Fig. 6.3 shows the transition characteristics of the films obtained for these runs. For +6kV applied to the electrode, a near perfect film was obtained with a $T_c(0)$ of 91K and ΔT_c of about 1K. The -6kV film showed degraded transition characteristics with a $T_c(0)$ of 70K. The drastic improvement of the film quality observed for the positive applied voltage in relation to the negative voltage, was unexpected. The superconducting transition was one of the best ever measured for YBCO thin films deposited with our PLD equipment. However, the difficulties associated with the constant electrode failure made this technique nearly impossible to apply with any reliability or repeatability. Due to these difficulties, we decided to find a new design for the electrode.

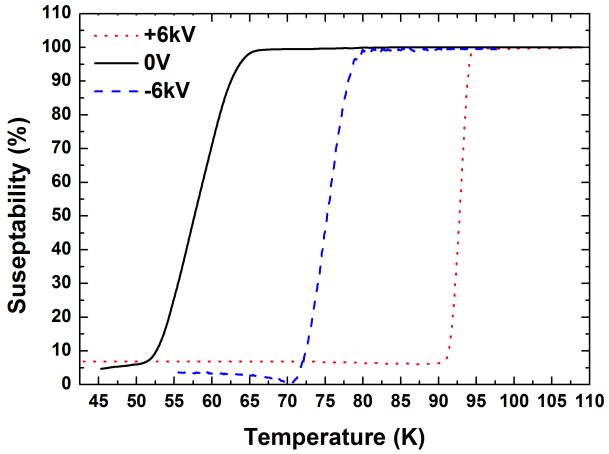

Figure 6.3: The measured superconducting transitions of the YBCO thin films deposited with the off-axis parallel plate electrode configuration.

6.1.2 HV Wire Ring Electrodes

We noticed that during deposition the HV wire never melted, yet it was exposed to the same conditions as the electrodes that failed. Therefore, we decided to fashion electrodes from HV wire. To reduce the uneven film deposition, it was decided to position the substrate in the more

conventional in-line configuration. Using HV wire allowed us to make hollow ring electrodes, through which the plume could pass to the substrate.

A number of trial wire ring electrodes were tested, examples of these are shown in Fig. 6.4. The electrodes were formed using 5 mm thick HV wire, curled into a loop. Various loop diameters were tested, however the a final loop diameter of 60 mm was used. This allowed the plume to easily pass through the loop, without the laser being obstructed from striking the target. Inside the PLD chamber, the open end of the wire was insulated with a HV stub, which can be seen in Fig. 6.4(c). The other end was connected to the HV source outside the chamber. No significant current flowed in the wire and therefore it did not produce any significant magnetic fields.

To offer added heat resistance, the HV wire was threaded through moulded quartz tubing, shown in Fig. 6.4(d). This also helped to give the electrode its shape. Heat shielding fabric was also tested (see Fig. 6.4(a-c)), however the quartz tubing provided the best heat resistance.

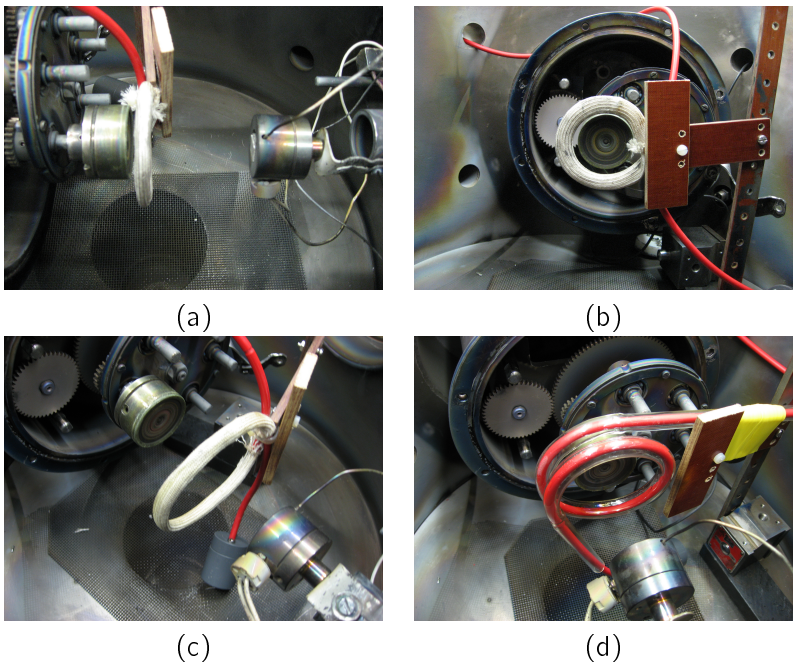

Figure 6.4: Photos showing some of the initial trial runs using the high voltage wire as the electrode. a) and b) are the front and side views of a small ring close to the target, c) is a larger ring positioned midway between the target and substrate, d) shows an improved design using moulded quartz tubing to insulate the HV wire from the extreme heat of the substrate heater.

In-line configuration

Fig. 6.5 shows a schematic illustration of the in-line electrode placement during deposition and annealing. The electrode was placed halfway in between the target and substrate. The substrate and electrode were positioned directly in front of the ablation plume, so that the plume could pass directly through the centre of the electrode. The HV potential was applied to the electrode only

during deposition and annealing. The entire PLD chamber, target-holder and substrate-heater were electrically grounded.

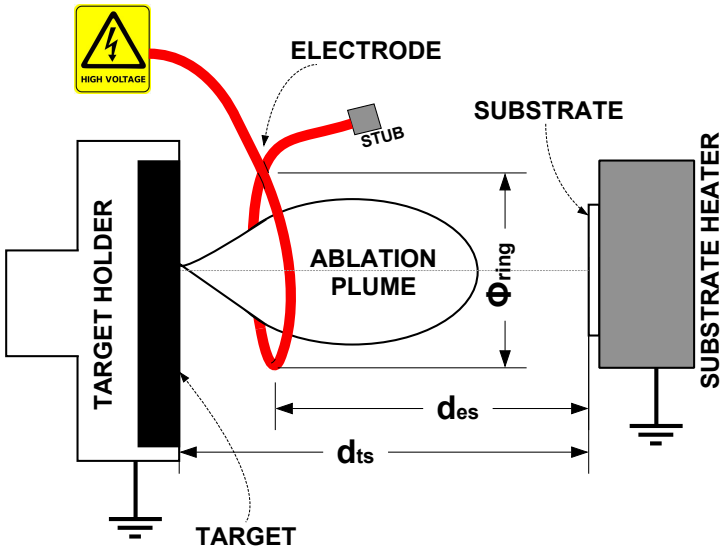

Figure 6.5: The in-line experimental setup used with the new HV wire ring electrode.

The YBCO thin films were deposited using the depostion parameters shown in Table 6.2. Three electrode bias voltages were considered: -1kV, 0V and +1kV. The measured superconducting properties of the three films are shown in Fig. 6.6. The standard film that was deposited without any voltage applied to the electrode showed better superconducting properties than other films. It had a $T_c(0)$ of 88.5K and a ΔT_c of approximately 2.4K. The +1kV sample was nearly as good as the 0V sample. However, the negative bias voltage significantly deteriorated the -1kV sample's superconducting properties.

Table 6.2: Wire ring electrode YBCO deposition parameters

Target-Substrate Distance	90mm
Electrode-Substrate Distance	45mm
Laser Fluence	2.71 J.cm^{-2}
Laser Frequency	10Hz
Deposition Temperature	723°C
O_2 Deposition Pressure	7×10^{-2} mbar
Deposition Time	30min
Anneal Temperature	500°C
O_2 Anneal Pressure	1 bar
Anneal Time	30min

All the films deposited displayed very similar XRD patterns. An example of which is shown in Fig. 6.7. The films were predominantly *c*-axis oriented but also showed some *a*-axis texturing. All the films showed this mixed phase growth, even the films that had no electric field applied

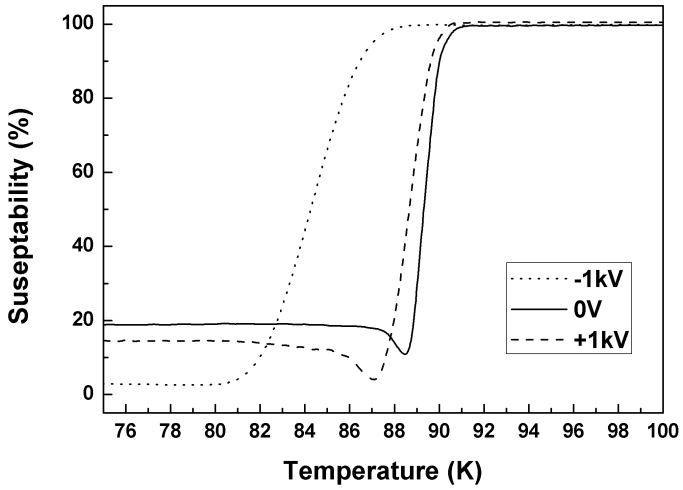

Figure 6.6: The measured superconducting transitions of the YBCO thin films deposited with the in-line electrode configuration.

during deposition. Table 6.3 summarizes the superconducting properties of all three films and also shows their full width at half maxima (FWHM) of the (005) peak as an indication of the films *c*-axis crystallinity. The films exhibiting best superconducting properties have narrower FWHM, and therefore sharper peaks.

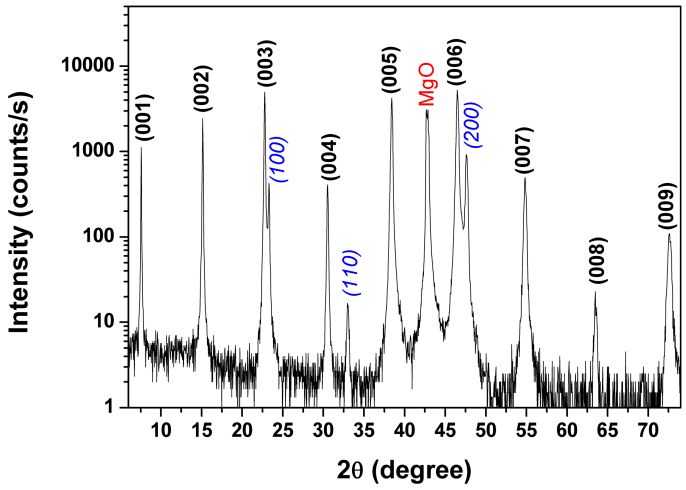

Figure 6.7: X-ray diffraction pattern of the best superconducting film (+1kV biased electrode configuration). The bold font indicates the *c*-axis diffraction peaks, the italic font the *a*-axis and *b*-axis peaks, and the normal font the MgO substrate peak.

Table 6.3: Summary of XRD and superconducting results for the insulated in-line wire ring electrode experiment

Applied Voltage [kV]	$T_c(0)$ [K]	$\triangle T_c$ [K]	FWHM (005) peak [°]
+1	87.1	3.3	0.318
0	88.5	2.4	0.294
-1	80.5	7.6	0.333

Discussion

used and cannot be attributed to application of electric fields. The long target-substrate distance (D) in comparison to the visible plume length (L) correctly accounts for the mixed *c*- and *a*-axis growth [130]. For our deposition D/L = 1.2 > 1. Moreover, the application of the high electric field during deposition was unable to remove this *a*-axis texturing.

This in-line electrode configuration was difficult to implement, due to the close proximity of the electrode to the substrate heater and its tendency to melt. Additionally, ensuring that the electrode does not block the laser beam can be tricky. Only two voltages were tested with this setup, because of repeated electrode failure. Therefore, we moved the electrode back to the position used for the parallel plate electrode configuration. Here it was further away from the substrate heater and thus less likely to melt. This new off-axis position for the ring electrode seemed a promising solution, considering that both techniques (the in-line ring electrode and parallel plate electrode) provided similar results.

Off-axis configuration

In this new configuration (Fig. 6.8), the electrode is placed out of the path of the ablation plume, 45° off-axis with respect to the target. The rest of the setup remained the same as for the in-line configuration. Voltages in the range of -1kV to +5 kV were applied and tested. The same deposition parameters from Table 6.2 were used.

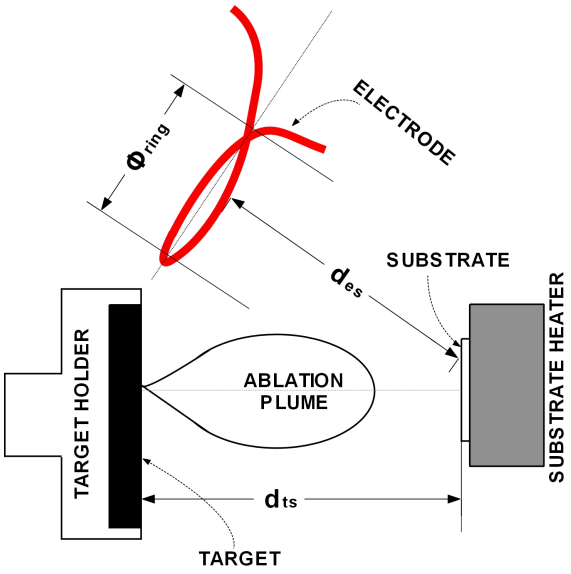

Figure 6.8: Schematic of the experimental setup of the wire ring electrode in the 45º off-axis configuration.

Fig. 6.9 displays the susceptibility measurement of the films deposited with the off-axis configuration. Once again, the negative applied voltage considerably reduces the T_c of the YBCO film. In contrast with the in-line electrode configuration, applying +1kV in this configuration dramatically

improves the films T_c to approximately 91K and reduces the ΔT_c by nearly half. However, higher positive voltages (+2kV and +5kV) tend to again decrease the superconducting properties of the deposited thin films.

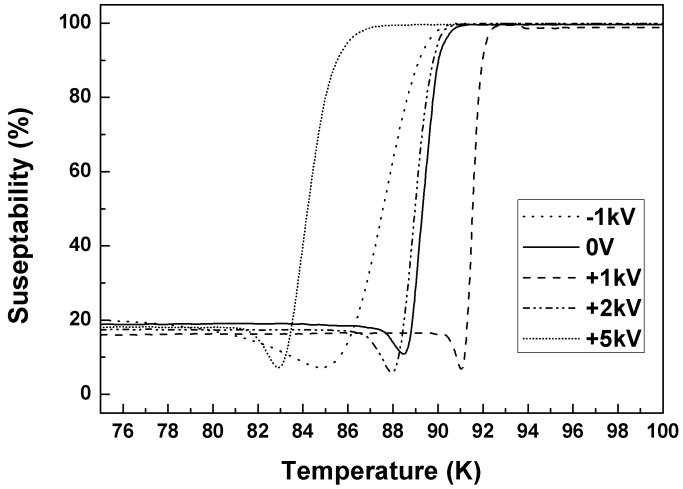

Figure 6.9: Susceptibility measurements of the YBCO thin films deposited with the off-axis electrode configuration, for various applied voltages.

To try to determine the contribution that annealing has to this behaviour, two films were deposited, applying 0V and +1kV respectively, without annealing after deposition. Instead of annealing at 500°C for 30min, the films were allowed to cool down rapidly to room temperature while increasing the oxygen pressure to 1 bar. Fig. 6.10 shows the susceptibility measurements for these films compared to those prepared with an in situ anneal. The films that were not annealed exhibit nearly identical behaviour to those that were annealed, but have a broader ΔT_c. A positively applied voltage of +1kV improves the thin film's superconducting properties, even without post-annealing. In both cases, annealing the films after deposition, results in roughly halving the film's ΔT_c. This suggests that the electric field only really has an effect during deposition and that applying the electric field during annealing in this configuration offers little to no improvement over regular annealing.

All the films deposited displayed similar XRD patterns to those determined before (see Fig. 6.7). The films are predominantly *c*-axis oriented with some *a*-axis texturing. The films with the best T_c had the sharpest *c*-axis peaks, as was measured with the FWHM of the (005) YBCO peak.

Table 6.5 summarizes the superconducting properties and FWHM for all the off-axis electrode deposited films.

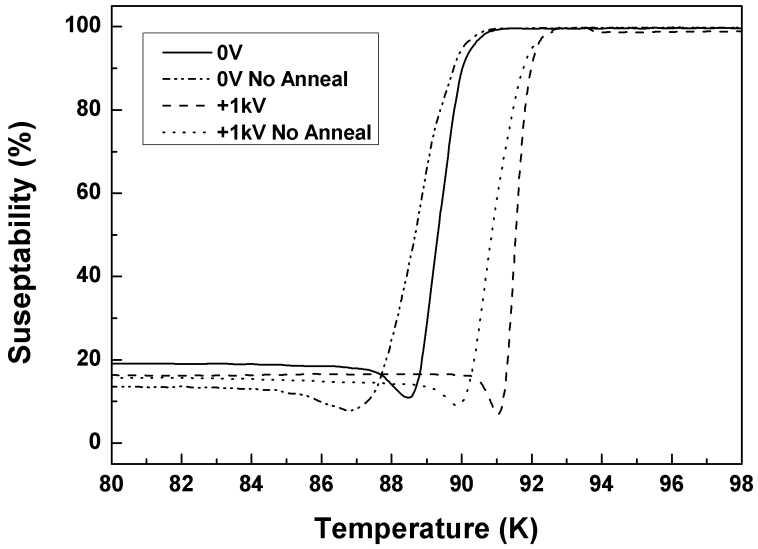

Figure 6.10: Susceptibility measurement results comparing annealed films deposited with the off-axis configuration to ones that were not annealed.

Table 6.5: Summary of XRD and superconducting results for the insulated off-axis ring electrode experiment

Applied Voltage [kV]	Anneal	$T_c(0)$ [K]	$\triangle T_c$ [K]	FWHM (005) peak [°]
0	No	86.9	3.8	0.308
+1	No	89.9	2.8	0.233
-1	Yes	84.8	5.4	0.306
0	Yes	88.5	2.4	0.294
+1	Yes	91.1	1.4	0.216
+2	Yes	88.0	2.6	0.303
+5	Yes	82.9	4.3	0.278

6.1.3 Discussion

This final off-axis HV wire ring electrode configuration (see Fig. 6.8) was extremely stable during all deposition runs. It did not melt or cause any unwanted arcing inside the chamber. Furthermore, by applying a suitable positive bias voltage to the electrode the superconducting film qualities of the PLD deposited YBCO films could be reliably enhanced. This therefore represents a very useful technique, as it introduces an extra parameter that can be used to modulate the superconducting qualities of the YBCO films deposited. This parameter is not essential for deposition to occur, however, it does influence the deposition, and its effectiveness is influenced by the deposition parameters used.

By applying a potential of +1kV in an off-axis electrode configuration, thin films with a T_c of 91K

and ΔT_c of 1.4K were obtained. Applying a negative voltage deteriorates the superconducting properties of the films. The exact mechanisms responsible for this improvement are unknown. We can only speculate as to the reason why the in-situ application of E-field during deposition affects the superconducting properties of the YBCO thin films in the manner observed.

A possible explanation might be that the localized electric field may cause the target surface to charge up. The ablation of the charged target material enriches the ionic species available in the ablation plume. The plume is therefore more reactive, improving the superconductor crystal growth. The resulting films therefore show better superconducting properties. Furthermore, the E-fields effect on the electrons in the plume may be significant. The electrode may attract or repel electrons in or out of the plume changing its neutrality and affecting its reactivity.

Fig. 6.11 shows the results of electrostatic simulations [131] for these two electrode configurations, ignoring the effect of the plume and its dynamics. The simulations show that the in-line configuration creates a relatively uniform perpendicular electric field in the region of the substrate and target (see Fig. 6.11(a)). With the off-axis configuration, all the E-field lines are concentrated to the side of the target closest to the electrode, producing practically no field at the substrate (see Fig. 6.11(b)).

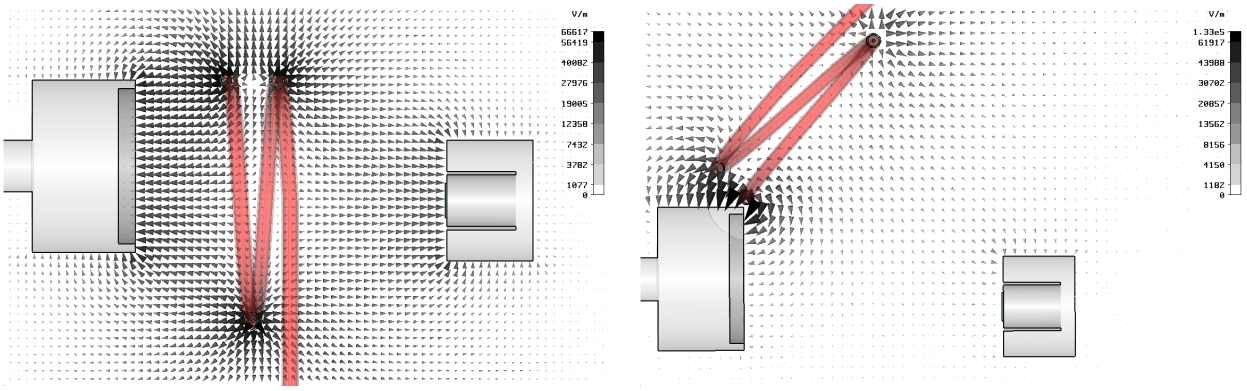

(a) (b)

Figure 6.11: Simulations of the static electric fields inside the PLD chamber for an applied voltage of +1kV, the two different electrode configurations: (a) in-line configuration, (b) 45° off-axis configuration. The arrowheads indicate the direction of the electric field. Darker, larger arrowheads indicate higher fields. The target-holder and target are on the left. The substrate and substrate-heater are on the right. The figures shows a top-view of the E-fields on a cross-section through the centre of the substrate.

For a positive applied voltage with the in-line setup, the electric field is directed away from the electrode towards the target and substrate, as can be seen in Fig. 6.11(a). The fields may initially accelerate the electrons out of the plume reducing the plume neutrality, and causing enhanced collisions with the gas. Before the electrode is reached, after the electrode the opposite would occur, pulling electrons back into the plume neutralising the plume and reducing its reactivity. This could be why we did not see an improvement over the 0V case for this configuration. It was

however still better than the -1kV case. For the negative voltage the fields will tend to repel the mobile electrons into the plume immediately after ablation neutralising it and reducing it reactivity. The more neutral plume will therefore also be less reactive after passing through the electrode and the resultant films show poorer superconductivity.

In the case of an optimum positive voltage applied in the off-axis electrode configuration, the electric field is concentrated at the target and is much weaker at the substrate (see Fig. 6.11(b)). This may attract electrons out of the plume and cause the plasma to become ion rich and more reactive with the ambient oxygen environment. The off-axis nature of the field may enhance this removal effect. The close proximity to the target could also further draw the electrons in the target towards the electrode leaving an ion rich region where the laser strikes the target and leading to the enrichment of the ionic species available in the ablation plume. This would tend to amplify the previously mentioned effect.

Increasing this voltage above optimum may start to cause the acceleration of the ions present in the plasma plume, affecting the stoichiometry of material that arrives at the substrate.

A negative bias may accelerate electrons towards the plume and tend to neutralise it as previously mentioned.

The electrostatic simulations seem to indicate that the enhancement is an effect localized at the target (due to the high electric field concentrated here) and therefore the shape of the ring electrode is not that important. Only the close proximity of the electrode to the target is required so that charge can be induced on the target and also affect the electrons present in the at an early stage of the ablation. As a next step, the wire electrode shape was further simplified to only be a straight wire positioned near to the target.

6.1.4 Single wire electrode

To test whether another shape electrode would also work if placed close to the target, the insulated high voltage wire was run down next to the target (see Fig. 6.12 (a) and (b)). This shape (or lack thereof) electrode gave us more freedom to position the electrode in the deposition chamber's confined space. We tested using two positions of the electrode on either side of the target, the near-side and far-side position as shown in Fig. 6.13. This was to see if the exact positioning of the electrode affected the quality of the films produced.

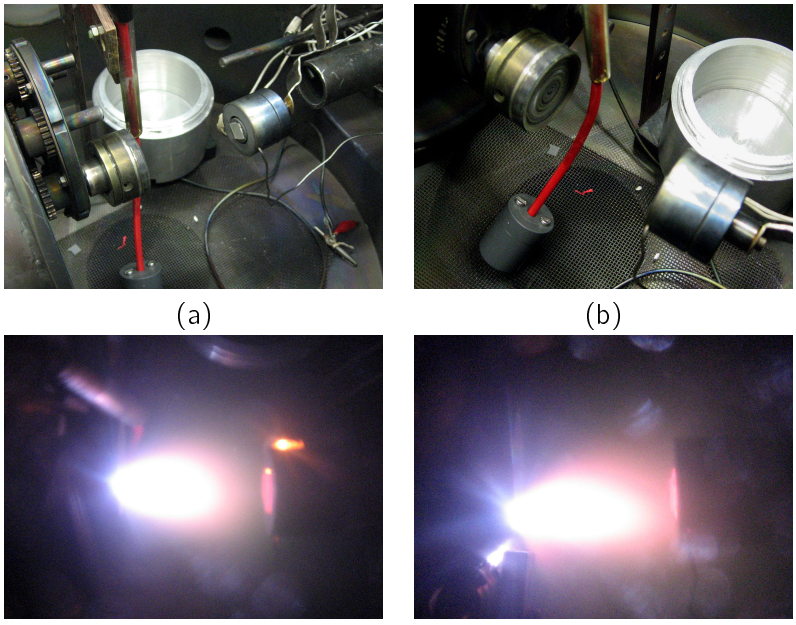

Figure 6.12: The deposition configuration used with a single straight piece of wire. (a) (b) actual setup (far-side position) before depostition, (c) during deposition farside, (d) near-side.

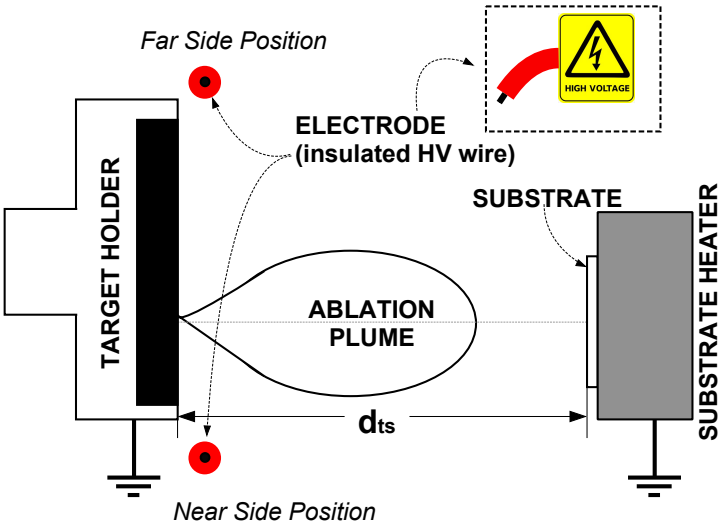

Figure 6.13: Schematic of the deposition configuration used with a single straight piece of wire, indicating the near- and far-side electrode positions.

The deposition parameters used are summarised in Table 6.7. Only +1kV was tested as this gave the best results previously. These films were compared to those prepared without voltage applied. Figure 6.14 shows the susceptibility measurements of three of the films deposited. Both films deposited with +1kV applied to the wire electrode have higher T_c's and narrower transition widths

than those deposited without voltage applied. All of the films showed good c-axis growth as can be seen in Fig. 6.15. The +1kV films were smoother than the 0V films, as is shown in Fig. 6.16 and Fig. 6.17. The 0V film had a surface roughness of 74nm, approximately double that of the +1kV samples (R_a =33nm). The position of the electrode did not seem to effect the quality of the films produced. Table 6.8 summarises the results for a number of films deposited under these conditions. This electrode configuration showed good repeatability.

Table 6.7: Wire ring electrode YBCO deposition parameters

Target-Substrate Distance	55mm
Laser Fluence	2.3 J.cm^{-2}
Laser Frequency	10Hz
Deposition Temperature	723°C
O_2 Deposition Pressure	7×10^{-2} mbar
Deposition Time	30min
Anneal Temperature	500°C
O_2 Anneal Pressure	1 bar
Anneal Time	30min

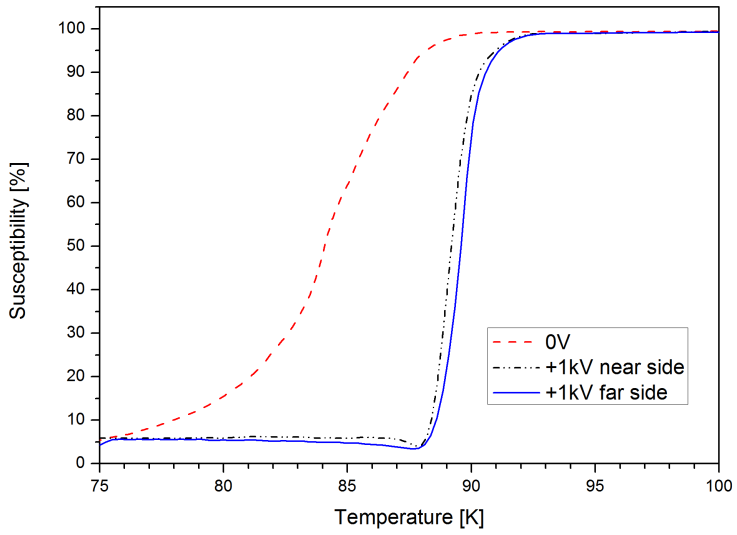

Figure 6.14: Susceptibility measurements comparing films with voltage applied to the electrode in different positions to films without voltage applied.

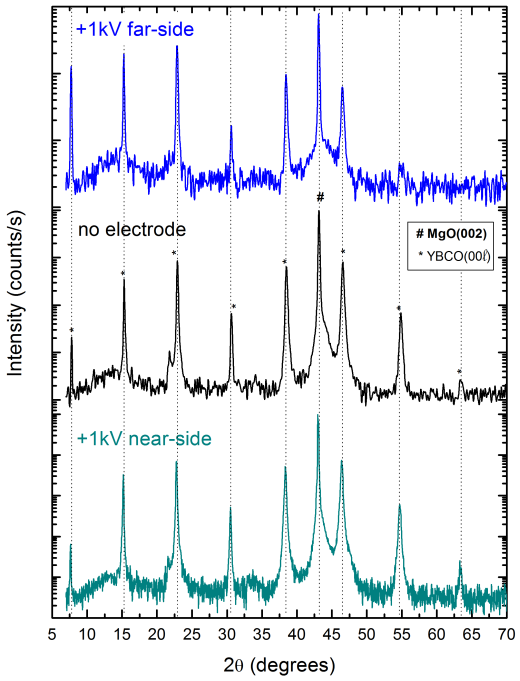

Figure 6.15: XRD results of the films deposited with the wire electrode placed in different positions.

Table 6.8: Summary of XRD and superconducting results for various films from the single wire electrode experiment.

Electrode Position	Applied Voltage [kV]	$T_c(0)$ [K]	$\triangle T_c$ [K]	(005) peak Center [degrees]	FWHM (005) peak [degrees]
Far	0	75.0	7.2	38.50	0.25
Far	0	74.0	9.0	38.33	0.27
Near	1	88.4	2.2	38.39	0.24
Near	1	88.0	2.7	38.31	0.23
Far	1	88.1	3.0	38.36	0.21
Far	1	88.2	2.9	38.46	0.21

6.2 Conclusion

We have successfully demonstrated how the in-situ application of electric field during the pulsed deposition of YBCO thin films can enhance their superconducting properties. A low-cost, simple and stable electrode design and configuration, which produced repeatable results, was identified. By applying a potential of +1kV in an off-axis electrode configuration, high quality superconducting

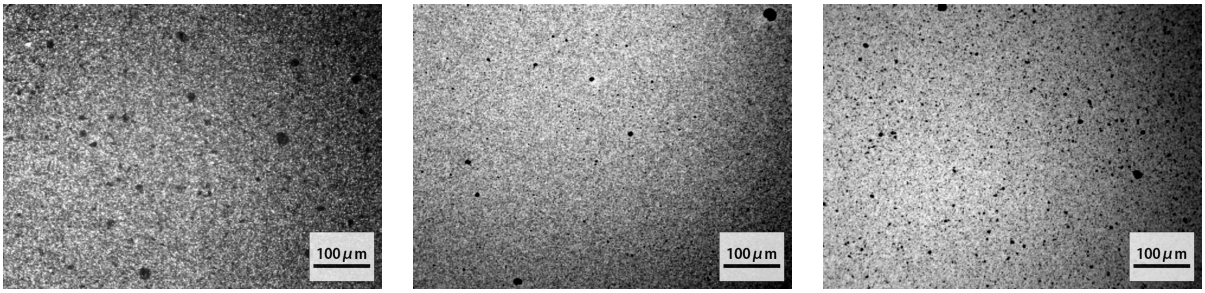

(a) (b) (c)

Figure 6.16: Microscope images of films prepared with (a) 0V, (b) +1kV far-side, (c) +1kV near side applied to the wire electrode.

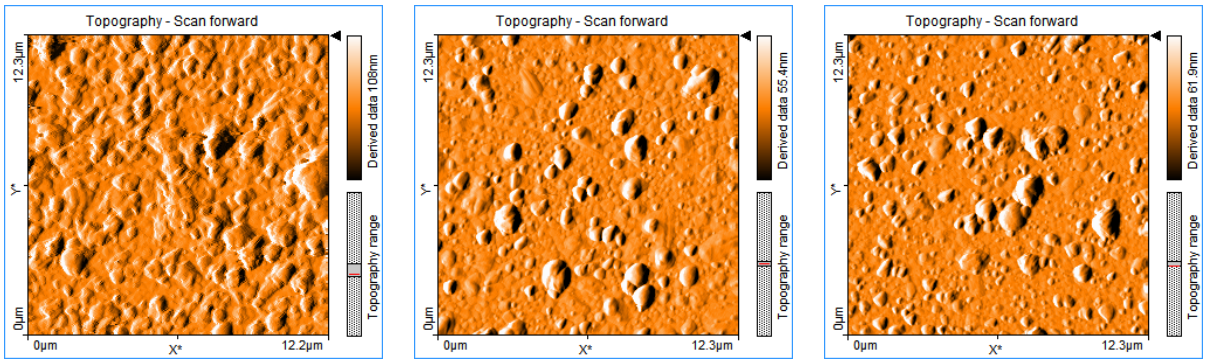

(a) (b) (c)

Figure 6.17: AFM scans of films prepared with (a) 0V, (b) +1kV far-side, (c) +1kV near side applied to the wire electrode.

YBCO thin films with T_c's of up to 91K could be routinely obtained. These results have been published [132].

Applying a positive voltage tends to improve the quality of the films grown and a negative voltage considerably reduces the superconducting film properties. The exact mechanisms responsible for this improvement and deterioration are unknown. A possible explanation might be that the localized electric field may attract and repel electrons in the plume and also cause the target surface to charge up. The ablation of this charged target material enriches the ionic species available in the ablation plume. The plume is therefore more reactive, improving the superconductor crystal growth. The resulting films therefore show better superconducting properties.

Chapter 7

Superconducting Dual-Mode Filter

Superconducting filters are a real world application of high-temperature superconductors that has been successfully commercially exploited in telecommunication systems and military applications [1, 2]. Their low surface resistance allows makes them particularly well suited for making ultra narrow-band filters, with minimal passband insertion loss and extremely high selectivity. High performance filters require high quality films and good fabrication processes. The construction of such a device therefore is a test of our research groups capabilities and the value of the high quality superconducting YBCO thin films. We therefore set ourself the goal of producing a compact bandpass filter.

At present, we are only able to uniformly deposit single-sided 10mm×10mm YBCO thin films on 0.5mm thick MgO substrates. This is the largest size that we can accommodate, due to the small spatial distribution of the PLD laser ablation plume. Therefore, considering our limited manufacturing capabilities we focused on making the filter as small as possible.

7.1 Dual-Mode Filter

Dual-mode microstrip filters have been widely studied by numerous researchers for its advantages in of small feature size, low mass and low loss. This type of filter therefore fits our depositing capabilities and fabrication limitations. The main advantage of this type of filter is that each dual-mode resonator used to make up these filters can be used as a doubly tuned resonant circuit. Therefore, the number of resonators required to realise a n-degree filter can be halved. These filters are realised in very compact configurations. Fig. 7.1 shows some typical dual-mode resonators and their size in comparison to the guide-wavelength of the fundamental resonant frequencies of the structure. All of the resonators have a two-dimensional symmetry, with a small perturbation applied at 45° from the two orthogonal modes of the resonator [41]. Meander loop resonators clearly offer the smallest size. Their characteristic size is smaller than a quarter of the fundamental resonant frequency of the resonator. We therefore chose this configuration for our dual-mode filter.

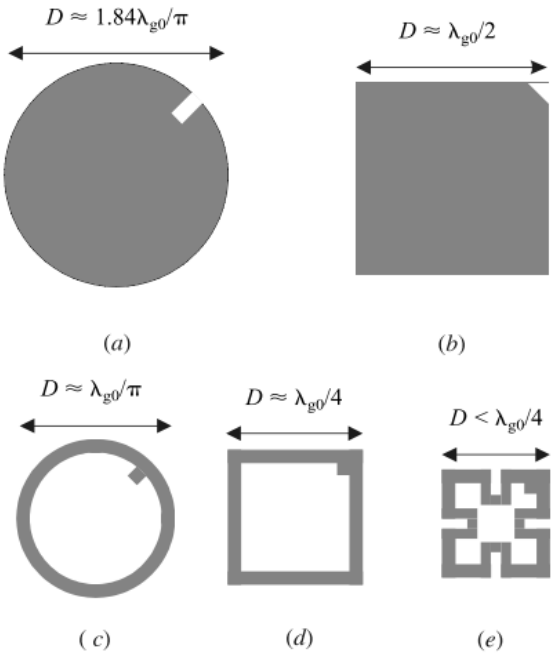

Figure 7.1: Various microstrip dual-mode filter resonator shapes and their size dimension D and in comparison to a the guide-wavelength of the fundamental resonant frequency λ_{g0}: (a) Disk, (b) squarepatch, (c) ring, (d) square loop and (e) meander loop resonators. [41]

The small perturbation in the symmetrical structure causes a coupling between these two orthogonal degenerate modes of the resonator, which causes resonance frequency splitting. The size of the perturbation changes the amount of coupling between the two modes and is therefore used to control the response of the filter. The coupling factor is given by

$$k = \frac{f_1 - f_2}{f_1 + f_2}, \tag{7.1}$$

where f_1 is the higher, and f_2 is the lower of the two split resonant modes. These are usually determined from accurate electromagnetic (EM) simulations of the structures. Knowing the coupling coefficient is an important step in the design of this type of filter. The coupling coefficient is used to translate the low pass filter prototype parameters into actual microstrip design parameters. Because we have no specification for our bandpass filter, we sought out a design from literature that was of a similar scale and on a similar substrate with properties close to those of MgO.

7.2 Design and Simulation

The simplest dual-mode filter is the two-pole bandpass filter using a single dual-mode resonator. After considering various designs from the literature [133–136], we chose to use the design reported

by [41], shown in Fig. 7.2. The filter consists of two meander-loop, dual-mode resonators, each of which has a 7 mm by 7 mm footprint. What attracted us to the design, was that one of the resonators would fit onto our 10mm×10mm YBCO thin films and the substrate parameters used are nearly identical to those of our MgO substrates (ϵ_r = 9.8 and thickness h = 0.5 mm).

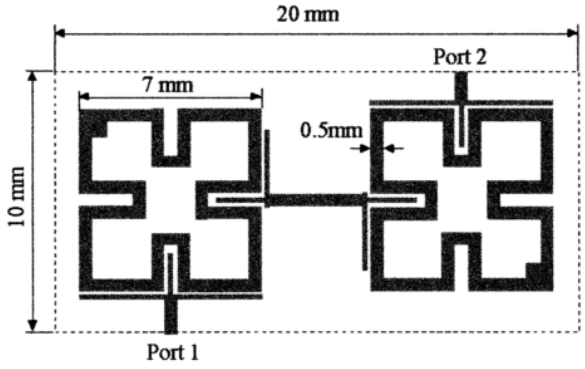

Figure 7.2: Layout of a four-pole, dual-mode microstrip bandpass filter on a 0.5 mm thick substrate with a relative dielectric constant of 9.8 [41].

Taking the dimensions of one of the resonators, the second order dual-mode filter structure shown in Fig. 7.3 was created as our prototype filter. The lengths were adjusted changed slightly, but the 0.5mm track width of the main resonator was kept.

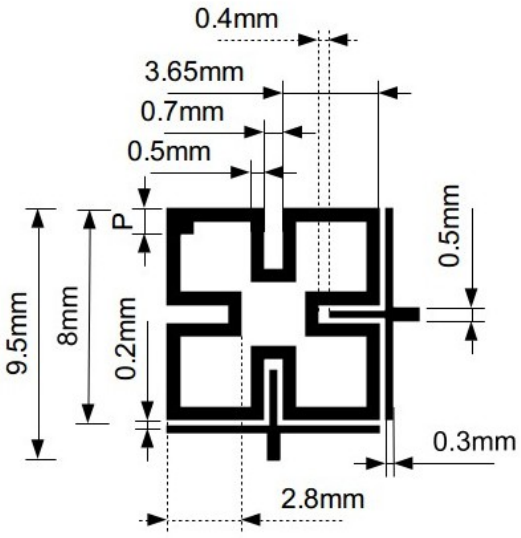

Figure 7.3: 2nd Order Dual-mode Microwave Filter design

This filter was then simulated and designed using a full-wave EM simulation package [131]. Simulations were performed adjusting the size of the perturbation patch (length P in Fig. 7.3) until the sharpest bandpass response was obtained. The results of the simulations are shown in Fig.

7.4. For the final design we chose P=1mm, and this resulted in a filter with a simulated centre frequency of 2.74GHz, a bandwidth of 70MHz and an insertion loss of -1.8dB.

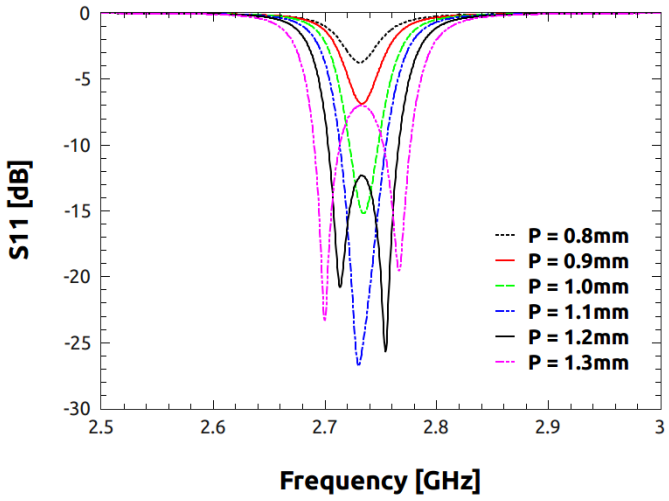

(a)

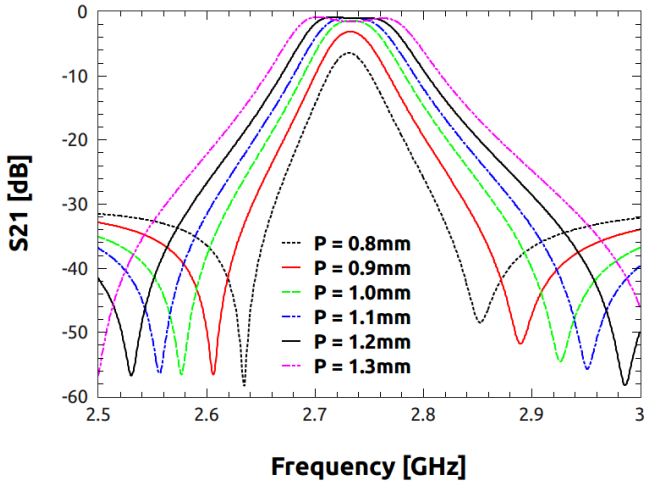

(b)

Figure 7.4: Simulated filter performance (a) S11 and (b) S21

7.3 Fabrication

Two superconducting YBCO thin films were used to construct two dual-mode filter prototypes. The YBCO layers had a thickness of approximately 300nm ($\approx 3\lambda_L$) as determined from AFM measurements. The two thin films where deposited using of the off axis wire electrode configuration reported in Chapter 6. One film was deposited without applying any voltage to the electrode and the other was deposited with a +1kV potential applied. The samples deposited in the same run as

the last batch reported in Chapter 6 and were therefore assumed to have the same characteristics, which are summarised in Table 7.1 for the readers' convenience.

Table 7.1: Summary of the superconducting results for two films used to construct filter devices.

Applied Voltage [kV]	$T_c(0)$ [K]	$\triangle T_c$ [K]
0	75.0	7.2
1	88.4	2.2

The dual-mode filter device was then manufactured according to the fabrication steps outlined in Chapter 4. Fig. 7.5 shows the completed filter, mounted on the testing circuit board.

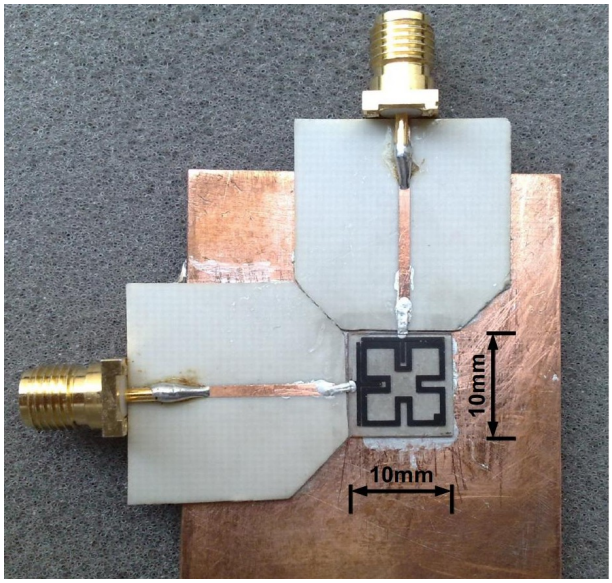

Figure 7.5: The completed filter and test structure of the +1kV YBCO sample.

7.4 Measurement

Once the prototype filter devices had been fabricated, they were then measured and compared to the EM simulation results. This was the last stage of verification of the devices after fabrication. A Rohde & Schwarz ZVB8 Vector Network Analyzer (VNA) was used to measure the filter's frequency response. The frequency range of the VNA is 300 kHz to 8 GHz. The filter designs fitted well within this range, hence the use of this equipment is applicable to the experiment.

The VNA was first calibrated using the standard SOLT (Short circuit, Open circuit, Line and Thru) calibration procedure and measurement of known standards. This procedure is detailed by [111]. By calibrating the VNA with these standards, only then it can compensate for its inherent imperfections in the test structure and coaxial cables and shifting the effective measurement planes to the ports of the device-under-test (DUT). The compensation corrections are calculated by measuring precision standards of with known characteristics. The ZVB8 VNA was able to calculate the transformation matrix and apply it to the measured S-parameters automatically. The microstrip SOLT standards developed by [111] were used for the calibration. Measurements could proceed after calibration. Care has to be taken not to disturb the measurement setup and to perform the measurement exactly as calibrated to ensure accurate results.

The two ports of the filter where connected to the VNA carefully. The filter device was then cooled to 77K by gradually submersing it in liquid nitrogen. Fig. 7.6 shows how the test structure was partially submersed in the liquid nitrogen. The entire superconducting part was in the liquid nitrogen and measurements were only taken once the liquid has stopped boiling. A 1000 point sweep was then made from 2GHz-6GHz, recording the S-parameters of the filter device. Fig. 7.7 (a) and (b) show the measured responses of the 0V YBCO sample and +1kV YBCO sample filter devices, respectively. The experiment results will be discussed in the following section.

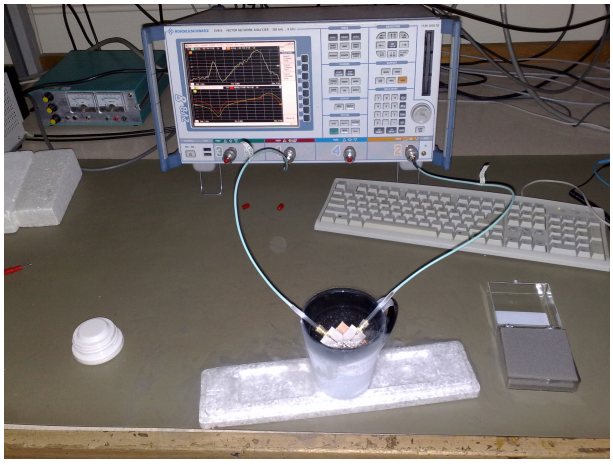

Figure 7.6: The filter response +1kV YBCO sample device measured at 77K with a Rohde & Schwarz ZVB8 VNA. The superconducting filter is immersed in liquid nitrogen.

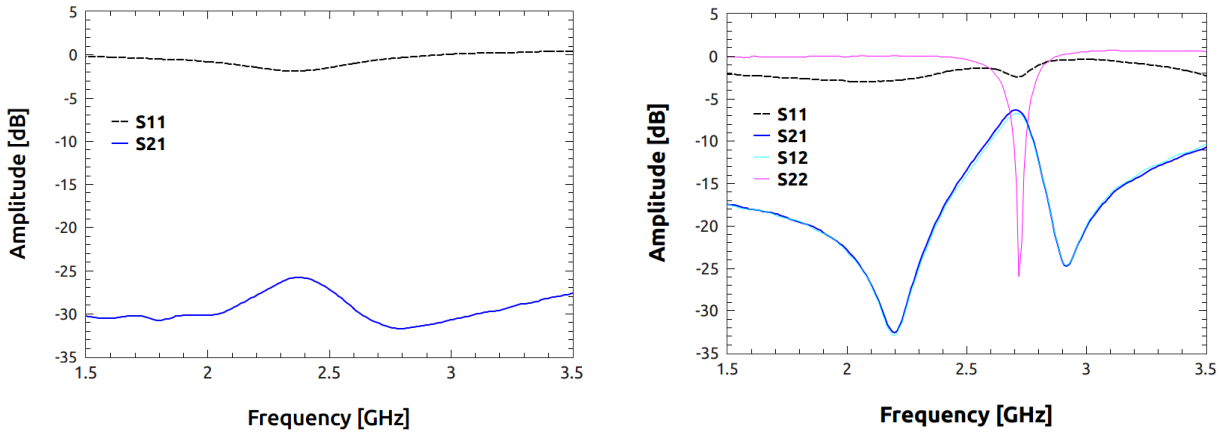

(a) (b)

Figure 7.7: Measured filter performance of the (a) 0V PLD sample filter and (b) the +1kV PLD sample filter.

7.4.1 Discussion

From Fig. 7.7 (a) we can see that the filter made from the normal PLD sample (0V applied) did not show much of a filter response at all. This is most probably due to the low transition temperature of this sample (see Table 7.1) and the sample was not fully superconducting at 77K.

The frequency response of the +1kV sample was much better (see Fig. 7.7). A bandpass filtering action is evident, with a centre frequency of 2.71GHz and 3-dB bandwidth ($S11 \leq -9.3$dB) of 160MHz and an insertion loss of -6.3dB. The out of band attenuation is quite poor. Although the filter is far from ideal, it does serve the purpose of proof-of-concept device. In comparison to the simulated response (centre frequency of 2.74GHz, a bandwidth of 70MHz and an insertion loss of -1.8dB) the device is reasonably close, although it does display much larger losses and an asymmetrical response as can be seen in see Fig. 7.7 ($S_{12} = S_{21}$). Fig. 7.8 shows a comparison of the measurement and simulation performed over a much wider range of frequencies.

The additional losses can be attributed to various non-ideal aspects in the filter's construction. The use of a printed transparency film as the UV lithography mask created much rougher edges on the device. This increases the surface resistance of the superconductor and its losses. A major source of losses is the poor electrical contact that the silver past makes with the superconductor. As was shown in Fig. 4.20 in Chapter 4, this silver connection has residual resistance of approximately 8 ohm. This results in poor coupling to the device. Furthermore, we suspect the imperfect nature of these connections is responsible for the asymmetry of the filter response. Parasitic coupling between the input and output can cause the additional transmission zeros.

Using silver paste as the ground plane and to make electrical contact also increases the losses. Silver conductive paint has a much higher resistivity ($\sim 1 \times 10^{-5}$ Ω.m) than gold (2.44×10^{-8} Ω.m), silver (1.59×10^{-8} Ω.m) and copper (1.72×10^{-8} Ω.m). The backside of the MgO substrate

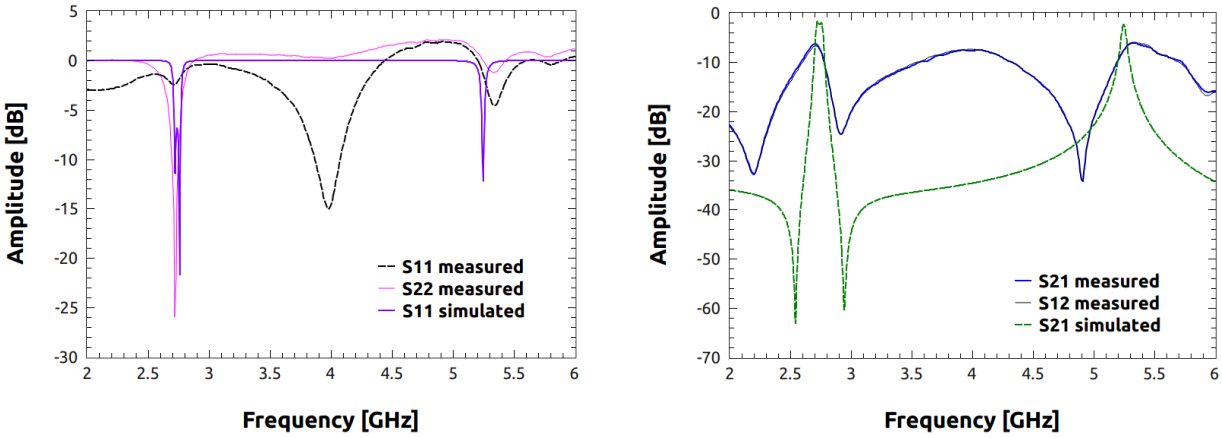

(a) (b)

Figure 7.8: Measured filter performance compared to the EM simulation results

is also very rough (single side polished substrate), which further increases the surface resistance of the ground plain. Furthermore, the meander loop filter is very sensitive to substrate thickness variations. This is because of the effect of all the corners along the meander [41].

The very small substrate made it difficult to make good connections to the filter and these connections were very close to the actual device. This could lead to distortion in the electromagnetic field distributions and effect the devices performance. Future research should focus on obtaining larger area, double-sided superconducting films, so that better performing devices can be constructed.

The test setup was not ideal either. The used filter device should be enclosed in a filter housing to shield the device and testing should be performed in a vacuum cooler or dewar. This should also allow the addition of tuning elements, as the high performance of this kind of filter is rarely achieved without considerable tuning.

To end on a positive note, considering all the fabrication and implementation limitations, the bandpass filter response of the device is clearly evident at approximately the correct frequency (1.9% error) and a 6% bandwidth. Furthermore, only the filter constructed from the film deposited with the novel E-field enhanced PLD technique developed in the previous chapter showed any type of filter response at 77K. This can be attributed to its superior thin film properties and superconducting properties. It is therefore a very valuable technique that can help to produce practical superconducting devices.

7.5 Conclusion

A simple superconducting filter device has been successfully constructed and tested. The filter device was fabricated completely in-house and showed a reasonably similar response in comparison to what was designed and simulated. The filter created from a compact dual-mode bandpass filter

design chosen to fit on the small 10mm×10mm superconducting YBCO thin film samples that we can fabricate. Various reasons for the poor response of the filter have been suggested and a future direction for this work is to try to improve on the various aspects highlighted and focus on increasing the size of YBCO samples that we can produce. These results serve as a final validation of the value of the novel E-field enhanced PLD method developed in this thesis. Only the samples prepared using this technique where of sufficiently high quality to allow a working device to be manufactured.

Chapter 8

Conclusions

The aim of this thesis was to developed a novel method to improve the quality of superconducting YBCO thin films produced with PLD. The PLD system at Stellenbosch University has never been able to match the quality of the thin films produced using the inverted cylindrical magnetron sputtering unit. Therefore, we aim to improve the quality of the superconducting thin films produced using this local PLD equipment. However, the broader aim was to produce a universal method that could be used for any PLD system. This method therefore needed to be simple to implement as an *"add-on"* to any existing system. Furthermore, the technique needed to work with existing deposition parameters and result in minimal modification of the deposition environment. An in situ technique was also desired, as excessive handling degrades the superconducting properties of YBCO thin films.

We began by looking at the properties of superconductors and continued to explore the material properties of YBCO thin films and the difficulties associated with their deposition. The sensitivity of YBCO to oxygen content has made the use of oxygen plasmas a popular method for improving the superconducting quality of thin films. DC glow discharges are popular methods of introducing plasmas into the PLD deposition chamber during deposition and its application has shown good results in the literature. The in situ application of electric fields and voltage biasing was therefore the starting point of our investigations. This method potentially satisfied many of the characteristics desired for the improvement technique we were looking for:

- simple easily controllable parameter (voltage bias),
- cost effective to implement,
- very little modification to the deposition environment,
- improves the results obtained with sub-optimal conditions (e.g. lower substrate deposition temperatures).

In the past this technique had shown potential for lowering the deposition temperatures required to deposit good quality YBCO thin films and therefore make them compatible with more materials. However, this DC Plasma Enhanced technique never gained widespread use. We investigated the problems of this method, by experimenting with its application in Chapter 5. We were able to show that, although the technique worked well, the plasma produced was unstable and tended to cause random arcing in the chamber. Arcing is undesirable due to its damaging effects and the instability it creates for a deposition process.

In Chapter 6 we modified the experimental setup to prevent these unwanted discharges from occurring. We investigated the effect of applying large static electric fields in situ during deposition, with insulated electrodes rather than bare metal electrodes. The insulated electrodes prevented the DC plasma discharge and we observed that by using this technique we could modulate the quality of the thin films grown, depending on the polarity of the applied voltage. Various electrode configurations were investigated and refined, resulting in a final electrode design that was stable and produced reproducible results of excellent quality.

Our novel method showed that an positively biased insulated electrode placed in close proximity to the target can have the same enhancing effect as has been previously shown with bare metal electrodes. The use of insulated electrodes allowed the exploration of a much wider range of bias voltages than has previously been explored in the literature. This technique could also be used for lowering the substrate temperature during YBCO deposition, as has been shown in the literature by similar techniques using bare metal electrodes. However, this was not tested in this research and should be explored in future work. This would potentially allow us to deposit YBCO thin films with a wider variety of materials, such as silicon.

Our results showed that a negatively biased electrode always deteriorated the film quality obtained. This has possible applications in T_c modulation for multilayer HTS fabrication processes. The technique developed is especially useful for improving sub-optimal deposition parameter sets, such as those experienced due to decreased laser energy and deteriorated targets, a common problem experienced in our research group.

Furthermore, this project's results shed new light on the possible cause for the film improvement observed. In the literature there is no strong consensus on the exact mechanisms responsible for the improvement of YBCO thin films using DC PE-PLD. The most common assertion is that the activated oxygen plasma is responsible for increased oxygenation of the thin films. This argument does not readily explain the reasons why the oppositely biased case degrades the thin films produced, as it has be shown that under these circumstance the plasma shows higher levels of excitement. In fact this case is very rarely reported in the literature. In this work we showed that this case definitely exists and give a plausible qualitative explanation that holds for both conditions, improvement and degradation. We propose that it is the effect of the E-fields on the electrons in the plasma plume and the charging of the target surface, rather than the DC plasma discharge itself that is responsible for the observed effects. This argument is plausible as no DC plasma exists

for our insulted electrode configuration, yet the similar results were observed.

We have therefore developed and demonstrated a novel technique to improve the quality of YBCO films grown by PLD. By introducing an insulated high voltage electrode into the chamber during deposition, the quality of the deposited thin films can be enhanced or degraded depending on the polarity of the voltage applied. The electrode is simple and cost effective to produce. It is made from a single HV wire that is placed close to the target. The entire chamber is grounded and only the electrode is electrified. Applying a positive voltage improved the films obtained. There was an optimal range of values for which this worked and applying too large a voltage degraded the quality of the deposited films. Applying a negative voltage always degraded the superconducting properties of the films. The insulating electrode prevented the DC glow discharge and all electrical discharging in the chamber. Therefore this configuration was very stable and produced repeatable results. We found that the method works best when the electrode is closest to the target. This tends to indicate that it is the localised effect of the electric field on the target material and plume, rather than an effect on the substrate that causes the enhancement.

The secondary aim of this project was is to construct a simple proof-of-concept device. A HTS microwave filter was chosen to demonstrate value of the technique developed. These filters can be constructed using a single superconducting layer and the quality of the superconducting layer directly affects the final device's performance. Chapter 7 summarizes the design, fabrication and testing of the superconducting band-pass filter.

The largest area that we can currently deposit YBCO films with reasonable uniformity is 10mm×10mm. We therefore had to focus on making the filter as small as possible. A 2^{nd} order dual-mode band-pass microwave filter was chosen for its extremely compact size. The filter was designed and simulated with EM simulation software to have a centre frequency of 2.74GHz, a bandwidth of 70MHz and an insertion loss of -1.8dB. Two filters were constructed from 300nm layer YBCO thin films deposited on MgO substrates. One film was deposited using normal PLD and the other with our novel enhancement technique. The films were then patterned with standard UV lithography and wet chemical etching.

Only the filter made with the YBCO deposited with the our novel PLD technique displayed the correct filtering action upon cooling to 77K. This could be attributed to the higher transition temperature and better superconducting films achieved by applying this technique. This filter had a centre frequency of 2.71GHz, a bandwidth of 160MHz and an insertion loss of -6.3dB. Although the filter was far from ideal it did serve as a proof-of-concept device. The additional losses could be attributed to various non-ideal aspects in the filter's construction.

Future research should focus on obtaining larger area, double-sided superconducting films, so that better filter devices can be fabricated. Furthermore, research should be instigated into developing proper test structures for these devices, such as sealed vacuum Dewars.

The major contributions presented in this thesis are as follows:

- In this research we successfully developed a novel in situ deposition technique to improve superconducting YBCO thin films (published in [132])
  - The technique is simple and cost effective
  - It does not require complex control circuitry or matching networks
  - This technique sheds new light on the possible reasons for applied electric fields improving film quality
  - Technique has application for other materials that require reactive deposition
  - We demonstrate for the first time that insulated electrodes can be used to improve the film quality
  - The developed technique offers drastic improvement in stability and reliability over previous efforts that utilise bare metal electrodes
  - We show for the first time that applying the appropriate potential the film growth can be improved and degrad*ed*. This has significant importance, as it can potentially be used to develop a novel multilayer process, where layers are tuned as required according to the deposition potential, while retaining virtually the same crystal structure
- The successfully design, manufacture and testing of a compact dual-mode HTS bandpass filter in the S-band is presented
  - We demonstrated the first HTS filter produced completely in-house for our research group
  - We show that even with the limited manufacturing and testing equipment that HTS filter manufacture is possible and a viable research avenue
  - Future research areas necessary to make this a viable commercial outlet for the department are also identified
    - large area deposition
    - double sided/ multilayer deposition
    - optimise and simplify electrical contact to the devices
    - permanent low temperature test fixture to test in a shielded environment

In conclusion, we have shown that the in situ application of DC E-fields via insulated electrodes during PLD is an effective method to produce high quality YBCO thin films suitable for practical device applications. Further research into this technique is strongly advised to be able to realise this technique's potential within the superconducting industry.

Bibliography

[1] S. Anders, M. Blamire, F.-I. Buchholz, D.-G. Crété, R. Cristiano, P. Febvre, L. Fritzsch, A. Herr, E. Il'ichev, J. Kohlmann, J. Kunert, H.-G. Meyer, J. Niemeyer, T. Ortlepp, H. Rogalla, T. Schurig, M. Siegel, R. Stolz, E. Tarte, H. ter Brake, H. Toepfer, J.-C. Villegier, A. Zagoskin, and A. Zorin, "European roadmap on superconductive electronics - status and perspectives," *Physica C: Superconductivity*, vol. 470, no. 23-24, pp. 2079–2126, Dec. 2010. [Online]. Available: http://linkinghub.elsevier.com/retrieve/pii/S0921453410005332 1, 2, 3, 6, 10, 21, 109

[2] O. Vendik, I. Vendik, and D. Kholodniak, "Applications of High-Temperature Superconductors in Microwave Integrated Circuits," *Mater. Phys. Mech*, vol. 2, pp. 15–24, 2000. [Online]. Available: http://194.226.210.10/e-journals/MPM/no_1200/vendik/vendik.pdf 1, 109

[3] T. P. Sheahen, *Introduction to High-Temperature Superconductivity*, S. Wolf, Ed. Kluwer Academic Publichers, 2002. 1, 9

[4] D. Yohannes, S. Sarwana, S. K. Tolpygo, A. Sahu, Y. A. Polyakov, and V. K. Semenov, "Characterization of HYPRES' 4.5 kA/cm^2 & 8 kA/cm^2 Nb/AlO$_x$/Nb Fabrication Processes," *IEEE Transactions on Applied Superconductivity*, vol. 15, no. 2, pp. 90–93, June 2005. 2

[5] M. Huang, P. Komissinski, A. Kidiyarova-Shevchenko, M. Gustafsson, E. Olsson, B. Hogberg, Z. Ivanov, and T. Claeson, "Small scale integrated technology for HTS RSFQ circuits," *IEEE Transactions on Appiled Superconductivity*, vol. 11, no. 1, pp. 558–561, Mar. 2001. [Online]. Available: http://ieeexplore.ieee.org/lpdocs/epic03/wrapper.htm?arnumber=919406 2

[6] S. Tanaka, "High-temperature superconductivity: History and outlook," *Japan Society of Applied Physics International*, vol. 4, no. 4, pp. 17–22, 2001. [Online]. Available: http://www.thirdwave.de/3w/tech/mnt/superconductorsppf.pdf 2

[7] S. Nishijima, S. Eckroad, A. Marian, K. Choi, W. S. Kim, M. Terai, Z. Deng, J. Zheng, J. Wang, K. Umemoto, J. Du, P. Febvre, S. Keenan, O. Mukhanov, L. D. Cooley, C. P. Foley, W. V. Hassenzahl, and M. Izumi, "Superconductivity and the environment:

a Roadmap," *Superconductor Science and Technology*, vol. 26, no. 11, p. 113001, Nov. 2013. [Online]. Available: http://stacks.iop.org/0953-2048/26/i=11/a=113001?key=crossref.f9bca89d1e8cd322837a1cf4b0709213 2, 3

[8] O. A. Mukhanov, "Energy-Efficient Single Flux Quantum Technology," *IEEE Transactions on Applied Superconductivity*, vol. 21, no. 3, pp. 760–769, Jun. 2011. [Online]. Available: http://ieeexplore.ieee.org/xpls/abs_all.jsp?arnumber=5682046http://ieeexplore.ieee.org/lpdocs/epic03/wrapper.htm?arnumber=5682046 2, 3

[9] A. Fujimaki, "Advancement of superconductor digital electronics," *IEICE Electronics Express*, vol. 9, no. 22, pp. 1720–1734, 2012. [Online]. Available: http://japanlinkcenter.org/DN/JST.JSTAGE/elex/9.1720?lang=en&from=CrossRef&type=abstract 2, 3

[10] K. K. Likharev, "Superconductor digital electronics," *Physica C: Superconductivity*, vol. 482, pp. 6–18, Nov. 2012. [Online]. Available: http://linkinghub.elsevier.com/retrieve/pii/S0921453412002481 2

[11] E. A. Gutiérrez-D., "Physics of Silicon at Cryogenic Temperatures," in *Low Temperature Electronics: Physics, Devices, Circuits, and Applications*, E. A. Gutiérrez-D., M. J. Deen, and C. Claeys, Eds. Academic Press, 2001, ch. 1, pp. 1–96. 3

[12] R. W. Simon, R. B. Hammond, S. J. Berkowitz, and B. A. Willemsen, "Superconducting Microwave Filter Systems for Cellular Telephone Base Stations," *Proceedings Of The IEEE*, vol. 92, no. 10, pp. 1585–1596, October 2004. 3

[13] D. Brock, O. Mukhanov, and J. Rosa, "Superconductor digital RF development for software radio," *IEEE Communications Magazine*, no. February, pp. 2–7, 2001. [Online]. Available: http://ieeexplore.ieee.org/xpls/abs_all.jsp?arnumber=900649 3

[14] R. R. Romanofsky and F. A. Miranda, "High-Temperature Superconductor / Semiconductor Hybrid Microwave Devices and Circuits," in *Low Temperature Electronics: Physics, Devices, Circuits, and Applications*, E. A. Gutiérrez-D., M. J. Deen, and C. Claeys, Eds. San Diego: Academic Press, 2001, ch. 7, pp. 841–900. 3

[15] T. Van Duzer and S. Kumar, "Semiconductor-superconductor hybrid electronics," *Cryogenics*, vol. 30, no. 12, pp. 1014–1023, Dec. 1990. [Online]. Available: http://linkinghub.elsevier.com/retrieve/pii/001122759090201M 3, 30

[16] J. Narayan, N. Biunno, R. Singh, O. Holland, and O. Auciello, "Formation of thin superconducting films by the laser processing method," *Applied Physics Letters*, vol. 51, no. 22, pp. 1845–1847, November 1987. 4, 31

[17] S. Witanachchi, S. Patel, H. S. Kwok, and D. T. Shaw, "As-deposited Y-Ba-Cu-O superconducting films on silicon at 400°C," *Applied Physics Letters*, vol. 54, no. 6, pp.

578–580, 1989. [Online]. Available: http://ieeexplore.ieee.org/xpls/abs_all.jsp?arnumber=4859193 4, 5, 31, 38, 44, 45, 72

[18] R. Eason, *Pulsed laser deposition of thin films: applications-led growth of functional materials*. John Wiley & Sons, 2007. [Online]. Available: http://books.google.com/books?hl=en&lr=&id=0jIO3cwkiOIC&oi=fnd&pg=PR7&dq=Pulsed+laser+deposition+of+thin+films:+applications-led+growth+of+functional+materials&ots=PVRVcu-QRM&sig=XGjcWR4-GFBPNh4rvvVfxqucxRg 4

[19] D. Dijkkamp, T. Venkatesan, X. Wu, S. Shaheen, N. Jisrawi, Y. Min-Lee, W. McLean, and M. Croft, "Preparation of Y-Ba-Cu oxide superconducting thin films using pulsed laser evaporation from high T_c bulk material," *Applied Physics Letters*, vol. 51, pp. 619–621, 1987. 4, 27

[20] T. Haugan, P. Barnes, L. Brunke, I. Maartense, and J. Murphy, "Effect of O_2 partial pressure on $YBa_2Cu_3O_{7-\delta}$ thin film growth by pulsed laser deposition," *Physica C*, vol. 397, pp. 47–57, 2003. 4

[21] M. Branescu, V. S. Teodorescu, G. S. a, I. B. b, C. D. c, and J. Jaklovszky, "Experiments On Pulsed Laser Deposition And Characterization Of Epitaxially In-situ Grown $YBa_2Cu_3O_{7-x}$ Thin Films," *Journal of Optoelectronics and Advanced Materials*, vol. 7, no. 2, pp. 967–972, April 2005. 4

[22] Y. Ishimaru, M. Ogura, O. Horibe, S. Adachi, H. Wakana, K. Nakayama, Y. Tarutani, U. Kawabe, and K. Tanabe, "Development of multilayer process with upper wiring layer for HTS circuit application," *Physica C*, vol. 445-448, pp. 908–911, July 2006. 4, 5, 31

[23] J. Talvacchio, M. G. Forrester, and J. R. Gavaler, "Properties of passive structures for multilayer HTS digital circuits," *IEEE Transactions on Appiled Superconductivity*, vol. 5, no. 2, pp. 3139–3142, 1995. [Online]. Available: http://ieeexplore.ieee.org/xpls/abs_all.jsp?arnumber=403257 5, 27, 31

[24] A. Inam, M. Hegde, X. Wu, T. Venkatesan, P. England, and P. Miceli, "As-deposited high T_c and J_c superconducting thin films made at low temperatures," *Applied Physics Letters*, vol. 53, no. 10, pp. 908–910, September 1988. 5, 31

[25] S. Witanachchi, H. S. Kwok, X. W. Wang, and D. T. Shaw, "Deposition of superconducting Y-Ba-Cu-O films at 400°C without post-annealing," *Applied Physics Letters*, vol. 53, no. 3, pp. 234–236, 1988. [Online]. Available: http://ieeexplore.ieee.org/xpls/abs_all.jsp?arnumber=4858164 5, 31, 36, 38, 44, 45, 72

[26] S. Funaki, Y. Yoshida, Y. Ichino, M. Miura, Y. Takai, K. Matsumoto, A. Ichinose, M. Mukaida, and S. Horii, "Enhancement of dislocation density in $YBa_2Cu_3O_y$ thin

films prepared by low temperature growth technique," *Physica C: Superconductivity*, vol. 463-465, pp. 644–648, Oct. 2007. [Online]. Available: http://linkinghub.elsevier.com/retrieve/pii/S0921453407008854 5, 31

[27] W. F. Van Staden, "The fabrication of PBCO buffered step-edge Josephson Junctions," MScEng, University of Stellenbosch, Electrical and Electronic Engineering, Dec 2007. [Online]. Available: http://hdl.handle.net/10019/483 5, 29, 48, 65, 69

[28] A. A. Elkaseh, "Fabrication of josephson junctions using afm nanolithography," PhDEng, University of Stellenbosch, Electrical and Electronic Engineering, Dec 2010. 5

[29] U. Büttner, "The development of equipment for the fabrication of thin film superconductor and nano structures," MScEng, University of Stellenbosch, 2011. 5, 29, 53, 56

[30] A. Mourachkine, *Room-Temperature Superconductivity*. Cambridge International Science Publishing, 2004. 8, 9

[31] K. A. Müller, "The search for new high temperature superconductors," *Superconductor Science and Technology*, vol. 19, pp. S1–S3, 2006. 8

[32] M. Wu, J. Ashburn, C. J. Torng, P. Hor, R. Meng, L. Gao, Z. Huang, Y. Wang, and C. Chu, "Superconductivity at 93K in a new mixed-phase Y-Ba-Cu-O compound system at ambient pressure," *Physics Review Letters*, vol. 58, pp. 908–910, 1987. 8, 27

[33] N. Khare, "Introduction to High-Temperature Superconductors," in *Handbook of High-Temperature Superconducting Electronics*, N. Khare, Ed. New York: Marcel Dekker, Inc., 2003, ch. 1. 9

[34] D. P. Norton, "Epitaxial Growth of Superconducting Cuprate Thin Films," in *Handbook of High-Temperature Superconductor Electronics*, N. Khare, Ed. New York: Marcel Dekker, Inc., 2003, ch. 2. 9, 18

[35] S. Uchida, "Forefront in the Elucidation of the Mechanism of High-Temperature Superconductivity," *Japanese Journal of Applied Physics*, vol. 51, no. 1, p. 010002, Jan. 2012. [Online]. Available: http://jjap.jsap.jp/link?JJAP/51/010002/ 9, 22

[36] C. P. Poole, Jr., H. A. Farach, R. J. Creswick, and R. Prozorov, *Superconductivity*, 2nd ed., ., Ed. Academic Press, June 2007. 9, 21

[37] M. Youssif, A. Bahgat, and I. Ali, "AC magnetic susceptibility technique for the characterization of high temperature superconductors," *Egyptian Journal of Solids*, vol. 23, no. 2, pp. 231–250, 2000. [Online]. Available: http://egmrs.powweb.com/EJS/PDF/vo232/231.pdf 10

[38] P. A. Atanasov, R. I. Tomov, and V. S. Serbezov, "Plasma assisted in situ laser depostition of $YBa_2Cu_3O_{7-x}$ superconducting thin films with laser heating and annealing," *Vacuum*, vol. 45, no. 12, pp. 1215–1219, 1994. 10, 43, 44, 45, 72

[39] M. P. Lisitskiy, C. Camerlingo, M. Salvato, A. Vecchione, and M. Russo, "Improvement of the homo-biepitaxial YBCO film fabrication process on Yttrium Stabilized Zirconia," *Journal of Physics: Conference Series*, vol. 43, pp. 1135–1138, 2006. 10

[40] T. Orlando and K. Delin, *Foundations of Applied Superconductivity*. Addison-Wesley Publishing Company, 1991. 13, 14

[41] J.-S. Hong and M. J. Lancaster, *Microstrip Filters for RF/Microwave Applications*. New York, USA: John Wiley & Sons, Inc., Jun. 2001, vol. 7. [Online]. Available: http://doi.wiley.com/10.1002/0471221619 17, 18, 19, 20, 25, 109, 110, 111, 116

[42] N. Klein, "High-frequency applications of high-temperature superconductor thin films," *Reports on Progress in Physics*, vol. 65, no. 10, pp. 1387–1425, Oct. 2002. [Online]. Available: http://stacks.iop.org/0034-4885/65/i=10/a=201?key=crossref.8acdc39937642ca3da42c9f3cde72ffc 19, 21, 23

[43] H.-U. Habermeier, "Thin films of perovskite-type complex oxides," *Materials Today*, vol. 10, no. 10, pp. 34–43, Oct. 2007. [Online]. Available: http://linkinghub.elsevier.com/retrieve/pii/S1369702107702432 22, 23, 25, 26, 27

[44] D. Dimos, P. Chaudhari, and J. Mannhart, "Superconducting transport properties of grain boundaries in $YBa_2Cu_3O_7$ bicrystals," *Physical Review B*, vol. 41, pp. 4038–4049, 1990. 24

[45] M. Hein, T. Kaiser, and G. Müller, "Surface resistance of epitaxial $YBa_2Cu_3O_{7-x}$ films on various substrates: Effects of pair condensation and quasiparticle scattering," *Physical Review B*, vol. 61, no. 1, pp. 640–647, 2000. [Online]. Available: http://prb.aps.org/abstract/PRB/v61/i1/p640_1 24

[46] J. Du, S. Gnanarajan, and a. Bendavid, "Characterization of MgO substrates for growth of epitaxial YBCO thin films," *Superconductor Science and Technology*, vol. 18, no. 8, pp. 1035–1041, Aug. 2005. [Online]. Available: http://stacks.iop.org/0953-2048/18/i=8/a=002?key=crossref.6e215d8c438a876c89e61d4b5ab60ec5 24, 26

[47] P. Seidel, F. Schmidl, C. Steigmeier, S. Linzen, K. Peiselt, M. Mans, H. Jacob, F. Schmidt, and J. Scherbel, "Thin YBCO films on different substrates and their use in Josephson junctions and SQUIDs," *Superconductor Science and Technology*, vol. 15, no. 3, pp. 462–467, Mar. 2002. [Online]. Available: http://stacks.iop.org/0953-2048/15/i=3/a=335?key=crossref.95db77b78602e915734371583eea7851 24, 25

[48] J. M. Phillips, "Substrate selection for high-temperature superconducting thin films," *Journal of Applied Physics*, vol. 79, no. 4, p. 1829, 1996. [Online]. Available: http://link.aip.org/link/JAPIAU/v79/i4/p1829/s1&Agg=doi 25, 26

[49] R. Hott, "Materials aspects of high-temperature superconductors for applications," in *High Temperature Superconductivity 1 - Materials*, A. V. Narlikar, Ed. Springer Berlin, 2004, no. September 2003, ch. 1, pp. 1–28. [Online]. Available: http://arxiv.org/abs/cond-mat/0306442 25, 31

[50] J. Krupka, R. G. Greyer, M. Kuhn, and J. H. Hinken, "Dielectric properties of single crystals of Al_2O_3, $LaAlO_3$, $NdGaO_3$, $SrTiO_3$, and MgO at cryogenic temperatures," *IEEE Transactions on Microwave Theory and Techniques*, vol. 42, no. 10, pp. 1886–1890, 1994. [Online]. Available: http://scholar.google.com/scholar?hl=en&btnG=Search&q=intitle:Dielectric+properties+of+single+crystals+of+Al2O3,+LaAlO3,+NdGaO3,+SrTiO3,+and+MgO+at+cryogenic+temperatures#1 25

[51] G. Koren, A. Gupta, E. A. Giess, A. Segmuller, and R. B. Laibowitz, "Epitaxial films of YBa2Cu3O7-d on NdGaO3, LaGaO3, and SrTiO3 substrates deposited by laser ablation," *Applied Physics Letters*, vol. 54, no. 11, pp. 1054–1056, 1989. 25, 31, 32, 33

[52] J. Du, S. Gnanarajan, and a. Bendavid, "Influence of MgO surface conditions on the in-plane crystal orientation and critical current density of epitaxial YBCO films," *Physica C: Superconductivity*, vol. 400, no. 3-4, pp. 143–152, Jan. 2004. [Online]. Available: http://linkinghub.elsevier.com/retrieve/pii/S092145340301431X 26

[53] S. Bhat, M. L. Hammond, K. C. Cadien, M. Keefer, R. Chow, W. Kern, G. J. Collins, W. S. Knodle, C. Dennison, J. J. McNally, J. Foggiato, J. R. McNeil, C. A. Moore, K. Seshan, R. Pinto, V. Singh, P. D. Reader, L. R. Thompson, S. Rossnagel, J. Turlo, L. B. Rothman, Z. qi Yu, D. J. Schepis, J. L. Zilko, and K. K. Schuegraf, *Handbook of Thin-Film Deposition Processes and Techniques*, 2nd ed., K. Seshan, Ed. Norwich, NY: Noyes Publications / William Andrew Publishing, 2002. 26

[54] B. Oh, M. Naito, S. Arnason, P. Rosenthal, R. Barton, M. R. Beasley, T. H. Geballe, R. H. Hammond, and A. Kapitulnik, "Critical current densities and transport in superconducting $YBa_2Cu_3O_{7-\delta}$ films made by electron beam coevaporation," *Applied Physics Letters*, vol. 51, no. 11, pp. 852–854, 1987. [Online]. Available: http://ieeexplore.ieee.org/xpls/abs_all.jsp?arnumber=4855938 27

[55] D. P. Norton, "Pulsed Laser Deposition Of Complex Materials: Progress Toward Applications," in *Pulsed Laser Deposition of Thin Films: Applications-Led Growth of Functional Materials*, R. Eason, Ed. Wiley Interscience, 2007, ch. 1, pp. 3–28, epitaxial growth of superconducting cuprate thin films. 27, 44

[56] H. M. Christen and G. Eres, "Recent advances in pulsed-laser deposition of complex oxides," *J. Phys.: Condens. Matter*, vol. 20, pp. 264 005–264 020, Jun 2008. 27

[57] H. Krebs, M. Weisheit, and J. Faupel, "Pulsed Laser Deposition (PLD) - A Versatile Thin Film Technique," in *Advances in Solid State Physics*, B. Kramer, Ed. Springer Berlin Heidelberg, 2003, vol. 43, pp. 505–518. [Online]. Available: http://link.springer.com/chapter/10.1007/978-3-540-44838-9_36 28

[58] J. Schou, "Physical aspects of the pulsed laser deposition technique: The stoichiometric transfer of material from target to film," *Applied Surface Science*, vol. 255, no. 10, pp. 5191–5198, Mar. 2009. [Online]. Available: http://linkinghub.elsevier.com/retrieve/pii/S0169433208022617 28

[59] R. K. Singh and D. Kumar, "Pulsed laser deposition and characterization of high-T_c $YBa_2Cu_3O_{7-x}$ superconducting thin films," *Materials Science and Engineering: R: Reports*, vol. 22, pp. 113–185, 1998. 28

[60] F. W. Graser, "A Reproducible Design and Manufacturing Process for SQUID Magnetometers," MScEng, University of Stellenbosch, 2005. 28, 29, 31, 48, 56, 65, 66, 69

[61] D. P. Norton, "Synthesis and properties of epitaxial electronic oxide thin-film materials," *Materials Science and Engineering: R: Reports*, vol. 43, no. 5-6, pp. 139–247, Mar. 2004. [Online]. Available: http://linkinghub.elsevier.com/retrieve/pii/S0927796X03001384 28

[62] C. Andreouli, T. Efthimiopoulos, S. Christoulakis, A. Tsetsekou, and C. Panagopoulos, "Influence of irradiated target modification on the quality of pulsed laser deposited $YBa_2Cu_3O_{7-x}$ thin films," *Journal of the European Ceramic Society*, vol. 24, no. 14, pp. 3623–3634, Nov. 2004. [Online]. Available: http://linkinghub.elsevier.com/retrieve/pii/S0955221903009130 28

[63] H. A. C. de Villiers, "A Process for the Manufacture of High Temperature Bi-epitaxial Josephson Junctions," MScEng, University of Stellenbosch, 2007. 29, 30, 32, 48, 56, 63

[64] J. F. I. Nturambirwe, "Non-destructive measurement of internal fruit quality using SQUID-NMR techniques," MScEng, University of Stellenbosch, 2012. 29, 48, 68

[65] E. H. Conradie, "The design and fabrication of dc SQUID magnetometers," MScEng thesis, University of Stellenbosch, 1998. 29, 30, 31, 48, 52

[66] E. Knox-Davies, "The Design and Fabrication of a High-Tc DC SQUID Gradiometer," MScEng, University of Stellenbosch, Electrical and Electronic Engineering, December 1999. 29, 30, 48, 56, 69

[67] P. A. Rottier, "Establishing a process for the fabrication of high-quality HTc SQUIDs," MScEng, University of Stellenbosch, Electrical and Electronic Engineering, 2002. 29, 30, 31, 48, 56, 57

[68] E. J. Maritz, "Flux creep in pulsed laser deposited superconducting $YBa_2Cu_3O_7$ thin films," MScEng, University of Stellenbosch, 2002. 29, 48, 49, 51, 80

[69] H.-U. Krebs, M. Weisheit, J. Faupel, E. Süske, T. Scharf, C. Fuhse, M. Störmer, K. Sturm, M. Seibt, H. Kijewski, D. Nelke, E. Panchenko, and M. Buback, "Pulsed laser deposition (PLD) - a versatile thin film technique," *Adv. Solid State Phys.*, vol. 43, pp. 505–517, 2003. 29

[70] J. .McKinnon, M.Ionescu, D. Q. Shi, and S. X.Dou, "On The Growth Mechanisms Of Thin Films Produced By Pulsed Laser Deposition," in *Advances in Cryogenic Engineering: Proceedings of the International Cryogenic Materials Conference - /CMC*, B. B. et al., Ed., vol. 48, 2002, pp. 547–554. 29, 56

[71] B. J. F. Muller, "The Development of a SQUID-based Gradiometer," MScEng, University of Stellenbosch, 2010. 30, 48

[72] A. Morimoto, K. Takezawa, T. Minamikawa, Y. Yonezawa, and T. Shimizu, "Low-temperature growth of YBCO thin films by pulsed laser ablation in reducing environment," *Applied Surface Science*, vol. 127-129, pp. 963–967, May 1998. [Online]. Available: http://linkinghub.elsevier.com/retrieve/pii/S0169433297007745 30, 31, 44

[73] M. Takahashi and Y. Takai, "Low-temperature growth of $YBa_2Cu_3O_x$ by pulsed laser deposition," *Superconductor Science and Technology*, vol. 11, no. 3, p. 265, 1998. [Online]. Available: http://stacks.iop.org/0953-2048/11/i=3/a=002 30

[74] H. S. Kwok, H. S. Kim, S. Witanachchi, E. Petrou, J. P. Zheng, S. Patel, and E. Narumi, "Plasma-assisted laser deposition of $YBa_2Cu_3O_{7-\delta}$," *Applied Physics Letters*, vol. 59, no. 27, pp. 3643–3646, 1991. 31, 38, 39, 45, 72

[75] J. Muyari, N. Kobayashi, S. Takahashi, K. Hayashi, a. Saito, and S. Ohshima, "Fabrication process of YBCO thin film starting from amorphous film for microstrip line device," *Physics Procedia*, vol. 27, pp. 280–283, Jan. 2012. [Online]. Available: http://linkinghub.elsevier.com/retrieve/pii/S1875389212008814 31

[76] A. Gupta, B. Hussey, A. Kussmaul, and A. Segmüller, "Defect Formation caused by transient decrease in the ambient oxygen concentration during growth of $YB_2Cu_3O_{7-\delta}$ films," *Applied Physics Letters*, vol. 57, no. 22, pp. 2365–2367, November 1990. 31

[77] M. Tanaka, Y. Kawagoe, H. Tsukazaki, and K. Yamanishi, "Active oxygen generator by silent discharge and oxidation power in formation of oxide thin films," *Electrical*

Engineering in Japan, vol. 163, no. 1, pp. 1–7, Apr. 2008. [Online]. Available: http://doi.wiley.com/10.1002/eej.20671 31, 32

[78] J. G. López, D. H. A. Blank, and H. Rogalla, "Oxygen content of $YB_2Cu_3O_7$ thin films during growth by pulsed laser deposition," *Applied Surface Science*, vol. 127-129, pp. 1011–1016, 1998. 31, 56

[79] V. a. Shakhatov and O. a. Gordeev, "Thin film deposition by means of laser ablation of titanium oxide targets in oxygen radiofrequency electrode plasma," *High Energy Chemistry*, vol. 42, no. 2, pp. 141–144, Jan. 2011. [Online]. Available: http://link.springer.com/10.1134/S001814390802015X 31, 33

[80] R. Singh, L. Ganapathi, P. Tiwari, and J. Narayan, "Effect of processing geometry in oxygen incorporation and in situ formation of YBaCuO superconducting thin films by pulsed laser evaporation technique," *Applied Physics Letters*, vol. 55, no. 22, pp. 2351–2353, 1989. [Online]. Available: http://link.aip.org/link/?APPLAB/55/2351/1 32, 43, 44, 72, 91

[81] H. Izumi, K. Ohata, and T. Hase, "Superconductivity and crystallinity of $Ba_2Y_1Cu_3O_{7-\delta}$ thin films prepared by pulsed laser deposition with substrate bias voltage," *Journal of Applied Physics*, vol. 68, no. 12, pp. 6331–6334, 1990. [Online]. Available: http://ieeexplore.ieee.org/xpls/abs_all.jsp?arnumber=5088091 32, 40, 41, 44, 45, 72, 73, 79, 91

[82] B. C. Chung, C. H. Tsai, S. S. Hsu, C. S. Huang, T. Y. Tseng, and I. N. Lin, "Spectroscopic study of the microwave plasma enhanced pulsed laser deposition for $Y_1Ba_2Cu_3O_{7-x}$ superconducting thin films," *Applied Surface Science*, vol. 96-98, pp. 233–237, 1996. [Online]. Available: http://cat.inist.fr/?aModele=afficheN&cpsidt=3139085 33

[83] A. D. Giacomo and V. Shakhatov, "Plasma-assisted pulsed laser deposition for the improvement of the film growth process," *Applied Surface Science*, vol. 186, pp. 533–537, 2002. [Online]. Available: http://www.sciencedirect.com/science/article/pii/S0169433201007632 33

[84] M. Cantoro, N. Coppedè, a. Camposeo, F. Cervelli, F. Fuso, M. Allegrini, and E. Arimondo, "Laser ablation of ceramic oxides in the presence of a RF pulsed oxygen plasma," *Surface and Coatings Technology*, vol. 180-181, pp. 591–595, Mar. 2004. [Online]. Available: http://linkinghub.elsevier.com/retrieve/pii/S0257897203012581 33

[85] I. Safi, "Recent aspects concerning DC reactive magnetron sputtering of thin films: a review," *Surface and Coatings Technology*, vol. 127, no. 2-3, pp. 203–218, May 2000. [Online]. Available: http://linkinghub.elsevier.com/retrieve/pii/S0257897200005661 33, 44, 45, 74

[86] A. Bogaerts and R. Gijbels, "Similarities and differences between direct current and radio-frequency glow discharges: a mathematical simulation," *Journal of Analytical Atomic Spectrometry*, vol. 15, no. 9, pp. 1191–1201, 2000. [Online]. Available: http://xlink.rsc.org/?DOI=b000519n 33

[87] A. Bogaerts, E. Neyts, R. Gijbels, and J. van der Mullen, "Gas discharge plasmas and their applications," *Spectrochimica Acta Part B: Atomic Spectroscopy*, vol. 57, no. 4, pp. 609–658, Apr. 2002. [Online]. Available: http://linkinghub.elsevier.com/retrieve/pii/S0584854701004062 33, 34, 35, 36, 82, 91

[88] S. M. Rossnagel, J. J. Cuomo, and W. D. Westwood, Eds., *Handbook of Plasma Processing Technology : Fundementals, Etching, Deposition, and Surface Interactions*. Noyes Publications, 1990. 33

[89] S. Rossnagel, J. Cuomo, and W. Westwood, *Handbook of plasma processing technology: fundamentals, etching, deposition, and surface interactions*. Noyes Publications, 1990. [Online]. Available: http://scholar.google.com/scholar?hl=en&btnG=Search&q=intitle:Handbook+of+Plasma+Processing+Technology+Fundamentals,+Etching,+Deposition,+and+Surface+Interactions#0 33, 90

[90] A. Bogaerts, "The glow discharge: an exciting plasma!" *Journal of Analytical Atomic Spectrometry*, vol. 14, no. 9, pp. 1375–1384, 1999. [Online]. Available: http://xlink.rsc.org/?DOI=a900772e 34

[91] D. Miu, "Enhanced oxide emission in electrode-aided laser deposition of $YBa_2Cu_3O_{7-x}$ thin films," *Romanian Reports in Physics*, vol. 60, no. 3, pp. 797–806, 2008. [Online]. Available: http://www.nimp.ro/2008_60_3/37-797-806.pdf 36, 39, 44, 45, 72

[92] S. Witanachchi, S. Patel, D. T. Shaw, and H. S. Kwok, "Effect of buffer layers on low-temperature growth of mirror-like superconducting thin films on sapphire," *Applied Physics Letters*, vol. 55, no. 3, pp. 295–297, 1989. [Online]. Available: http://ieeexplore.ieee.org/xpls/abs_all.jsp?arnumber=4860002 37, 44, 45, 72

[93] S. Witanachchi, S. Patel, D. Shaw, and H. Kwok, "Low-temperature growth of mirror-like superconducting thin films on sapphire," *Materials Letters*, vol. 8, no. 1, pp. 53–56, 1989. [Online]. Available: http://www.sciencedirect.com/science/article/pii/0167577X8990096738

[94] R. K. Singh, J. Narayan, A. Singh, and J. Krishnaswamy, "In situ processing of epitaxial Y-Ba-Cu-O high-Tc superconducting films on (100) SrTiO3 and (100) YS-ZrO2 substrates at 500-650°C," *Applied Physics A: Materials Science & Processing*, vol. 54, no. 22, pp. 2271–2273, 1989. [Online]. Available: http://ieeexplore.ieee.org/xpls/abs_all.jsp?arnumber=4858906 38, 39, 44, 72, 91

[95] R. Singh and J. Narayan, "In-situ patterned laser deposition of high-Tc Y-Ba-Cu-O superconducting thin films," *Journal of Applied Physics*, vol. 67, no. 7, pp. 3448–3451, 1990. [Online]. Available: http://ieeexplore.ieee.org/xpls/abs_all.jsp?arnumber=508702539

[96] Q. Ying, D. Shaw, and H. Kwok, "Spectroscopic study of plasma-assisted laser deposition of Y-Ba-Cu-O," *Applied physics letters*, vol. 53, no. 18, pp. 1762–1764, 1988. [Online]. Available: http://ieeexplore.ieee.org/xpls/abs_all.jsp?arnumber=4857793 39, 40, 43, 79

[97] J. Zheng, Q. Ying, S. Witanachchi, Z. Q. Huang, D. T. Shaw, and H. S. Kwok, "Role of the oxygen atomic beam in low-temperature growth of superconducting films by laser deposition," *Applied Physics Letters*, vol. 54, no. 10, pp. 954–956, 1989. [Online]. Available: http://ieeexplore.ieee.org/xpls/abs_all.jsp?arnumber=4858430 39

[98] S. Pramanick and J. Narayan, "Effect of processing geometry on $YBa_2Cu_3O_{7-x}$ plasma emission during superconducting thin film growth by pulsed laser evaporation technique," *Journal of Applied Physics*, vol. 73, no. 1, p. 316, 1993. [Online]. Available: http://link.aip.org/link/JAPIAU/v73/i1/p316/s1&Agg=doi 39

[99] H. Takahashi, H. Izumi, K. Ohata, T. Hase, M. Sasaki, T. Morishita, and S. Tanaka, "Crystal structure of $YBa_2Cu_3O_{7-x}$ thin films prepared by pulsed laser deposition with substrate bias voltage," *Physica C: Superconductivity*, vol. 190, no. 4, pp. 427–432, Jan. 1992. [Online]. Available: http://linkinghub.elsevier.com/retrieve/pii/092145349290701Dhttp://www.sciencedirect.com/science/article/pii/092145349290701D 40

[100] D. Fried, T. Kushida, G. P. Reck, and E. W. Rothe, "The effects of the electric field associated with a laser-induced pulsed discharge on the ablation-generated plumes of $YBa_2Cu_3O_{7-x}$," *Jounal of Applied Physics*, vol. 72, no. 3, pp. 1113–1125, August 1992. 41, 42, 73, 91

[101] P. Yeates and E. T. Kennedy, "Diagnostics of laser plasma plume dynamics within an electrically biased confining cavity," *Journal of Applied Physics*, vol. 110, no. 6, p. 063303, 2011. [Online]. Available: http://link.aip.org/link/JAPIAU/v110/i6/p063303/s1&Agg=doi 42

[102] D. S. Mirsa and S. B. Palmer, "Growth of as-deposited superconducting thin films of $Y_1Ba_2Cu_3O_{7-\delta}$ using Nd:YAG laser," *Journal of Applied Physics*, vol. 68, no. 3, pp. 1403–1406, 1990. 43, 44, 45, 72, 79, 93

[103] D. Misra, A. Lourenco, and S. Palmer, "Use of Nd: YAG laser for in situ growth of thin films of $Y_1Ba_2Cu_3O_{7-\delta}$," *Bulletin of Materials Science*, vol. 14, no. 2, pp. 517–520, 1991. [Online]. Available: http://link.springer.com/article/10.1007/BF02747366 43

[104] A. Narazaki, T. Sato, Y. Kawaguchi, H. Niino, A. Yabe, T. Sasaki, and N.Koshizaki, "Pulsed laser deposition of semiconductor-ITOcomposite films on electric-field-applied substrates," *Applied Surface Science*, vol. 197-198, pp. 438–441, 2002. 44

[105] C. Hirose, Y. Matsumoto, Y. Yamamoto, and H. Koinuma, "Electric field effect in pulsed laser deposition of epitaxial ZnO thin film," *Applied Physics A*, vol. 79, no. 4-6, pp. 807–809, Jul. 2004. [Online]. Available: http://link.springer.com/10.1007/s00339-004-2568-3 44

[106] H. S. Park, S. H. Nam, and S. M. Park, "Laser Ablation of a Zn Target in Electric Field," *Journal of Physics: Conference Series*, vol. 59, pp. 384–387, Apr. 2007. [Online]. Available: http://stacks.iop.org/1742-6596/59/i=1/a=081?key=crossref.4b60b18931cd4497717db89b72d19d14 44

[107] W. S. Hu, Z. G. Liu, Y.-Q. Lu, S. N. Zhu, and D. Feng, "Pulsed-laser deposition and optical properties of completely (001) textured optical waveguiding $LiNbO_3$ films upon SiO_2/Si substrates," *Opt. Lett.*, vol. 21, no. 13, pp. 946–948, July 1996. 44, 89, 90

[108] J. Jones, A. Voevodin, and J. Zabinski, "Characterization of plume fluence for laser ablation of yttria stabilized zirconia in mixed oxygen and argon environments," *Surface and Coatings Technology*, vol. 146-147, pp. 258–262, 2001. 44

[109] R. I. Tomov and M. Blamire, "Pulsed Laser Deposition of $SrBi_2Ta_2O_9$ Thin Films on Si Substrate," *Plasma Processes and Polymers*, vol. 3, pp. 241–247, 2006. 44

[110] G. Norton and B. Carter, "Effect of substrate temperature and oxygen pressure on the microstructure of thin $YBa_2Cu_3O_{7-\delta}$ film deposited on MgO by pulsed-laser ablation," *Physica C: Superconductivity*, vol. 182, no. August, pp. 30–38, 1991. 44

[111] C. van Niekerk, "An Investigation into the Manufacture and Measurement of Superconducting microwave Devices," MScEng, University of Stellenbosch, Electrical and Electronic Engineering, December 1995. 48, 56, 114

[112] H. L. Snetler, "High-temperature superconductor step-edge fabrication for the implementation of RSFQ circuits /," MScEng, University of Stellenbosch, 2005. 48, 56, 65, 68, 69

[113] A. A. Elkaseh, "Fabrication of High-Temperature Superconducting nanobridges Using Atomic Force Microscopy," MscEng, University of Stellenbosch, Electrical and Electronic Engineering, Dec 2006. [Online]. Available: http://hdl.handle.net/10019/1019 48, 56

[114] ——, "Fabrication of Josephson junctions using AFM Nanolithography," PhD Eng, University of Stellenbosch, 2010. 48, 65, 68, 69

[115] C. Schenke, "An Investigation into the Fabrication of Nanomechanical Switches," MScEng, University of Stellenbosch, 2010. 48, 58, 67

[116] S. Xu, Y. Tian, H. Lü, D. Cui, Z. Chen, L. Li, and G. Yang, "The effect of laser energy density and target-substrate distance on the quality of YBCO films," *Superconductor Science and Technology*, vol. 7, p. 435, 1994. 52

[117] D. Chambonnet, C. Fages, C. Belouet, H. Moriceau, M. Schwerdtfeger, J. Villégier, and D. Keller, "Optimization of YBCO thin films grown on MgO for microwave applications," *Journal of Alloys and Compounds*, vol. 195, pp. 243–246, 1993. 56

[118] D. C. Montgomery, *Design and analysis of experiments*, 5th ed. John Wiley & Sons, Inc, 2001. 56

[119] A. F. Botha, "An Investigation into the Research and Development of Nanostructured Photovoltaic Cells," MscEng, University of Stellenbosch, Electrical and Electroninc Engineering, March 2010. 56

[120] S. Proyer, E. Strangl, M. Borz, B. Hellebrand, and D. Bäuerle, "Particulates on pulsed-laser deposited Y-Ba-Cu-O films," *Physica C*, vol. 257, pp. 1–15, 1996. 56

[121] S. Duhalde, A. Lamagna, M. Villafuerte, A. Schwartzman, L. Correra, and G. Quintana, "Influence of the deposition parameters on the structural and transport properties of YBaCuO thin films prepared by pulsed laser deposition," *Applied Surface Science*, vol. 127-129, pp. 520–524, 1998. 56

[122] P. Paturi, K. Schlesier, and H. Huhtinen, "Effect of target density on YBCO thin films deposited from nanograined targets," *Physica C: Superconductivity*, vol. 469, no. 14, pp. 839–842, 2009. [Online]. Available: http://www.sciencedirect.com/science/article/B6TVJ-4WC1169-1/2/555fb8b2393d12048c33a4b794a50989 56

[123] J. K. Heinsonn, D. Reimer, A. Richter, K. O. Subke, and M. Schilling, "Interaction of process parameters in the laser depostition of $YBa_2Cu_3O_7$ films," *Physica C*, vol. 299, pp. 99–112, 1998. 57

[124] A. Eulenburg, E. Romans, Y. Fan, and C. Pegrum, "Pulsed laser deposition of $YBa_2Cu_3O_7$ and $NdBa_2Cu_3O_7$ thin films: a comparative study," *Physica C*, vol. 312, pp. 91–104, 1999. 57

[125] H. Bubert, J. Rivière, H. Arlinghaus, and H. Hutter, *Surface and Thin-Film Analysis*, H. Burbert and J. Jennet, Eds. Wiley-VHC Verlag GmbH, 2002, vol. 4. [Online]. Available: http://onlinelibrary.wiley.com/doi/10.1002/14356007.b06_023/full 60, 61

[126] C. Brundle, C. E. Jr, and S. Wilson, *Encyclopedia of materials characterization: surfaces, interfaces, thin films*, L. E. Fitzpatrick, Ed. Manning Publications Co., 1992. [Online]. Available: http://www.lavoisier.fr/livre/notice.asp?ouvrage=1068460http://books.google.com/books?hl=en&lr=&id=i7XYEp0TVc4C&oi=fnd&pg=PR9&dq=

Encyclopedia+of+materials+characterization:+surfaces,+interfaces,+thin+films&ots=opAg9fVT_u&sig=1rST8RNf5CSvXChcGWKkA4b4A0U 61

[127] J. Reibenspies, A. Clearfield, and N. Bhuvanesh, *Principles and applications of powder diffraction*. Wiley, 2008. [Online]. Available: http://www.lavoisier.fr/livre/notice.asp?id=RKOWARAX333OWX 62, 63

[128] S. Rossnagel, "Sputtering and Sputter Deposition," in *Handbook of Thin Film Deposition Processes and Techniques*, 2nd ed., K. Seshan, Ed. Noyes Publications / William Andrew Publishing, 2002, ch. 8, pp. 319–348. 81

[129] B. Moeckly and W. Ruby, "Growth of high-quality large-area MgB_2 thin films by reactive evaporation," *Superconductor Science and Technology*, vol. 19, pp. L21–L24, 2006. 90

[130] J. Garcia López, D. H. A. Blank, and H. Rogalla, "Oxygen content of $YBa_2Cu_3O_{6+x}$ thin films during growth by pulsed laser deposition," *Applied Surface Science*, vol. 127-129, pp. 1011–1016, 1998. 100

[131] Cst em studio 2006b. Online. Darmstadt, Germany, CST Computer Simulation Technology. Bad NauheimerStr. 19, D-64289. [Online]. Available: http://www.cst.com/ 103, 111

[132] G. L. Hardie, U. Büttner, and W. J. Perold, "The Enhancement of Superconducting $YBa_2Cu_3O_{7-x}$ Thin Films by Electric Field Application During Deposition," *IEEE Transactions on Appiled Superconductivity*, vol. 19, no. 3, pp. 3387–3390, 2009. 108, 121

[133] Y. Wang, B. Wang, and J. Wang, "A compact square loop dual-mode bandpass filter with wide stop-band," *Progress In Electromagnetics Research*, vol. 77, pp. 67–73, 2007. [Online]. Available: http://onlinewww.jpier.org/PIER/pier.php?paper=07072707 110

[134] S. Shen, R. Ramer, M. Banciu, and R. Mansour, "Design and realisation of star-geometry dual-mode bandpass filter." *Optics express*, vol. 13, no. 24, pp. 9753–7, Nov. 2005. [Online]. Available: http://www.ncbi.nlm.nih.gov/pubmed/19503182 110

[135] S.-W. Fok, P. Cheong, K.-W. Tam, and R. Martins, "A novel microstrip square-loop dual-mode bandpass filter with simultaneous size reduction and spurious response suppression," *Microwave Theory and Techniques, IEEE Transactions on*, vol. 54, no. 5, pp. 2033–2041, May 2006. 110

[136] W.-H. Tu, "Compact double-mode cross-coupled microstrip bandpass filter with tunable transmission zeros." *IET Microwaves, Antennas & Propagation*, vol. 2, no. 4, pp. 373 – 377, 2008. [Online]. Available: http://search.ebscohost.com.ez.sun.ac.za/login.aspx?direct=true&db=aph&AN=32079038&site=ehost-live 110

Appendix A

Datasheets

A.1 ma-P 1225 : Positive Photoresist

micro resist technology GmbH
Koepenicker Straße 325
12555 Berlin-Koepenick
Germany
Telephone +49 30 65762192
Fax +49 30 65762193
E-Mail mrt@microresist.de
www.microresist.de

ma-P 1200 — Positive Tone Photoresist Series

Resists for UV Lithography

Resist patterning with mask aligner, broadband exposure

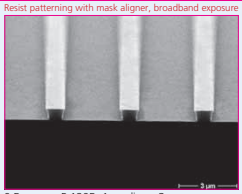

0.5 µm ma-P 1205, 1 µm lines, 3 µm spaces

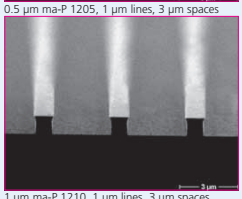

1 µm ma-P 1210, 1 µm lines, 3 µm spaces

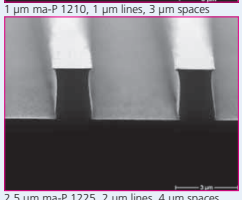

2.5 µm ma-P 1225, 2 µm lines, 4 µm spaces

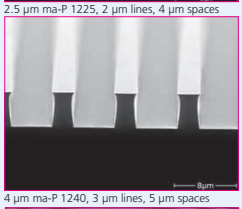

4 µm ma-P 1240, 3 µm lines, 5 µm spaces

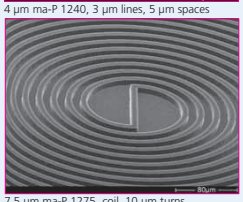

7.5 µm ma-P 1275, coil, 10 µm turns

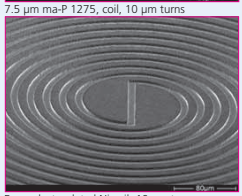

5 µm electroplated Ni coil, 10 µm turns

Unique features

- Outstanding pattern stability in wet etch processes and acid and alkaline plating baths
- Highly stable in dry etch processes e.g. CHF_3, CF_4, SF_6
- Aqueous alkaline development
- Easy to remove
- Resists available in a variety of viscosities

Applications

Mask for etching e.g.

- Si, SiO_2
- Metals
- Semiconductors

Mask for ion implantation

Moulds for electroplating

Process flow

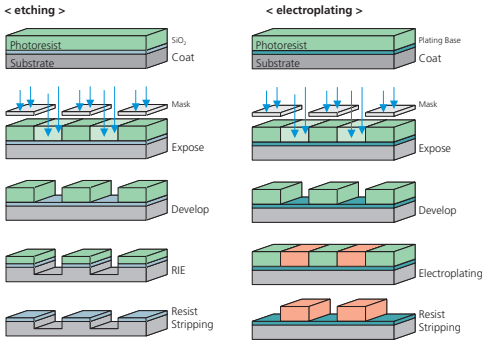

Technical data

Resist		ma-P 1205	ma-P 1210	ma-P 1215	ma-P 1225	ma-P 1240	ma-P 1275
Film thickness	µm	0.5	1.0	1.5	2.5	4.0	7.5
Spin coating	U min^{-1} s	3000 30					
Spectral sensitivity		broadband, g-, h-, i-line					
Dose @ 365 nm (broadband exposure)	mJ cm^{-2}	35	35	45	55	110	210

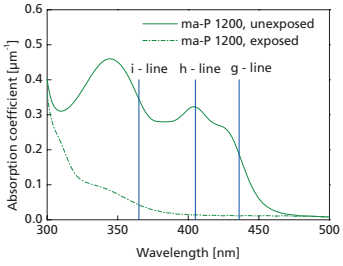

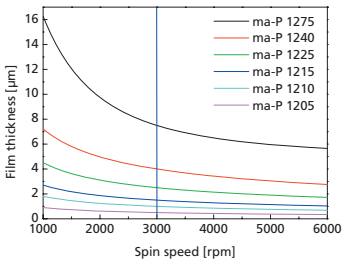

Figure A.1: Positive Photoresist : ma-P 1225 Datasheet